Report Title: Final Scientific/Technical Report of Project Methods to Enhance Wellbore Cement Integrity with Microbially-Induced Calcite Precipitation (MICP) - REVISED

Type of Report: Final Scientific/Technical Report

Reporting Period Start Date: October 01, 2014

Reporting Period End Date: September 30, 2019

Principal Author: Adrienne Phillips, Ph.D., Principal Investigator

Date Report was Issued: March 3, 2020

DOE Award Number: DE-FE0024296

Name and Address of Submitting Organizations:

Montana State University (MSU)
Energy Research Institute
P.O. Box 172465
Bozeman, MT 59717-2465
Dr. Robin Gerlach, Dr. Lee Spangler, Dr. Al Cunningham, Dr. Catherine Kirkland, and Dr. Adrienne Phillips

Southern Company (SC):
Post Office Box 2625 / Bin B263
Birmingham, AL 35202-2625
Dr. Richard Esposito

University of Alabama at Birmingham (UAB):
Business & Engineering Complex 358C
1150 10th Avenue South
Birmingham, Alabama 35294-4440
Dr. Peter Walsh

University of Stuttgart (Stuttgart):
Pfaffenwaldring 61
Stuttgart 70569
Germany
Dr. Rainer Helmig, Dr. Johannes Hommel

Montana Emergent Technologies (MET):
160 W Granite Street
Butte, MT 59701
Randy Hiebert, Brian Park, Jay McCloskey, Robert Hyatt

Loudon Technical Services (LTS):
611 Loudon Heights Road
Charleston, WV 25314
Jim Kirksey

Disclaimer

ACKNOWLEDGEMENTS

This work was supported by funding from the Department of Energy DOE Award No.: DE-FE0024296 Methods to Enhance Wellbore Cement Integrity with Microbially-Induced Calcite Precipitation (MICP). Any opinions, findings, conclusions or recommendations expressed herein are those of the authors and do not necessarily reflect the views of the Department of Energy (DOE). Collaborators on this project include Southern Company (SC), the University of Alabama at Birmingham (UAB), the University of Stuttgart (Stuttgart), Montana Emergent Technologies (MET), and Loudon Technical Services (LTS). Dr. Richard Esposito (SC) conducted geologic site characterization and obtained rock core samples from the field for laboratory analysis. Dr. Peter Walsh (UAB) conducted multiple core tests on field and laboratory sandstone rock core samples. Dr Rainer Helmig (Stuttgart) supervised simulation modeling in collaboration with CBE researchers. Randy Hiebert (MET) and Jim Kirksey (LTS) assisted in designing and performing the field tests, evaluation of the field delivery system, and analyzing results to ensure the effectiveness of the biomineralization sealing process. The authors also acknowledge the SubZero Science and Engineering Research Facility at Montana State University, which is supported by funding from the NSF-MRI Program and the M.J. Murdock Charitable Trust, for use of the X-ray μ-CT and assistance with data processing and analysis. This work was performed in part at the Montana Nanotechnology Facility, a member of the National Nanotechnology Coordinated Infrastructure (NNCI), which is supported by the National Science Foundation (Grant# ECCS-1542210).

ABSTRACT

The goal of this project was to develop improved methods for sealing compromised wellbore cement in leaking oil and gas wells, thereby reducing the risk of unwanted upward fluid migration. Novel methods for improving wellbore integrity, such as microbially induced calcite precipitation (MICP), can reduce leakage potential, improve the safety of fossil fuel extraction, improve the public perception of hydraulic fracturing, and promote environmentally-prudent unconventional oil and gas development. Microbes, with the urease enzyme, can catalyze the chemical reaction of urea hydrolysis to induce the precipitation of calcium carbonate which can be used as a cementitious material to seal leakage pathways. In this project, methods to promote robust bio-composite cementitious materials were designed and tested in the laboratory. Scale-up of those methods were tested in meso-scale reactor systems and in field applications. In this report, in Section One, we describe laboratory efforts to develop injection strategies to promote precipitation in wellbore analogs and determine the strength of the bio-composite cements as compared to fine cement. In Section Two, we describe the efforts to scale up the work and study the use of materials that can be used in field application, for example exploring the use of calcium chloride ice melt or urea fertilizer as source chemicals. In Section Three, the three field trials (methods and results) performed as part of the project are described and summarized. At the end of the report is a comprehensive summary and conclusion section which highlights the key findings of the project. The work performed during this project significantly advanced the technology readiness level (TRL) of the MICP wellbore sealing strategy.

EXECUTIVE SUMMARY

This project aims to promote environmentally prudent oil and gas production by developing improved methods for sealing compromised wellbore cement in leaking oil and gas wells--thereby reducing the risk of unwanted upward migration of greenhouse gases. The project has focused on development of a novel sealing technology known as microbially induced calcite precipitation (MICP). MICP promotes the hydrolysis of urea (aka ureolysis) to change mineral saturation which, in the presence of calcium, results in the precipitation of copious amounts of calcium carbonate ($CaCO_3$). The precipitated $CaCO_3$ seals fractures in compromised wellbore cement and free pore space in rock formations, effectively reducing permeabilities to low levels. MICP has been researched for a wide range of engineering applications[1] including improving construction materials [2-4], cementing porous media[5-9], and environmental remediation [10-14].

Traditional methods for wellbore rehabilitation usually rely on cement, in particular fine cement [15, 16], that can be injected into gaps as small as 120 µm, but high viscosity can limit access to smaller fractures. The MICP technology developed herein can be delivered via fluids of essentially aqueous viscosity, resulting in the ability to plug small aperture leaks including fractures and pore space in the near-wellbore environment.

The R&D strategy employed in this project combined laboratory experimentation at multiple scales and ultimately, field demonstrations. The three project objectives were: (1) conduct thorough laboratory testing of MICP sealing and develop a field test protocol for effective MICP placement and control, (2) prepare for and conduct an initial MICP field test aimed at sealing a

poor well cement bond, and (3) after analysis of the results from the first field test, conduct a second MICP field test using improved MICP injection methods. During the project, an additional field project was performed, and a mobile laboratory was designed and fabricated.

This report is organized according to the scaling (laboratory to field) strategy. In Section One, the laboratory efforts and reactor systems used to develop methods for field demonstrations are described. In Section Two, larger laboratory scale reactor systems and research methods to grow larger volumes of microbes using technically and economically feasible chemicals (such as urea, calcium and yeast extract) are described. In Section Three, the field demonstration projects are highlighted, including the details of the mobile laboratory design and construction project.

During this project, significant advancement of the MICP sealing technology was achieved. At the beginning of this project, MICP had yet to be deployed to seal a wellbore leakage pathway and had not been used in an environment that contained hydrocarbons. The starting Technology Readiness Level (TRL) was TRL3-4, defined as "Analytical and experimental critical function and/or characteristic proof of concept" and "Component and/or system validation in laboratory environment". The work described in Section One and Two of this report used laboratory-based wellbore analog reactors to move this technology to TRL5 defined as "Laboratory scale, similar system validation in relevant environment".

The first field deployment was conducted in a stratigraphic test well which exhibited surface casing vent flow. This field deployment was successful with well logs showing the annular space leakage pathway was sealed over a significant distance and that the pressure-flow response changed dramatically. However, the biomineralization-promoting solutions were mixed in the back of a U-Haul truck and the delivery method involved use of a bailer, which had to be manually filled before delivery of those solutions downhole. Prior to the second field test which was performed in an oil well in the presence of hydrocarbons, a mobile laboratory was designed and constructed but a similar bailer delivery system was used. These tests moved the technology towards TRL 6 defined as "Engineering/pilot-scale, similar (prototypical) system validation in relevant environment". The bailer delivery method was not typical to operations in the oil and gas industry, thus prior to test three, continuous injection methods were designed, and the mobile laboratory was further modified to include custom designed microbial growth systems to promote the development of large volumes of microbes. In the third test, continuous injection of solutions down the wellbore was deployed which moved significantly more fluid volume compared to the bailer delivery method. The success of the continuous injection in the third field test moved the technology much closer to commercialization. Supplemental funding for this mobile laboratory was critical to move the technology to TRL 7 "Full-scale, similar (prototypical) system demonstrated in relevant environment".

Montana Emergent Technologies (MET), a partner to MSU and subcontractor on this project, helped design and build-out the mobile laboratory and used the lessons learned during its field deployment to build a similar system more targeted at oilfield operations. MET's efforts have moved MICP specifically for the purpose of sealing channels in the annular space of wellbores to the TRL 8 "Actual system completed and qualified through test and demonstration" level by commercializing the technology under the name BioSqueeze™. MET has successfully sealed 13

wells in two states in commercial environments. This included four problematic wells that other "exotic" and more expensive sealing technologies failed to remediate ($300,000 - $1M spent on each well before Biosqueeze™). MET has had a significant success rate, but probably has not yet "operated over the full range of expected mission conditions" which defines TRL 9.

It is worth re-iterating that these TRL levels for MICP are being defined specifically for sealing leakage pathways in the annular space of wellbores. There are other potential sub-surface applications of MICP targeting permeability modification of the rock formation which are lower on the readiness scale (TRL 2-4). Future avenues for exploratory research include applications such as modification of lost circulation materials, sealing fractures prior to re-fracturing to open new source rock, solidifying unconsolidated materials in drilling operations, reducing proppant flowback, and reducing permeability to improve sweep efficiency for injected fluids.

There were key lessons learned in this project: 1) faithful laboratory analogues allow for trial and error that dramatically improves probability of success in field pilots, 2) bringing oilfield expertise (Jim Kirksey of Louden Technologies) into the project team was critical to understanding technical issues to address and for coordination of the field activities and 3) developing a working technology is necessary but not sufficient for its adoption, even if it is unique in its ability to solve a challenging problem. Operations and deployment are also very important if that technology targets an existing industry which may be reluctant to adopt un-proven technologies. The work performed during this project significantly advanced the technology readiness level (TRL) of this wellbore sealing strategy, which can now be used reliably to reduce the potential for leakage from oil and gas wells, reducing the environmental impact of conventional or unconventional oil and gas wells.

TABLE OF CONTENTS

CONTENTS

Report Layout

As mentioned above, the report is laid out in sections according to the scaling strategy. Each section includes excerpts from produced peer reviewed or draft journal publications, theses, or conference papers. Each subsection contains an Abstract, Experimental Methods, Results and Discussions, and Conclusion segment. These segments are designated as such with parentheses behind the corresponding journal heading for example "(Abstract)". The Conclusion at the end of the report encompasses the entire project.

ABSTRACTS: Abstracts are included in each section of this final report.

EXPERIMENTAL METHODS: Experimental methods are described within each section of this final report.

RESULTS AND DISCUSSIONS: Results and discussions are written within each section of this final report.

CONCLUSIONS: Conclusions are drawn for each of the individual sections and also in a comprehensive overall conclusion statement at the end of the report.

Section One: Laboratory Efforts

In this section, we describe the laboratory scale experiments that were used to develop injection strategies to promote biomineralization in gaps or fractures and studies on the fundamental properties of the biomineral. These injection strategies and properties were studied to determine what might work best in the field applications and scale up efforts that will be described in Section Two and Section Three. The results of the laboratory scale studies were published in three papers and two graduate student theses. Section 1.1 describes visualizing the distribution of mineral in an engineered fracture with wellbore cement on each side of the fracture. The injection strategies were altered to promote a more homogenous distribution of mineral. Section 1.2 describes activities to design a representative wellbore analog reactor system and promote mineral in an engineered gap between the cement annulus and the outside polycarbonate of the reactor. Section 1.3 includes the assessment of the strength of the biomineral and the comparison to the material properties of typical oil and gas well cement. This study was performed because the strength of the biomineral influences the success of the treatment in fractured gaps in the field and the resistance to flow of fluids through those gaps. This section describes the efforts used to meet the objectives as described in the proposal:

Objective 1: After thorough laboratory testing of MICP sealing, develop a field test protocol for effective MICP placement and control.
Objective 2: Prepare for and conduct an initial MICP field test aimed at sealing a poor well cement bond.
Objective 3: After thorough analysis of the results from the first field test, conduct a second MICP test using improved MICP injection methods.

Section 1.1 is comprised of the following manuscripts (with permission from Elsevier- see Appendix A) and thesis:

- Kirkland, C, Norton, D, Firth, O, Gerlach, R, and Phillips, AJ. (2019) Visualizing MICP with X-ray µ-CT to enhance cement defect sealing, *International Journal of Greenhouse Gas Control* 86: 93-100 https://www.sciencedirect.com/science/article/pii/S1750583618308831
- Norton, D. Visualizing and Quantifying Biomineralization in Wellbore Analog Reactors. MS Thesis, Environmental Engineering, Montana State University, June 2017

Section 1.2 is comprised of the following conference paper/thesis:

- Kirkland, C, Norton, D, Cunningham, A, Thane, A, Gerlach, R, Hiebert, R, Hommel, J, Kirksey, J, Esposito, R, Spangler, L, Phillips, AJ. (2019) Biomineralization and wellbore integrity: a microscopic solution to subsurface fluid migration 14th Greenhouse Gas Control Technologies Conference Melbourne, Australia October 21-25, 2018 (SSRN published online April 2019) https://papers.ssrn.com/sol3/papers.cfm?abstract_id=3366088
- Norton, D. Visualizing and Quantifying Biomineralization in Wellbore Analog Reactors. MS Thesis, Environmental Engineering, Montana State University, June 2017

Section 1.3 is comprised of the following conference paper/thesis:

- Beser, D, West C, Daily, R, Cunningham, A, Gerlach, R, Fick, D, Spangler, L and Phillips, AJ. (2017) Assessment of ureolysis induced mineral precipitation material properties compared to oil and gas well cements. American Rock Mechanics Association 51st Annual Meeting Proceedings, June 25-28, 2017, San Francisco, CA. (Paper # 588) https://www.onepetro.org/conference-paper/ARMA-2017-0588

- Beser, GD. Ureolysis induced mineral precipitation material properties compared to oil and gas well cements. MS Thesis, Civil Engineering, Montana State University, April 2018

Section 1.1 Visualizing MICP with X-ray µ-CT to enhance cement defect sealing

Abstract (Abstract)

Concerns about leakage exist when storing fluids like CO_2 or natural gas in the subsurface given their potential to damage functional groundwater aquifers or be emitted to the atmosphere. Defects in the cement surrounding the wellbore undermine the integrity of subsurface storage systems. Microbially induced calcite precipitation (MICP) is a technique that uses low viscosity fluids and microorganisms (~2 µm diameter) to seal defects like micro-annuli, cracks, and channels in well cement. This study quantified MICP in a cement channel defect using X-ray computed microtomography (X-ray µ-CT). Following control and replicate experiments conducted with a low injection flow rate, and which produced X-ray µ-CT data showing precipitation predominately occurred near the inlet, the injection strategy was modified for a third MICP experiment. The revised injection method used an increased flow rate and more frequent nutrient pulses resulting in 1) fewer calcium media pulses to seal the defect and 2) a more homogeneous distribution of mineral compared to the replicate experiments. Observations made during these experiments will aid in improving the safety and efficacy of subsurface fluid storage systems.

Introduction

Subsurface reservoirs can provide long-term storage of hydrocarbon fuels or CO_2 injected as part of a carbon capture and storage (CCS) project. Concerns about fluid leakage arise given the potential for damage to functional groundwater aquifers and emission to the atmosphere (Figure 1).[17-19] The risk of leakage in storage systems is heavily dependent on the ability of the well cement to maintain a seal against subsurface fluids.[17, 19-22] In the case of subsurface carbon storage, cement defects also enhance the possibility of acidic fluids corroding well materials.[17, 23-27] The wells that are used to access the subsurface typically consist of a steel casing nested inside a borehole drilled into the rock formation. During installation of the casing, cement is pumped down through the inner casing to the bottom of the well and then forced up into the annular space between the casing and the formation. The cement's return to the surface implies that the annular space was filled.[19] This cement is designed to hold the casing in place, create a bond between the casing and formation, fill fractures that might develop during drilling, and thus stop vertical fluid migration.

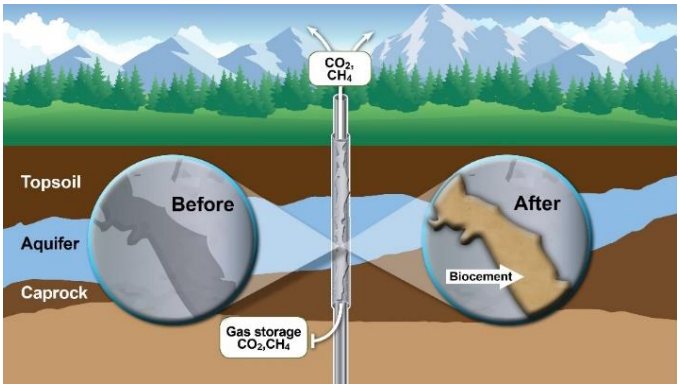

Figure 1. An Illustration of MICP formation in a wellbore cement defect and leakage pathway. The resulting mineral seal could mitigate fluid leakage to functional aquifers or the atmosphere.

Wellbore cement defects form in a variety of ways. In some cases, cement may return to the surface without being evenly distributed around the well, especially if the casing is not centered in the open hole. Physical stresses, such as geological shifts and thermal expansion or contraction, can also produce cement defects, thereby creating potential leakage pathways.[19, 21, 22] Interface defects form in the presence of residual drilling mud,[21] excess water in the cement paste,[19] variable temperatures (thermal cycling),[19] or mechanical stresses (pressure cycling) in the wellbore.[28, 29] While it is possible to minimize the risk of some types of cement defects by use of best practices in well construction, some degree of physical stress is inevitable over the lifetime of a well. Thus, optimization of wellbore leakage mitigation strategies will only become more important over time as more wells are drilled and existing wells age. Models and experimental analogs have been developed to assess defect formation and methods to repair defects at interfaces between the cement and casing, or cement and formation, as well as within the body of the annular cement.[17, 21, 23, 30]

Current technologies to seal leakage pathways in the annular space surrounding the well generally consist of the use of cement or resins.[31] Large defects can be sealed by injecting cement into the annular space, known as a "squeeze job."[32] This approach may fail in small aperture defects, where viscous cement slurries may require excessive (fracture inducing) pumping pressures to inject. The resulting fluid migration in small aperture defects may pose significant risks – particularly when storing low viscosity fluids such as vapor phase hydrocarbons or gaseous CO_2 at reservoir temperatures and pressures.

The process of microbially induced calcite precipitation, or MICP, is proposed to seal small aperture defects in the wellbore environment using microbes and low viscosity fluids to promote the formation of bio-cement. MICP binds discrete particles together and modifies formation permeability by filling pore spaces with mineral deposits. MICP has been proposed for a variety of engineering applications such as suppressing dust, improving soils, remediating contaminated groundwater, sealing ponds or reservoirs, mitigating wellbore leakage, and enhancing oil recovery.[14, 33-37] Several studies have also proposed or implemented treatment of the subsurface using MICP to restrict fluid flow.[1, 38-45]

MICP can occur via multiple biochemical pathways including ureolysis, sulfate reduction, and photosynthesis.[1, 46] The work described within this final report utilizes ureolysis-driven MICP. Ureolysis-driven MICP utilizes the enzyme urease, produced by microbes, to hydrolyze urea, generating ammonia (NH_3) and CO_2 [Eq 1]. The presence of NH_3 increases the solution pH [Eq. 2] creating conditions where the carbonate equilibrium shifts toward the production of carbonate ions, CO_3^{2-} [Eq. 3]. In the presence of sufficient calcium ion activity, Ca^{2+} and CO_3^{2-} can precipitate as calcium carbonate ($CaCO_3$), [Eq 4].

$$CO(NH_2)_2 + H_2O \rightarrow NH_2COOH + NH_3 \rightarrow 2NH_3 + CO_2 \quad \text{(urea hydrolysis)} \quad [1]$$

$$2NH_3 + 2H_2O \leftrightarrow 2NH_4^+ + 2OH^- \quad \text{(pH increase)} \quad [2]$$

$$CO_2 + 2OH^- \leftrightarrow CO_3^{2-} + H_2O \quad \text{(carbonate formation)} \quad [3]$$

$$CO_3^{2-} + Ca^{2+} \leftrightarrow CaCO_{3(s)} \quad \text{(precipitation)} \quad [4]$$

Ureolysis-driven MICP depends on (1) calcium concentration, (2) dissolved inorganic carbon concentration, (3) pH, and (4) the availability of nucleation sites.[46] The first three factors affect the saturation of dissolved $CaCO_3$ through the manipulation of the aqueous chemistry surrounding the cell, where the saturation of $CaCO_3$ in solution can be described by [Eq 5]:

$$S = \frac{[Ca^{2+}][CO_3^{2-}]}{K_{so}} \quad [5]$$

in which S is the saturation state of $CaCO_3$, $[Ca^{2+}]$ and $[CO_3^{2-}]$ are the activities of the calcium and carbonate ions respectively, and K_{so} is the solubility constant of $CaCO_3$ (5×10^{-9} at 25°C). An increase in either calcium or carbonate species will increase the saturation state of $CaCO_3$, meaning that precipitation is more likely. Conditions are favorable for $CaCO_3$ precipitation when $S > 1$.

The fourth factor controlling ureolysis-driven MICP, the availability of nucleation sites, is related in part to the presence and activity of microbes. Cells may act as nucleation sites for the mineral, leading to localized precipitation on the biofilm surface.[47, 48] *Sporosarcina pasteurii*, a urease-producing microbe, is approximately 2 µm in length, allowing cells to enter small defects in the wellbore which would be difficult to seal with cement slurry injection.[40, 49] The localized precipitation around the biofilm can help to concentrate precipitation into defects, creating a seal capable of halting fluid flow along the wellbore in subsurface fluid storage systems.

Balancing fluid injection and reaction (precipitation) rates may help to control the spatial deposition of bio-cement. If the reaction rate exceeds the transport rate, precipitation may occur during injection. This typically produces more spatially heterogeneous $CaCO_3$ precipitation with most occurring near the inlet, called entry point plugging.[42, 50, 51] For example, Mortensen et al. (2011) correlated a larger precipitation deposition near the entrance of a column to a slower fluid injection rate.[50] Since many applications of MICP benefit from a more homogeneous distribution of $CaCO_3$ precipitation, pulsed-flow injection strategies have been developed. In this study, the injection of the calcium solution was performed using high and low injection flow rates to manipulate the transport/reaction processes. Following injection, the flow was halted to allow the reaction rate to dominate and to promote homogeneous precipitation along the well-cement flow

path. The more homogeneous distribution of $CaCO_3$ resulting from the pulsed flow injection method may create a more effective bio-cement seal.[52, 53]

The experiments described here utilize the ureolytic bacterium, *S. pasteurii* to facilitate MICP. The objective of this study was to visualize and quantify fluid flow restrictions resulting from MICP in cement defects. Control and replicate MICP experiments were conducted in a model cement defect reactor compatible with measurement by X-ray computed microtomography (μ-CT). Using the results of these studies, a third MICP experiment was conducted with a modified injection strategy that included a faster injection flow rate and more frequent nutrient pulses. The void fraction of the cement defect was quantified over time using X-ray μ-CT as MICP occurred within the reactor. X-ray μ-CT provides a means to non-invasively and non-destructively quantify the change in void fraction due to MICP in space and time.

Materials and Methods (Experimental Methods)

Reactor Design and Assembly

A reactor (Figure 1) was designed to accommodate a Skyscan 1173 X-ray micro-tomograph (MSU Subzero Science Laboratory). The 3.4 cm-diameter, 11.4 cm-long PVC reactor housed a 5 cm-long cement core with a central longitudinal channel defect. New cement cores were made for each of the four experiments: the control experiment, CEC; the replicate experiments, CE1 and CE2; and the modified experiment, CE3. Each cement core was cast as two separate half-cylinders and then joined together in the reactor, producing a channel defect initially measuring 5 cm long x 0.25 cm wide x 0.05 cm deep. The estimated open volume within the reactor was approximately 30 mL and included the volume of the defect (0.0625 mL) and the void space above and below the cement core. The cement cores were prepared using a blend of equal parts Class H cement and pozzolan additives with an additional 6% by weight bentonite (supplied by Schlumberger). To prepare the cement slurry, water was added to the Class H cement to create a 0.4 water to cement ratio by mass (400 g water, 1000 g cement) mixture. The slurry was mixed in a blender for approximately 1 minute before it was poured into the half-cylinder molds for curing. Once poured, the cement set at room temperature in the molds for four days. The cores were removed from the molds and immersed in water saturated with $Ca(OH)_2$ for a minimum of 7 days. After curing, the reactor was assembled with a cement core inside; end caps were attached to seal the reactor (Figure 2). The reactor was equipped with quick-release valve fittings at the influent and effluent ports so that the reactor could be detached from the pumps and tubing and imaged in the X-ray μ-CT scanner periodically throughout each experiment. Flow was from bottom to top of the reactor.

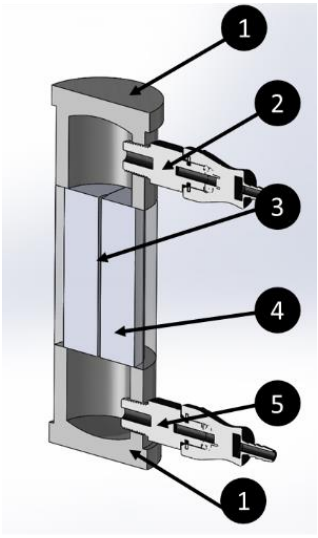

Figure 2. Cross-section schematic of the core reactor created in SolidWorks showing the (1) end caps; (2) effluent fluid port; (3) cement space defect 5 cm x 0.25 cm x 0.05 cm; (4) halves of the cement core; and (5) influent fluid port. The same reactor design was used for all four experiments in this study. Flow direction is from bottom to top.

Media Solutions

The experiments used three different solutions to promote MICP: (1) an inoculum culture of *S. pasteurii*, (2) a nutrient solution to stimulate bacterial growth (24 g/L urea (Potash Corp., Saskatoon, Canada), 1 g/L yeast extract (Acros Organics, Geel, Belgium), 1 g/L NH_4Cl (BASF USA, Florham Park, NJ) and 24 g/L NaCl (Morton's)), and (3) a source of calcium to induce the precipitation of calcium carbonate within the reactor (nutrient solution amended with 49 g/L $CaCl_2$-$2H_2O$ (Peladow, Occidental Chemical Corp., Dallas, TX)).

Inoculum Preparation

Microbes were grown by adding 1 mL of *S. pasteurii* (ATCC 11859) thawed frozen stock to 100 mL of autoclaved Brain Heart Infusion (BHI) solution (37 g/L (Becton Dickinson)) amended with 2% urea by weight. The organisms were incubated at 30°C on a shaker at 150 rpm for 16 hours. After the incubation period, the culture was transferred to fresh nutrient solution at a ratio of 1 mL of culture per 100 mL of nutrient solution. The transferred culture was then incubated at room temperature for 24 hours prior to its use as the inoculum for the reactor. For all subsequent days following the first frozen stock culture, an aliquot of the 24-hour culture was used to inoculate fresh nutrient solution in place of the frozen stock.

Injection Strategy

Four experiments were performed: three biomineralization experiments where inoculation of the reactor with *S. pasteurii* occurred (CE1, CE2, and CE3) and one negative control experiment without reactor inoculation (CEC). CEC, CE1, and CE2 employed identical methods and injection strategy including a design injection flow rate of 1 mL/min (Table 1). In the CE1 and CE2 experiments, 60 mL of inoculum culture was injected for the initial inoculation of the reactor. After a 4-hour stationary attachment period, 120 mL of nutrient solution was injected to stimulate biofilm formation and ureolysis. After approximately 15 hours, the reactor was flushed

with 60 mL of brine solution (NaCl 24 g/L (Morton's)). This brine rinse was performed between injections of different solution types to prevent instantaneous precipitation in the influent region upon the introduction of calcium species or microbe-rich fluids. Following the brine rinse, 4 pulses of calcium media, 30 mL each, were injected each day with a 60-minute stationary period between injections. The periods of no-flow were included in the injection strategy to allow additional time for the MICP process to occur once fluids had been introduced. The reactor was re-inoculated each night after a brine rinse. The negative control experiment, CEC, followed the same injection strategy but replaced inoculum injections with injections of nutrient solution. All CEC fluids were amended with 25 mg/L Chloramphenicol (Fisher-Scientific), an antibiotic known to inhibit growth and protein production of *S. pasteurii* [54].

Table 1. Detailed injection strategies used in the core reactor experiments.

CE1, CE2, and CEC	Fluid	Duration (hr)	Volume (mL)	Flow rate (mL/min)
Day 1	inoculum	1	60	1
	nutrient	2	120	1
	-	15.25		
Day 2+	brine rinse	1	60	1
	calcium media	0.5	30	1
	-	1		
	calcium media	0.5	30	1
	-	1		
	calcium media	0.5	30	1
	-	1		
	calcium media	0.5	30	1
	-	1		
	*u-CT scanning**	1.5		
	brine rinse	1	60	1
	inoculum	1	60	1
	-	13.5		

** CEC was scanned on Day 0, Day 4, and Day 8 only.*

CE3	Fluid	Duration (hr)	Volume (mL)	Flow rate (mL/min)
Day 1	inoculum	1	60	1
	nutrient	2	120	1
	-	15.25		
Day 2+	brine rinse	0.25	30	2
	calcium media	0.25	30	2
	-	1		
	nutrient	0.25	30	2

-	1		
calcium media	0.25	30	2
-	1		
nutrient	0.25	30	2
-	1		
calcium media	0.25	30	2
u-CT scanning	1.5		
brine rinse	0.25	30	2
inoculum	0.5	60	2
-	16.25		

The injection strategy for CE3 was modified to promote a more homogeneous distribution of $CaCO_3$ along the length of the cement defect (Table 1). Specifically, the injection flowrate was doubled from 1 mL/min to 2 mL/min after Day 1. Also, the daily pattern of media injection was changed from nightly inoculation followed by 4 calcium pulses the next day as done in CE1 and CE2, to nightly inoculation followed by alternating calcium and nutrient solution injections the next day. The cycle included 3 calcium media pulses with 2 nutrient solution pulses interspersed between them. This adaptation was designed to maintain high ureolytic activity by the microbes in the reactor and increase the total amount of $CaCO_3$ produced.

Sampling Procedure

Effluent samples were taken at the beginning and end of each fluid pulse to assess the bio-chemical conditions within the reactor at large. A volume of 1 mL was filtered with a 0.2 µm syringe filter and refrigerated for urea quantification with the Jung Assay[55, 56]. An unfiltered sample was used for pH measurement with a VWR Symphony SB70P pH meter, which was calibrated daily.

Apparent permeability

Intrinsic permeability describes a formation's capacity to transmit fluids and is a property of the porous medium itself. Apparent permeability, on the other hand, incorporates the hydraulic properties of a system and can be calculated from pressure and flow data using Darcy's Law [Eq 6], [57]

$$k = \frac{Q}{A} * \frac{\Delta L}{\Delta P} * \mu \qquad [6]$$

where k is the apparent fracture permeability, $Q\ is\ t$he volumetric flow rate, A is the cross-sectional area of the defect, ΔL is the length of the defect, ΔP is the pressure drop along the flowpath, and μ is the dynamic viscosity of the fluid. Pressure measurements were collected using Omega Engineering, Inc. PX309 series pressure transducers and flow rate monitoring was performed through the pump control operating software (LabVIEW, National Instruments). Fluids were delivered to the reactors using a Cole Palmer 210 syringe pump at a flow rate of 1

mL/minute for CEC, CE1, and CE2, and at 2 mL/min for CE3. These flow rates correspond to approximately 30-minute and 15-minute fluid residence times in the reactor, respectively, and initial velocities in the defect of 13 mm/s and 26 mm/s, respectively, during periods of flow. Flow rate and differential pressure measurements for both experiments were averaged over the final 60 seconds of each injection. This averaging was done to minimize the impact of the signal noise from the pressure transducer. As permeability declined in each inoculated core (CE1, CE2, CE3) near the end of the experiment, the flow rate was reduced to allow continued injection. Final permeability was measured in each inoculated core using a flow rate of 0.1 mL/min. Aperture size was calculated using the cubic law for fracture flow (Eq 7)[57]

$$b = \left(\frac{12*\mu*Q*L}{w*\Delta P}\right)^{\frac{1}{3}} \qquad [7]$$

where b is the aperture size, Q is the volumetric flow rate, L is the fracture length, w is the aperture width, μ is the dynamic viscosity of the fluid, and ΔP is the pressure drop along the flowpath. The value returned for b is an estimate for the narrowest aperture in the fracture since that dimension governs the pressure-flow relationship.

X-ray μ-CT Imaging and Analysis

Imaging was performed using a Skyscan 1173 X-ray microtomograph before and after MICP treatment as well as between the final calcium injection each day and nightly inoculation of the reactor. Flat field calibration was performed prior to each scan to determine the initial intensity of the beam. Scans were performed every 0.7° for 180° to create a full image of the reactor. All scans were performed at a voltage of 130 kV and a current of 60 μA with an unfiltered beam. Image resolution was 25 μm.

The μ-CT scanner produced a 2D stack of projection radiographs showing signal attenuation through the reactor. Raw data was pre-processed to remove noise using Gaussian kernel smoothing and then the data was reconstructed using NRecon software (Bruker), using the Feldkamp algorithm,[58] to produce a series of 2D images. Once reconstructed, a rectangular region of interest (ROI) 2 mm x 9 mm was drawn around the defect at the center of the core for each 2D slice (Figure 2). A linear attenuation coefficient, corresponding to the material density through which the beam passed, was assigned to each pixel based upon the change in X-ray signal intensity.

Thresholding of the images was performed in CTAn software (Bruker) to distinguish the cement from the water within the image ROI. The data was sorted into two bins based upon the attenuation of each voxel: open pixels representing fluids in the channel (Figure 3, in black), and closed pixels representing cement and MICP (Figure 3, in white).[59] This threshold was then applied to all scans to determine how the ROI void space changed over the course of the experiment. Finally, the series of 2D images was stacked using CTAn to create a 3D reconstruction of the channel. Quantitative comparison of the pre- and post-MICP reconstructions provides an estimate of the void fraction reduction achieved in each experiment. After the experiments were terminated, the reactor was de-constructed and the cement cylinder

was separated into the two halves for light microscopy imaging using a Leica Model MDG41 stereomicroscope.

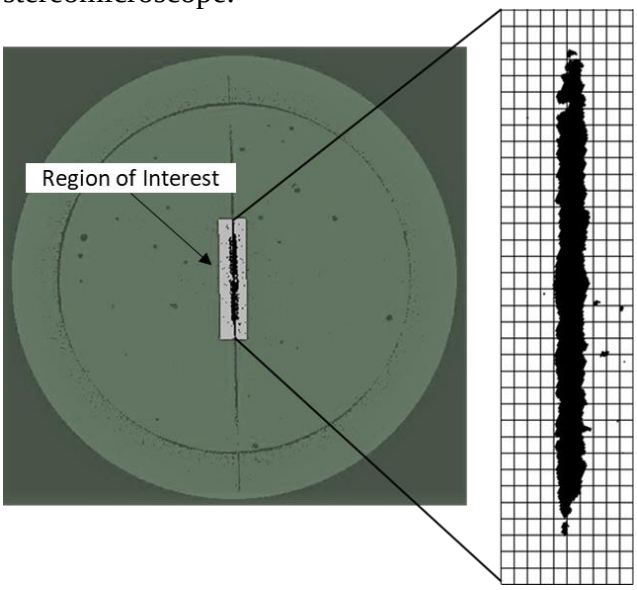

Figure 3. Two-dimensional radiograph and representative pixilation of the region of interest (ROI). Black pixels represent void space in the cement defect; white pixels represent solids (cement or calcium carbonate).

Results (Results and Discussion)

The objective of this study was to quantify and visualize calcium carbonate precipitation in a cement defect following promotion of MICP. First, changes in apparent permeability within the cement defect reflect the change over time in the fluid's ability to pass through the defect. Second, analysis of the X-ray images provides spatial and temporal resolution, showing where in the reactor the flow restrictions occurred at what time during the experiment. Stereoscopic imaging at the end of the experiments, while not quantitative, was compared with the µ-CT imaging results. A summary of the results is provided in Table 2.

Table 2. Comparison of core reactor experiments.

	CEC	CE1	CE2	CE3
Initial apparent permeability (mD)	$>5.6x10^5$	$>5.9x10^5$	$>5.6x10^5$	$7.8x10^6$
Final apparent permeability (mD)	$>2.9x10^5$	357	263	264
Approximate viable cells injected (cfu)	0	2.3×10^{10}	9.4×10^9	9.7×10^{10}
Inoculum pulses delivered (60 mL)	0	8	6	7
Nutrient pulses delivered (30 mL)	10	4	4	16
Calcium pulses delivered (30 mL)	22	29	22	18
Aperture reduction (%)	0%	97.4%	97.6%	97.6%
3D void fraction reduction (%)	10.7%	23.1%	23.6%	38%

Apparent permeability

The initial apparent permeability observed prior to MICP treatment was between $5.6x10^5$ and $5.8x10^5$ mD for CEC, CE1, and CE2 which represents the maximum permeability measurable by the pressure transducer for a flow rate of 1 mL/min through the reactor. The initial permeability for CE3, approximately $7.8x10^6$ mD, was higher because the higher flow rate used to collect the pressure measurement, 22 mL/min, created a larger pressure drop across the cement core and produced a more accurate initial permeability measurement than was recorded in the earlier experiments. The apparent permeability recorded during the initial inoculation of CE3 was $5.6x10^5$ mD. This measurement was collected using a flow rate of 1 mL/min and is consistent with the previous three core reactor experiments. It is therefore likely that the initial apparent permeability in CEC, CE1, and CE2 would also have been higher if measured with a similarly high flow rate since the cores and reactor were identical.

Final apparent permeability was recorded during injection of nutrient solution at 0.1 mL/min after the pressure and flow limitations of the reactor system were achieved. Each of the inoculated cores eventually achieved in excess of three orders of magnitude reduction in apparent permeability (Figure 4). The final apparent permeabilities of CE1 and CE2 were 357 mD (after 29th calcium pulse) and 263 mD (after 22nd calcium pulse), respectively. An increase in apparent permeability was observed in CE1 during the 26th pulse of calcium media. A possible explanation is that some mineral broke free and was washed out of the reactor, re-opening a flow path. Two subsequent pulses of calcium media were injected on the same day before the next µ-CT images were collected. The apparent permeability calculated from the 28th calcium pulse is very similar to that calculated from the 24th calcium pulse, suggesting that any mineral lost during the rapid change in pressure may have been replaced in subsequent calcium pulses. This transient increase in apparent permeability in CE1 may also explain, in part, the additional number of calcium pulses required to achieve the final permeability in CE1 relative to CE2.

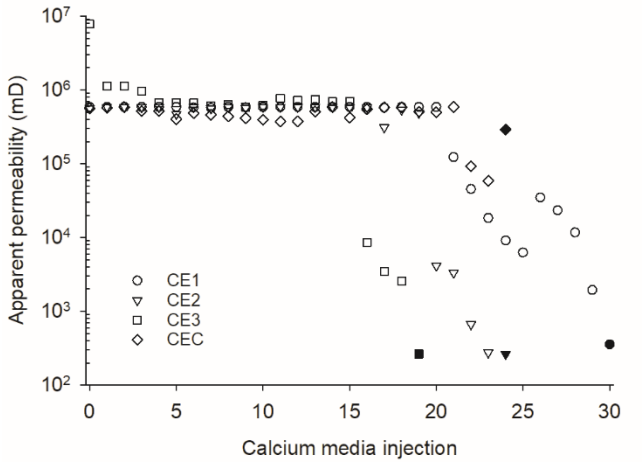

Figure 4. Apparent permeability of CER experiments as a function of calcium pulses delivered. The apparent permeability was reduced three orders of magnitude in the MICP treated cores, presumably due to mineral precipitation in the defect. The antibiotic-treated control core, CEC, showed variability in the permeability calculation, attributed to noise at the lower end of the

pressure transducer's calibration range as no mineralization was observed to form in the defect. The final data point shown for each experiment (solid marker) represents a final injection test made using nutrient solution rather than calcium media.

Experimental conditions in CE3 produced a more rapid decrease in apparent permeability, where a final apparent permeability of 264 mD was achieved after 18 calcium pulses. CE3 required 38% fewer calcium injections than CE1 and 21% fewer than CE2 to achieve equivalent final apparent permeabilities. Minimal change in apparent permeability was observed in the control experiment (CEC) which was attributed to the noise in the pressure transducer readings since no mineral was observed upon opening the reactor. The similarities between the final apparent permeability values for CE1, CE2, and CE3 are a result of system limitations for flow and pressure.

Aperture depth was approximated using the cubic law for fracture flow (Eq 7). The initial defect aperture depth was 0.05 cm. The final calculated aperture sizes for CE1, CE2, and CE3 were 0.0013 cm, 0.0012 cm, and 0.0012 cm, respectively, at the narrowest point in the defect. In each case, the final aperture size approximations represent a greater than 97.4% change from the cast aperture size of 0.05 cm. The calculated aperture size for CEC did not change over the experiment.

Void Fraction

MICP treatment success was quantified by measuring changes in the void fraction of the defect using µ-CT. The void fraction of the region of interest (ROI) was quantified for each slice and plotted as a function of distance along the fracture flow path for each day. ROI void fraction plots were compared visually to light microscopy imaging performed following the termination of each experiment (Figure 5).

In the uninoculated, antibiotic-treated control (CEC) (Figure 5, top left), little to no change in void fraction was observed in the first half of the fracture, 0 to 22.5 mm. Regions of variable void fraction were observed past 30 mm from the inlet in the final scan. One possible explanation of this reduction measured by µ-CT, although not observed when images were taken, is air that could have been trapped on the walls of the defect during the initial µ-CT scan resulting in a slightly inflated initial void volume. If those potential air bubbles were flushed out with subsequent injections, the void volume measured by µ-CT would appear to decrease. The light microscopy imaging shows no evidence of mineral precipitation in the defect.

In CE1 (Figure 5, top right), the greatest reduction in void fraction was seen within 5 mm from the fracture inlet in the data collected after the 29^{th} calcium pulse. The accumulation of mineral near the inlet was first apparent in the µ-CT image collected after the 24^{th} calcium pulse on day 7 and correlates to a significant drop in apparent permeability observed between calcium pulses 21 – 24. This observation also correlates well with post-experimental light microscopy imaging of the reactor, where a large quantity of $CaCO_3$ deposition was observed within 5 mm from the fracture inlet. More $CaCO_3$ precipitation was also observed in CE2 (Figure 5, bottom left) in the first 25 mm of the defect than in the latter half, though the effect is less pronounced than in CE1. The observation of heterogeneous $CaCO_3$ distribution similar to that seen in CE1 and CE2 has

been observed in previous works and thus is not unique to this experiment.[1, 60-62] Flow rates in these experiments were slow and the inlet volume of the reactor was large relative to the defect volume which could have led to increased precipitation in the beginning of the flow path.

Modifications to the injection strategy implemented during CE3 included doubling the injection flow rate to 2 mL/min and alternating calcium media and nutrient solution pulses. A more homogeneous distribution of $CaCO_3$ in the cement defect resulted (Figure 5, bottom right). Of particular interest, is the observation that the void fraction changed significantly between the 1st and 12th calcium pulse while there was no significant change over the same period in the apparent permeability of the defect (Figure 4). Conversely, small changes in the void fraction the last several days of the experiment produced changes in apparent permeability over four orders of magnitude. In CE1, however, the most significant changes in both void fraction and apparent permeability occurred in the latter half of the experiment, but only at the inlet.

3D Void Fraction

Analysis of the core experiments in 3D was performed based upon the 2D void fraction data and the slice height from X-ray µ-CT imaging. The total void fraction of the ROI for each day was calculated as a summation of the open voxel area divided by the total voxel area for all slices. The reduction in void fraction between the initial and final measurements was 23.1% for CE1, 23.6% for CE2, and 38% for CE3. The reduction in void fraction for CEC was 10.7%. The reduction in void fraction for CEC is most likely a measure of the error associated with scanning and data analysis methods or the presence of an air bubble in the fracture during the initial scan.

Discussion (Results and Discussion)

Several factors in these observations deserve mention. First, increasing the flow rate favors transport of media through the cement defect with minimal reaction/precipitation. Once the flow is stopped the reaction/precipitation process occurs homogeneously along the flow path. This may explain, in part, the more homogeneous distribution of mineral observed in CE3 versus CE1 and CE2. Second, replacing some of the calcium media injections with nutrient solution injections in CE3 may have helped maintain microbial activity and may have promoted biofilm formation throughout the reactor. Cells can become encased in mineral, hindering their ability to reproduce or perform urea hydrolysis.[63] More frequent injections of nutrient solution, in the absence of calcium, may promote bacterial growth in the bulk fluid and lead to higher ureolytic activity of new cells which could then provide additional nucleation sites for precipitation along the length of the defect. Cell count data from the inoculated reactors support the supposition that there were higher numbers of suspended cells in CE3 after the final daily calcium pulse compared to CE1 and CE2. Third, this hypothesized regeneration of cells and formation of new biofilm (which was not measured) may also help explain why CE3 required less calcium by mass to seal the defect.

In CE3, microbes, dispersed through the reactor and stimulated with additional substrate, may have produced a homogeneous distribution of calcite crystals early in the experiment, based on the calculation of the void fraction. Crystal growth could have proceeded outward from these initial calcite crystals until a significant portion of the flow paths were blocked, causing a rapid decrease in apparent permeability. The reactors were not imaged with the stereoscope until the

end of the experiment and the potential calcite crystals were not directly observed, though the data supports such an interpretation. It should also be noted that there were limitations to the observations using the X-ray µ-CT images, where the pixel size (25 µm) may limit resolution of small features. In CE1 and CE2, on the other hand, the reactor was inoculated nightly but was not otherwise stimulated solely with nutrient solution. Microbial cells may have become inactivated by entombment following the first subsequent calcium pulse leading to limited conversion of urea and precipitation of calcium in the remaining three calcium injections. Data from the Jung assay, which quantifies ureolysis, was consistent with this interpretation (data not shown). Both the apparent permeability calculations and the void fraction measurements by X-ray µ-CT show little change until after the 21st calcium pulse (Day 7) for CE1. Once flow restriction occurred because pathways were blocked, further precipitation in those regions rapidly reduced permeability and void fraction simultaneously.

The observation of greater flow restriction for the biomineralization experiments as compared to the control experiment coincide with the observations for both the apparent permeability and 2D analysis made previously. Additionally, the larger void fraction reduction observed in CE3 compared to CE1 and CE2 demonstrates the utility of controlling the relationship between reaction and transport rates and also stimulating bacterial growth during the promotion of MICP to achieve more homogeneous mineral distribution.

Conclusions (Conclusions)

This study used X-ray µ-CT imaging to assess the treatment of cement defects with MICP to observe spatial and temporal changes. Pressure and flow relationships were used to estimate apparent permeability and fracture aperture in a cement core reactor with a well-defined channel defect before, during, and after MICP. Apparent permeabilities of all three biomineralized reactors decreased by more than 3 orders of magnitude following $CaCO_3$ precipitation, and the estimated fracture apertures in all three reactors decreased by more than 97% at the narrowest point. These similarities, however, disguised significant differences in the deposition of the $CaCO_3$ within the defect, highlighting important implications for the design of injection strategies for real-world applications of the technology to seal subsurface leakage pathways. This study shows that an increase in injection flow rate and more frequent stimulations of the bacterial community with nutrient solution can lead to a greater reduction in void fraction and a more homogenous MICP seal.

Further research should concentrate on the effects of defect size, attachment of microbes and biofilm growth on cement and steel surfaces, and refinement of injection strategies to promote MICP formation. MICP may not be an effective tool for all defects but changing the size and shape of defects in these systems could lead to an understanding of the defect sizes where MICP is an effective tool. Manipulation of the injection strategies will aid in understanding the best method for the delivery of fluids to promote biofilm attachment and growth, as an active biofilm could create optimal conditions for the MICP process to occur. Determination of the limitations of the MICP technology will provide those in the oilfield a valuable resource when selecting the treatment strategy that suits each unique system.

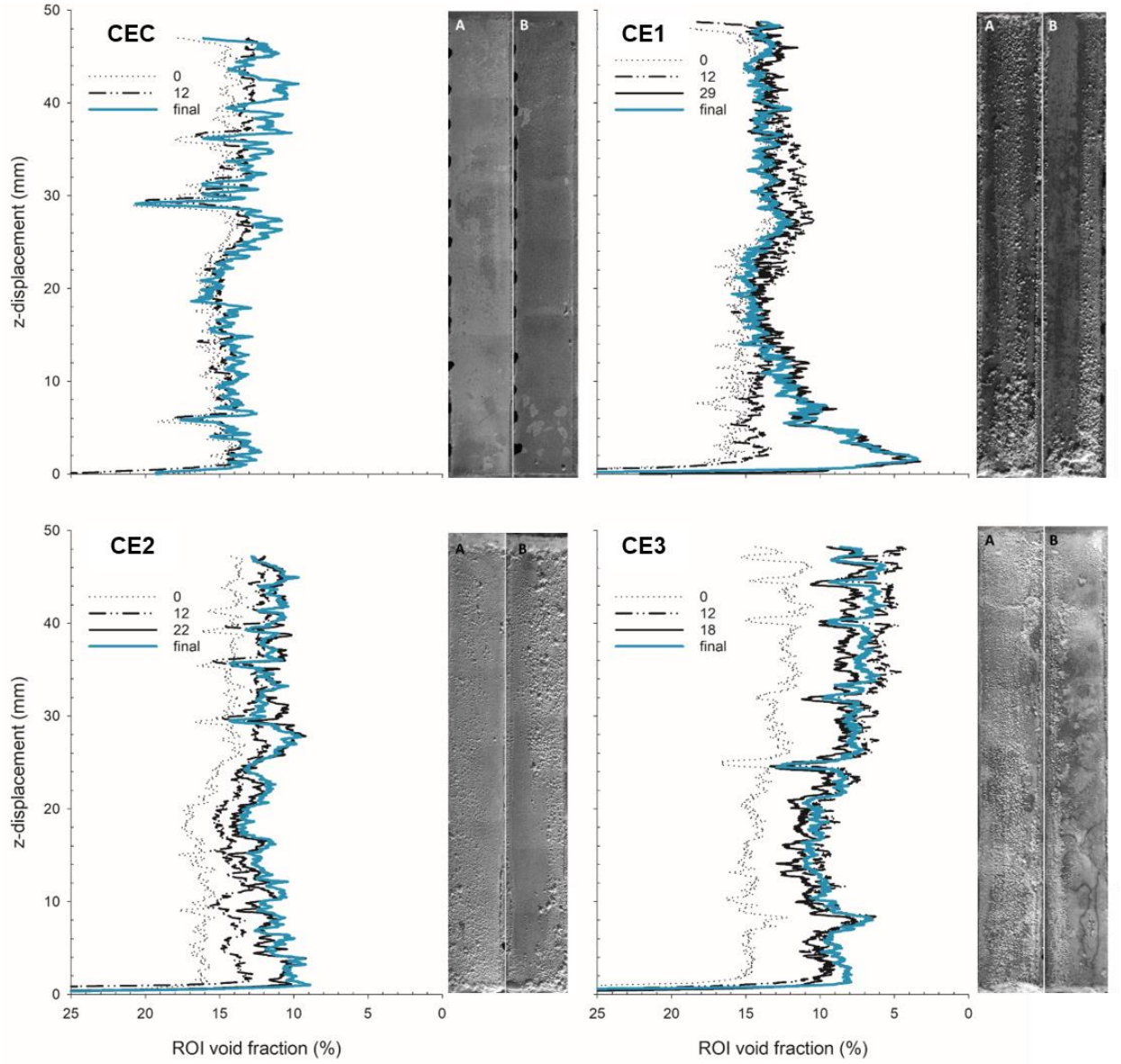

Figure 5. Void fraction and light microscopy imaging for CEC (top left), CE1 (top right), CE2 (bottom left) and CE3 (bottom right). Left panel: Void fraction of the ROI along the length of the defect was calculated after thresholding from the black (void) pixel space over the total pixel space. Void fraction distributions are shown in terms of number of calcium media pulses delivered: initial measurements (0), after 12 pulses of calcium media (12), and after the last calcium pulse delivered (number varies). The final measurement was collected during the last injection of the experiment (nutrient solution) prior to opening the reactor for light-microscopy. Right panel: Light-microscopy image of the defect taken during the post-experimental deconstruction stage. A and B each represent separate half-cylinders of the cement core.

Section 1.2 Biomineralization and wellbore integrity: a microscopic solution to subsurface fluid migration

Abstract (Abstract)

The keystone of subsurface fluid storage is the ability to inject and sequester fluids in underground reservoirs for extended periods of time. Concerns about leakage exist when storing fluids like CO_2 or natural gas in the subsurface given their potential to damage functional groundwater aquifers or to be emitted to the atmosphere. Microbially-induced calcite precipitation (MICP) is showing significant promise as an emerging technology for subsurface engineering applications including sealing defects in wellbore cement and modifying the permeability of rock formations. MICP uses low viscosity fluids and micro-organisms (~2 μm diameter) to induce calcium carbonate precipitation which can seal defects like micro-annuli, cracks, or channels. Calcium carbonate precipitation can be controlled to form seals capable of bridging small fluid migration pathways. In a laboratory study, MICP sealing of interface defects was visualized in a reactor designed to simulate a wellbore surrounded by a cement annulus. Apparent permeability decreased by over three orders of magnitude during an 8-day experimental period. The observations made during this experiment suggest that in a channel defect of variable dimensions encountered in a downhole system, MICP would likely first form at a constriction in the primary flow path before filling secondary flow paths. Building on laboratory experiments such as this, the authors conducted three successful MICP-based field demonstrations using the ureolytic bacterium, *Sporosarcina pasteurii*, to promote calcium carbonate precipitation in a variety of fracture and defect geometries.

Introduction

To securely store fluids in the subsurface methods are needed to ensure the fluids can be sequestered for extended periods of time. Concerns about leakage of stored CO_2, natural gas or other fluids exist given their potential to damage functional groundwater aquifers or to be emitted to the atmosphere[64-68]. Buoyancy and/or pressure gradients between the storage reservoir and the surface may create a driving force for fluid migration to the surface, thus requiring an effective seal to provide containment of subsurface fluids. The primary seal in the near wellbore environment is the cement in the annular space between the casing and the rock. Any defects in this cement surrounding the wellbore can undermine the integrity of subsurface storage systems[69-73]. When defects or leakage are detected, the common method to repair the problems involve the use of fine cement, resins, or other materials that can fill the defect and repair the leak[74-78]. These fluids may have high viscosity which can limit the aperture of defect they can effectively seal. While these current wellbore remediation technologies are effective for large defects, they can be inadequate in addressing smaller aperture defects that may persist. As described in Section 1.1 microbially-induced calcite precipitation (MICP) is showing strong promise as an emerging technology for subsurface engineering applications including sealing defects in wellbore cement and modifying the permeability of rock formations [42, 79-81].

Previously successful demonstrations have been performed to seal fractures and channeled cement in a field test well. However, there are few ways to visually observe the MICP formation in the field[40, 82] . To determine injection strategies and methods to control the placement of the

mineral seal, laboratory reactor systems were designed to mimic the near wellbore environment. The Wellbore Analog Reactor (WBR) was designed and constructed to investigate MICP sealing along the cement-casing interface (Figure 6). Studies were conducted to promote mineralization and to visualize and understand where the mineral seal formed in channelled cement.

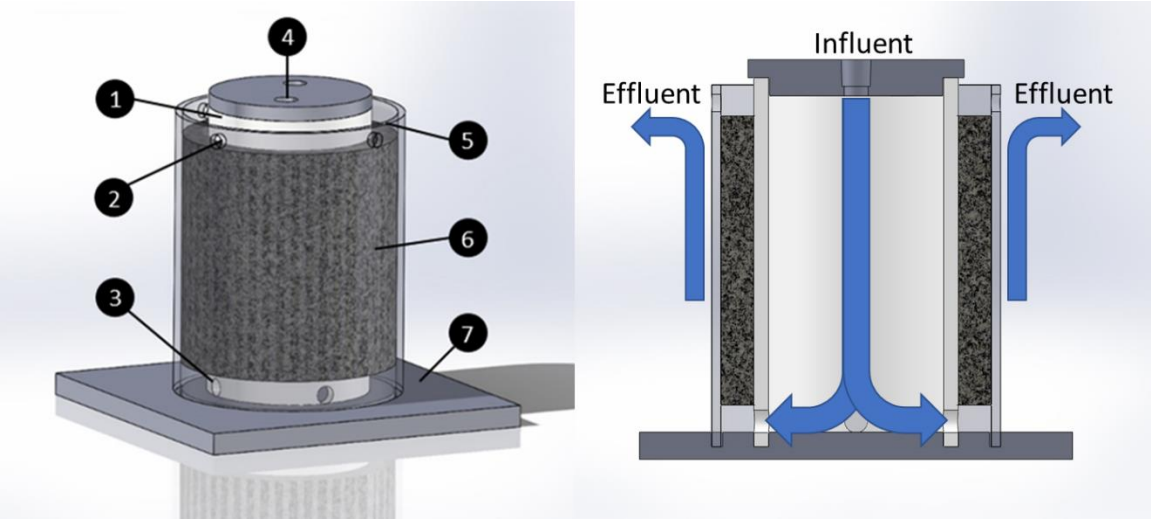

Figure 6. Left: Computerized drawing of the Wellbore Analog Reactor (WBR) created in SolidWorks: (1) inner casing; (2) effluent fluid ports; (3) casing perforations allowing fluids from the inner casing to reach the annulus space; (4) injection port; (5) clear polycarbonate outer casing for visualizing the mineral formation; (6) cement annulus with engineered defects, for example, channels cut into the cement; (7) base plate. Right: Cross sectional image of WBR indicating the flow path which fluids take through the reactor.

Materials and Methods (Experimental Methods)

Laboratory Wellbore Analog Reactor

The WBR consisted of an inner casing and a clear polycarbonate outer casing 12.7 cm high with an outer diameter of 10.2 cm. The annular space between the inner casing and polycarbonate exterior was filled with cement. Ports were constructed at the bottom of the inner casing to simulate wellbore perforations. The WBR was constructed to be approximately one-quarter scale compared to an actual well used for MICP field-testing.

The annular space cement (Schlumberger) was the same as had been used in the field at the Gorgas #1 well as described in Phillips et al. (2016). The cement was a blend of Class H cement and pozzolan additives with an additional 6% by weight D020 bentonite added (Jim Kirksey, personal communication). To prepare the cement slurry, water was added to the Class H cement to create a 0.4 water to cement ratio by mass (400 g water, 1000 g cement) mixture. The slurry was mixed in a blender for approximately one minute before pouring into the WBR for curing. Following a 14-day curing time, a Dremel cutting tool was used to create a channel defect in the cement at the cement-polycarbonate interface. The defect width tapered from 74 mm at the influent to 14 mm at the effluent.

Fluids were injected (Teledyne ISCO 1000D or Cole Palmer Model 270 syringe pump) through the inlet port fitting at the top of the inner casing. The fluids flowed down through the inner casing, out the perforations and up the interface between the outer casing and the cement. The fluid injection rate was set to achieve a 30-minute residence time within the reactor. This flowrate was maintained until the differential pressure increased, after which the flow rate was decreased to avoid over-pressurization of the reactor. Pressure measurements were taken using Omega Engineering Inc. PX309 series pressure transducers. Flow rate monitoring was performed continuously through the pump control operating software (LabVIEW, National Instruments). Flow rate and differential pressure measurements were collected for the final 60 seconds of each injection. This data was then used to calculate the apparent permeability and the aperture defect of the constructed defect using Darcy's law and Cubic's law for fracture flow as described in Section 1.1. The initial aperture was 800 µm.

The WBR experiments used three different solutions to promote MICP: (1) an inoculum which was the source of the ureolytic bacteria *Sporosarcina pasteurii*, (2) a nutrient solution to stimulate the growth of the bacteria, and (3) a source of calcium to induce the precipitation of calcium carbonate within the reactor. These solutions have been described previously in Section 1.1 and other studies[42, 83, 84]. Briefly, the reactor was inoculated with a microbial suspension after which a 4-hour stationary period (no flow) occurred to allow attachment of the microbes. Following the 4-hour stationary period, nutrient solution was injected to promote microbial growth followed by an overnight (no-flow) batch period. Then calcium solution was injected four times per day to promote mineralization. The reactor was re-inoculated with a microbial suspension at the end of the day and allowed to sit overnight prior to re-starting calcium injections the following day. A brine rinse preceded the first daily calcium solution injection to minimize instantaneous precipitation within the inner casing. Samples were collected from the effluent after each injection for analysis as described in Section 1.1.

At the end of the experiment, a section of the channel defect was cut from the reactor using a diamond blade Dremel cutting tool. The section selected was a large formation of biomineralization approximately 20 cm from the entrance region of the channel defect. The polycarbonate outer casing was then removed from the cement-polycarbonate interface, leaving behind the wellbore cement and MICP for imaging with the Zeiss Field Emissions Electron Microscope (MSU ICAL) and light microscopy images were taken using a Leica Model MDG41 stereomicroscope (CBE Imaging Facility).

Results and Discussion (Results and Discussion)

An 800 µm deep channel in the WBR was treated using MICP over eight days resulting in a three order of magnitude permeability reduction (Figure 7). The calculated final apparent permeability of the defect was 55 millidarcy (mD). The decrease in apparent permeability observed shows that over the course of the experiment it became more difficult for fluids to travel through the defect due to mineral precipitation. Cubic's law approximations for the final aperture size was 9 µm, correlating to a 98.9% reduction in aperture size.

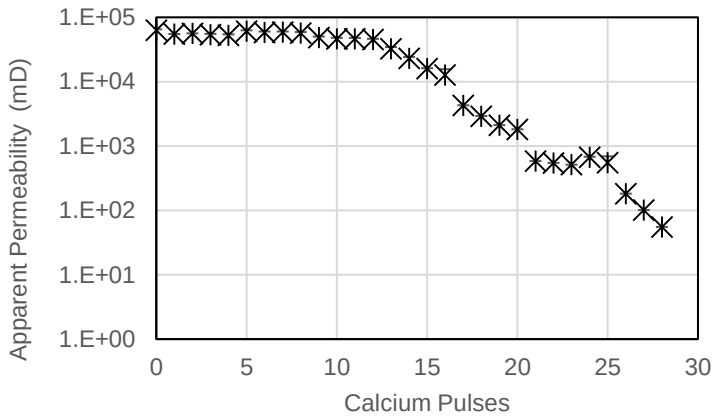

Figure 7. The apparent permeability of the channel defect in the WBR was reduced by three orders of magnitude following 28 calcium medium injections over a period of eight days.

Throughout the experiment, urea concentration was the metric used to quantify microbial activity within the reactor. The concentration of urea remaining inside the reactor after each batch period was determined and plotted as the ratio of effluent urea concentration to influent urea concentration as a function of the fluid pulse from which those fluids were injected (Figure 8). Influent concentrations were measured at the beginning of each day and effluent concentrations were measured at the beginning of each fluid pulse. Overall, the effluent to influent ratio was observed to increase throughout each day as the number of calcium pulses delivered increased. After nightly inoculation of the reactor, a decrease in the ratio was seen during the first pulse of the subsequent day. The decrease in this ratio indicated that more urea hydrolysis occurred post inoculation. Factors such as cell washout [85], reaction product inhibition[86, 87], or entombment[88] could be contributors to the loss of urea hydrolysis over the course of the day. None of these potential factors were specifically investigated by the experiment, therefore conclusions in regards to these parameters cannot be made.

Regardless of the mechanism for the inhibition of ureolysis an overall conclusion can be made that there exists an inverse relationship between urea hydrolysis (activity) and an increasing number of calcium pulses delivered without resuscitation of the microbial community. A reduction in urea hydrolysis would lead to less dissolved inorganic carbon being produced, potentially leading to less mineral precipitation in the defect. Proper spacing of microbial inoculations or resuscitation pulses could minimize the loss of ureolytic activity, maintaining the rate of MICP formation, and reduce the time needed to seal subsurface leakage pathways.

Formation of significant mineral deposits was observed over time in the channel (Figure 8). The observations made during this experiment suggest that in a channel defect of variable dimensions encountered in a downhole system, MICP would likely first form at a constriction in the primary flow path. In this experiment, the precipitates accumulated such that fluids eventually migrated to secondary flow paths, suggesting the bio-cement barrier would eventually form in the smaller secondary defects in addition to the primary flow paths.

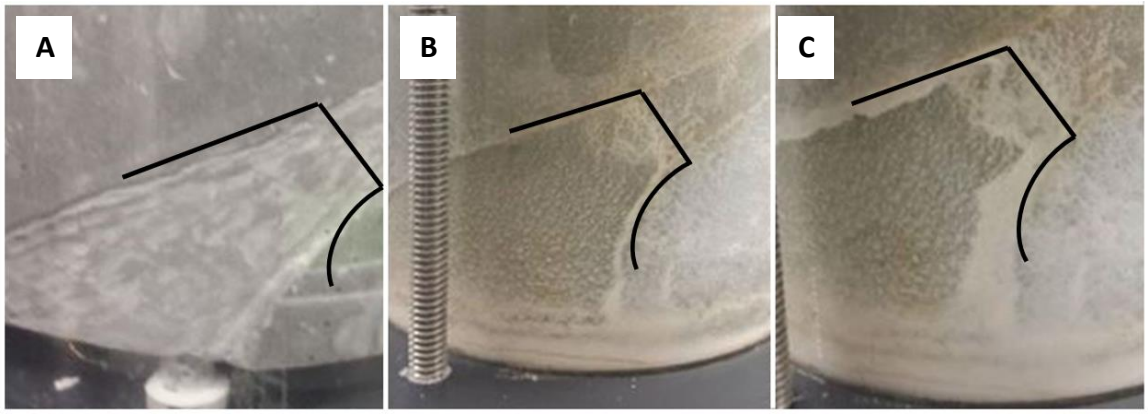

Figure 8. Calcium carbonate formation as a result of MICP treatment. A - C: Calcium carbonate formation over time in channel defect constriction point in the WBR. Lines indicate the edges of the channel.

Light microscopy and Field Emission Scanning Electron Microscopy (FE-SEM) was used to produce high resolution images of this formation, which was hypothesized to have created the flow restriction (Figure 9).

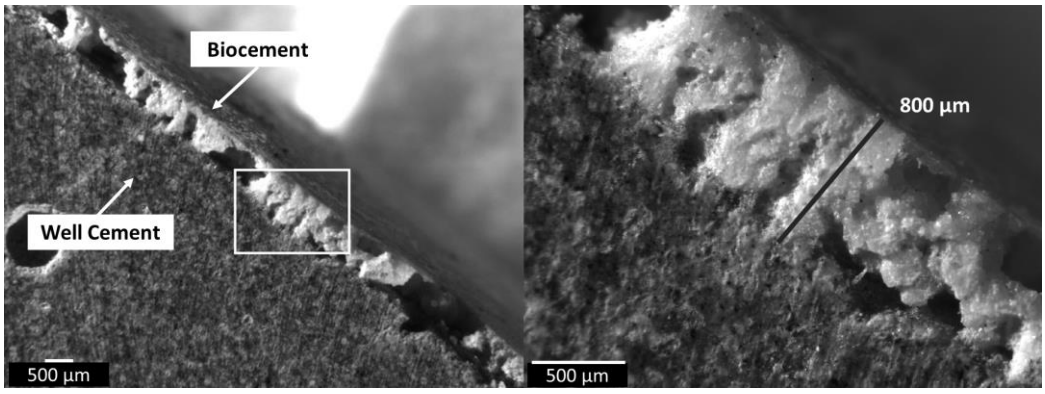

Figure 9. Light microscopy of WBR biocement. Left: Image taken of an approximately 800 µm thick layer of biocement bonded to the well cement at 7.81x magnification. Right: Framed portion of the left image viewed at 28.3x magnification showing the bond between the mineral formation and the cement.

From Figure 9, the layer of biocement was approximated to be 800 microns in thickness. When examined closely, the biocement and wellbore cement appeared to be bonded together. Initial attempts to image the interface between the biocement and wellbore cement showed little sign of microorganisms, hypothesized to be a result of entombment during the experiment. A brief acid wash however produced an image where rod shaped cells consistent with the dimensions of *S. pasteurii* were observed. In Figure 10, a biofilm (false colored green) can be seen on the biocement side of the interface of the biocement and wellbore cement. Observing cells inside the calcium carbonate layers provided evidence that cells are associated with precipitation of calcium carbonate and therefore may have an influence on where precipitation occurs. Stocks-Fischer (1999) observed *S. pasteurii (Bacillus pasteurii)* acting as nucleation sites for the

precipitation of calcite crystals. The hypothesis of cells acting as nucleation sites in the case of the WBR cannot be proved or disproved however, as specific analysis of this phenomena was not performed.

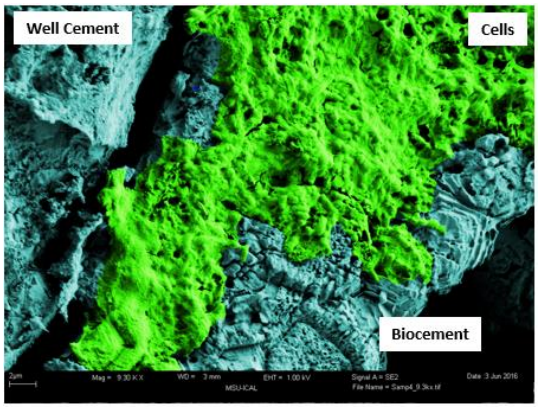

Figure 10. Bacilli (rod) shaped bacteria (false colored green) assumed to be Sporosarcina pasteurii observed in close proximity to the cement-biocement interface of the MICP seal. The cement appears on the left-hand side of the image while the calcium carbonate makes up the right-hand side of the interface.

Conclusions (Conclusions)

Development of methods on the laboratory scale has the aided the design of injection strategies for field application. It was shown that the laboratory wellbore analog reactor systems can be used to visualize and quantify the production of biomineralization in 800 μm engineered gaps in wellbore cement. Understanding the results of field experiments has challenges, such that laboratory experimentation combined with numerical model simulations help to determine the success of the field studies[53, 83, 89, 90]. The University of Stuttgart modelled the field experimental conditions and a recent manuscript highlighted the results of the model to field correlations[91].

Section 1.3 Assessment of ureolysis induced mineral precipitation material properties compared to oil and gas well cements

Abstract (Abstract)

Novel methods are needed to prevent or mitigate subsurface fluid leakage, for example stored carbon dioxide, fuels during unconventional oil and gas resource development or nuclear waste disposal. Ureolysis-induced calcium carbonate precipitation (UICP) has been investigated as a method to plug leakage pathways in the near-wellbore environment and in fractures. The enzyme urease catalyzes the hydrolysis of urea to react with calcium to form solid calcium carbonate (similar to limestone). UICP test specimens were prepared in triplicate by filling 2.5 cm (diameter) x 5 cm (length) and 5 cm x 10 cm cylindrical molds with sand and injecting both microbial and plant-based enzymes with urea and calcium solutions to promote precipitation. Sources of urease included jack bean enzyme and the microbe *Sporosarcina pasteurii*, resulting in both enzyme- and microbe-induced calcite precipitation (EICP, MICP) specimens. For comparison, Class H well- and Type I-Portland specimens were made by mixing cement paste (API 10B) with sand (ASTM C305). Fine cement specimens were also included in the comparison and were made both by mixing and injecting into the sand-filled molds to match the process used to make the biocement specimens. For the 2.5 cm x 5 cm specimens, the addition of nutrient broth to the enzyme specimens (ENICP) resulted in increased compression strengths compared to specimens without nutrient (EICP). The average compression strengths of these ENICP specimens reached 77% and 66% of the compressive strength of the 28-day well cement and Type I cement mortars, respectively and were over two times larger than the 28-day strength of the fine cement specimens. For 5 cm x 10 cm specimens, compression strengths of MICP, ENICP, and EICP specimens reached 42%, 38%, and 16% of the 28-day injected fine cement specimens. The average modulus of elasticity of ENICP was 17,316 ± 1,430 MPa with 8.3 ± 1.8% $CaCO_3$ content (g/g sand) and was approximately 30% larger than the average modulus measured for the fine cement specimens. The results of this study indicate that the UICP produced specimens may have adequate strength and stiffness for field applications.

Introduction

Construction consumes a large amount of non-renewable resources, which has an adverse impact on the environment. Portland cement is one of the most commonly used materials in civil infrastructure, even though its production releases a significant amount of CO_2, accounting for approximately 5 to 7% of greenhouse gas emissions in the world[92]. Production of cement in 2017 increased to 86.3 million metric tons in the United States and 4100 million metric tons in the world[93]. Constructing with sustainable materials must be considered in order to reduce the associated impacts on the environment. To reduce environmental impacts, more sustainable approaches are necessary.

As described in Section 1.1 ureolysis induced calcium carbonate precipitation (UICP) is an alternative cementation method where microbial or plant-based enzymes produce calcium carbonate ($CaCO_3$) to bond particles together. Microbial urease sources have been used extensively for various engineering applications as described in Section 1.1. A second source of urease that also precipitates calcium carbonate through enzyme induced calcite precipitation

(EICP) is the urease enzyme in a plant, for example from the jack bean. This plant source differs from *S. pasteurii* in that a period of microbial growth is not required prior to injection into the sand columns.

One proposed method to remediate cracks or fractures in concrete is to fill the cracks with a solution of urea and calcium with microbes that precipitate calcium carbonate after being deposited in the cracks. According to results from Tittelboom et al. (2010) MICP is an option as a biological technique for concrete repair[94]. In their study, ureolytic bacteria, *B. sphaericus*, were shown to precipitate $CaCO_3$ which can fill the cracks in concrete. Rectangular concrete samples cast using Type I Portland cement were split until cracks between 0.05 mm and 0.87 mm formed. These cracks were then repaired by injecting the microbes immobilized in silica gel. The research concluded that some form of enhanced crack repair might be obtained through a biological treatment in which a *B. sphaericus* culture is incorporated in a gel matrix and a calcium source is provided[94]. Studies have also been conducted where UICP have been used as a substitute to cement or concrete products, or mixing directly with cement materials have showed an increase in compressive strength within these specimens[95-98]. Also, data collected in the field is limited to pressure and flow measurements which can be used with observations from subsurface logging tools to estimate the wellbore integrity after treatment. Thus, it is difficult to assess material properties of the seals formed down-hole. These unknowns drive the question of how these UICP bonds develop strength, and whether they can be used as an alternate product to cement-based materials in field applications.

In this study, to investigate the bio-composite materials strength and stiffness characteristics, 2.5 cm diameter x 5 cm length and 5 cm diameter x 10 cm length sand columns were injected with *S. pasteurii* (MICP) and jack bean (EICP) solutions. Compression strengths and moduli of elasticity were measured and compared with Class H well-, fine-, and Type I-Portland cement specimens, mixed according to both the American Petroleum Institute[99] and ASTM Standards[100, 101]. The influence of nutrient broth, synthetic fibers, and a combination of jack bean and *S. pasteurii* were also investigated to identify their effect on material properties. The specific objectives were to: 1) determine the strength and stiffness characteristics of UICP specimens made from *S. pasteurii* and jack bean enzyme, 2) evaluate the influence of nutrient broth, synthetic fibers, and combined microbe and enzyme specimens on material properties, 3) compare the bio-composite specimen material properties to oil and gas well cement specimens, and 4) identify calcite precipitation formations through scanning electron microscope and stereoscope analyses.

Materials

Sand Columns

The sand used for the 2.5 cm (diameter) x 5 cm (length) and 5 cm x 10 cm cylindrical specimens was 2095 Granusil silica sand with effective filtration size of 1 mm. This course particle size was chosen for easy injection of water-cement mortars, with enough surface area for adequate attachment zones for microbe and enzyme. The columns were made from PVC material and fitted with screens, caps, and fittings for the solution injections.

Microbe and Enzyme Suspensions

MICP promoting cultures were grown by aliquoting 1000 µL of *Sporosarcina pasteurii* (ATCC 11859) from a thawed frozen stock to 100 mL of autoclaved brain heart infusion broth (BHI, Becton Dickinson) amended with 2% urea (20 g/L urea, Fisher Scientific). The cultures were incubated overnight at 30°C on a 150 rpm shaker. After incubation, 100 mL of this culture were added to 300 mL of growth promoting media. EICP promoting solutions were prepared by adding 5 g/L of jack bean meal (JBM) (Sigma Aldrich, St. Louis, MO) to distilled water prior to mixing overnight on a magnetic stir plate at room temperature.

Biocement Promoting Solutions

After injection of the microbial or JBM suspensions into the sand columns, different fluids were used to provide the substrates necessary for microbial growth, ureolysis, and subsequent calcium carbonate precipitation. These water based-biocementation fluids included 20 g/L urea (Fisher Scientific), 49 g/L $CaCl_2$-$2H_2O$ (Fisher Scientific), 10 g/L NH_4Cl (Sigma Aldrich), and 3 g/L nutrient broth (Beckton Dickinson). The urea-Ca^{2+} molar ratio was set to 1:1 at 0.333M. The growth solution described in Ebigbo et al.[83] was used to resuscitate or re-grow *S. pasteurii* and promote increased ureolytic activity, whereas the calcium containing solution was used to promote ureolysis induced calcium carbonate precipitation. The growth promoting solutions did not contain calcium.

Nutrient broth was provided to the MICP specimens to provide a carbon source for the microbes. In the initial 2.5 cm x 5 cm specimens, nutrient broth was added to the solution that was used to promote EICP even though not necessary. When scaled up to 5 cm x 10 cm specimens, nutrient broth was either added or left out of the ECIP promoting solutions to evaluate the impact of organics on the material properties.

Cement

Class H well cement and fine cement samples were procured from collaborators at Schlumberger. The Class H cement was proprietary blended well cement with 6 % bentonite and additives. Fine cement (SqueezeCRETE), and Type I Portland cement were used to prepare mortar specimens to compare with the UICP specimens. A 0.63 water-to-cement ratio was used for the fine cement and 0.38 water-to-cement ratio was used for well cement specimens.

Fibers

FORTA Super-Sweep Fine fiber was used for the ENFICP specimens. It is a homopolymer polypropylene fiber. The length of the fibers used in this study was 3.175 mm. The results from Li et al. showed that the optimum fiber content in the MICP-treated sand was 0.2–0.3% and a 0.2% fiber content was selected.

UICP Specimens

Five types of UICP specimens were produced using the plant-based enzyme (jack bean meal) and/or the microbial enzyme (*S. pasteurii).* The following specimens were prepared:

- EICP: Enzyme induced calcite precipitation produced without a nutrient broth.
- ENICP: Enzyme with nutrient broth induced calcite precipitation.

- ENFICP: Enzyme with nutrient broth and fibers induced calcite precipitation
- MEICP: Microbially and enzyme induced calcite precipitation
- MICP: Microbially induced calcite precipitation

The plant-based enzyme source was from jack bean meal (JBM) without nutrient broth and will be referred to as EICP (enzyme induced calcite precipitation), JBM with nutrient broth will be referred as ENICP (enzyme with nutrient broth induced calcite precipitation), JBM with nutrient broth and fibers will be referred as ENFICP (enzyme with nutrient broth and fibers induced calcite precipitation), the mixture of JBM and *Sporosarcina pasteurii* will be referred to as MEICP (microbially and enzyme induced calcite precipitation). The microbial enzyme source was *Sporosarcina pasteurii* and will be referred to as MICP (microbially induced calcite precipitation) hereafter.

A total of 107 specimens were made to determine the strength and stiffness characteristics of the cement and biocement. Early tests were performed on 2.5 cm x 5 cm specimens because of the smaller volumes of solutions and more efficient injection process. These specimens were used to perform a preliminary characterization of the biocement. To meet specimen size requirements for compression strength and elastic modulus tests according to ASTM C39[100] and ASTM C469[102], 5 cm x 10 cm cylinders were later used to continue the strength and stiffness characterization. Fine cement specimens were made both by mixing according to API 10B[99] and ASTM C305 [103] and also injected to match the process used to make the biocement specimens.

Methods (Experimental Methods)

Flow-through Reactor Systems for Biocement and Fine Cement Specimens

Flow-through reactors were constructed using both 2.5 cm x 5 cm and 5 cm x 10 cm PVC pipe to produce cylindrical biocemented sand specimens, which can be seen in Figure 11 and Figure 12. These reactors were filled with the sand and water-based biocementation solutions were injected using syringe pumps (KD Scientific) set to 6 ml/min. For 5 cm x 10 cm specimens, inoculation of the MICP specimens was conducted by injecting 120 ml of *S. pasteurii* culture. The inoculum was allowed an overnight attachment period to enable microbial attachment to the sand. A total of 120 ml of JBM suspension (5g/L) was also injected into 5 cm x 10 cm cylindrical specimens to promote EICP, ENICP and ENFICP. For MEICP specimens, 5 g/L JBM suspension was mixed with the overnight *S. pasteurii* culture and injected and also allowed to incubate overnight without flow. The injection strategy was modified three days into the MEICP experiment when *S. pasteurii* was injected at night and allowed to attach prior to injecting the JBM suspension in the morning. The total process of four to six injections were made and between twenty four to twenty six samples were taken each day for the colorimetric Jung assay to determine the urea concentration in samples of the fluids extracted after each batch period. The experiments were conducted over a period of 7 to 13 days. The number of days varied because the experiments were terminated when the overall mass of urea hydrolyzed was approximately the same for each of the specimen types.

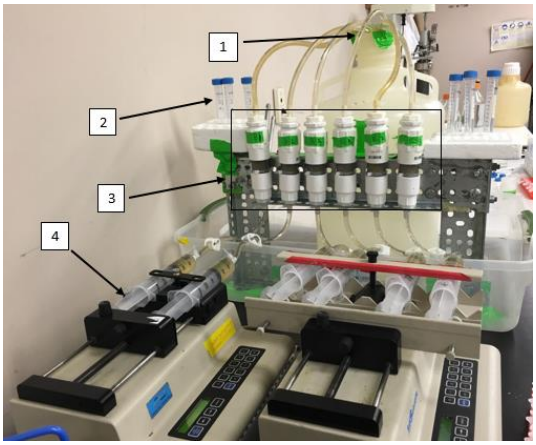

Figure 11. 2.5 cm diameter x 5 cm long specimen flow-through reactor system for MICP & EICP. Cylindrical flow-through reactors with (1) waste/outlet and sampling port (2) sampling collection tubes (3) specimens (4) syringe pump and 60 ml syringes.

Figure 12. Specimen flow-through reactor system for 5 cm x 10 cm MICP, EICP, ENICP, ENFICP and MEICP specimens.

For fine cement specimens, the same procedure was followed using 5 cm x 10 cm cylindrical specimens (Figure 13) where fine cement mortar with water-to-cement ratio of 0.63 was injected with syringes.

Figure 13. 5 cm x 10 cm fine cement injection system

Injections and Fluid Sampling

The experiments used pulsed injection strategies where fluids were injected to either promote precipitation or microbial growth, followed by reactive batch periods when the flow was stopped. Daily, between three and five injections of the calcium precipitation promoting solution (CMM+ solution) were performed for the MICP, EICP, ENICP, ENFICP and MEICP specimens. Each pulse permitted a no-flow period of one to two hours between injections. Samples were collected and analyzed using methods described in Section 1.1.

For MICP specimens, resuscitation or re-inoculation of microbes was conducted by injecting a growth promoting solution. JBM suspensions were also injected once per day prior to more calcium injections for both 2.5 cm x 5 cm and 5 cm x 10 cm biocement specimens. These re-injections were performed to promote increased ureolytic activity of the microbe and enzyme specimens after calcium precipitation, which has been observed to decrease activity after multiple calcium pulses over time[104]. These injection strategies and sampling methods were repeated daily until the total amount of urea hydrolyzed was approximately the same between the biocement specimens. It was observed that the EICP specimens more efficiently hydrolyzed the urea; therefore more calcium pulses were required in the MICP samples to reach an equivalent mass of urea hydrolyzed.

After the injections were terminated, the reactors were drained and the PVC molds were cut longitudinally to remove the cemented sand specimens. The biocement specimens were placed in an 80°C oven for 24 hours to deactivate any remaining active enzyme or microbe prior to compression strength testing. The influence of drying on the compression strength was not investigated. The compressive strength testing was performed as described in the strength testing section. After strength testing, digestion of the calcium carbonate from the biocement specimens was performed to determine mass of calcium carbonate achieved per mass of sand. Samples were crushed, mixed and then divided into triplicate 15 ml centrifuge tubes. Trace-metal-grade nitric acid (10%, Fisher Scientific) was added to dissolve the calcium carbonate. After 24 hours the liquid was removed, and the sand was placed in a 60°C oven to dry. The difference between the dried mass of sand before and after digestion and ICP-MS were used to estimate the total amount of $CaCO_3$ per mass of sand. A portion of the biocement samples were collected for microscopy. Image analysis was performed on the Leica M205FA stereoscope located at the Center for Biofilm Engineering Microscopy User Facility and the Zeiss Field Emission (FEM) scanning electron microscope in the Image and Chemical Analysis Laboratory at Montana State University. The specimens were coated with iridium prior to FEM scanning.

Cement Mortars

For comparison with the cylindrical biocement specimens, 2.5 cm x 5 cm and 5 cm x 10 cm cylinder specimens were made from the three cements using a water-to-cement ratio of 0.63 for the fine cement specimens and 0.38 for the well cement specimens. Sand quantities were calculated based on the recommended mortar proportions given in ASTM C109 for 5 cm x 5 cm x 5 cm cube specimens, which were re-calculated for the 2.5 cm x 5 cm and 5 cm x 10 cm well- and Type I- cylinder specimens tested in this study. API Specification 10B was used for mixing the water and well cements, followed by ASTM C305 for combining the slurry with the sand to create the mortar. ASTM C305 was also used to prepare the Type I cement mortar. After

molding, the test specimens were placed in a moist room with relative humidity of not less than 95% with a temperature range of 23.0 ± 2.0 °C. The cement specimens were stored in the curing room until tested.

Strength Testing

Compression testing was performed on the biocement and cement specimens with a 1000 kN MTS Static-Hydraulic Universal Test Frame using a load rate of 0.21 MPa/s (30 psi/s) in accordance with ASTM C39. Prior to testing, the ends of the 2.5 cm x 5 cm specimens were sanded, to create flat bearing surfaces. The 5 cm x 10 cm biocement specimens were also sanded and a grinding machine was used for the cement specimens to obtain a flat bearing surface. For the cement specimens, 7-, 14-, and 28-day compression strengths were measured. Because the biocement specimens were deactivated in the oven, an evaluation of strength vs. age was not made. Steel caps with neoprene pads were placed on top and bottom of the specimens for applying the load in accordance to ASTM C39.

Modulus of Elasticity

The modulus of elasticity was measured by installing strain gages on the test specimens according to Micro-Measurements Application Note TT-611[105] and then testing them tested per ASTM C469. Loads were applied with the same MTS Static-Hydraulic Universal Test Frame used for compression testing at a load rate of 1 mm/min.

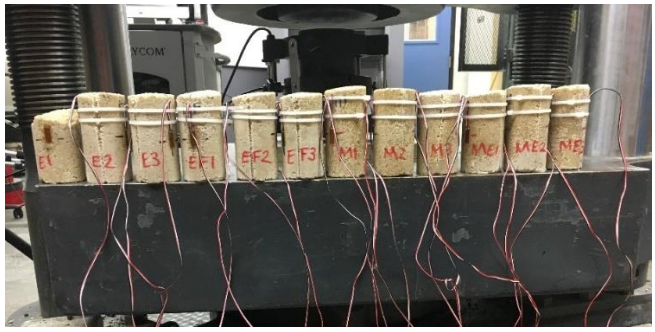

Figure 14. Installed strain gages on 5 cm x 10 cm biocement specimens

Statistical Analysis

One-way ANOVA tests were used to perform a statistical analysis for measured $CaCO_3$ content, strength and modulus of elasticity. Biocement specimens were compared to each other for the $CaCO_3$ content, and cement and biocement specimens were compared to each other for the strength and modulus of elasticity. If the Shapiro-Wilks test[106] for normality passed, t-tests were used for pairwise comparisons. If the normality test failed, Dunn's method [107] on ranks was substituted. It is noted that the small sample sizes (2, 3 or 4 replicates per treatment) and the inherent variability of some of the tests (modulus of elasticity, for example) result in situations where visual differences observed in box plots between means (or medians) are not corroborated by ANOVA analyses.

Results and Discussion (Results and Discussion)

Urea Hydrolysis

Due to the differences of ureolytic activity between the biocement specimens, the number of pulses distributed to each cylinder was based on the urea hydrolysis determined by the Jung Assay. This means for certain specimens' additional pulses were required to equalize the total urea hydrolyzed within biocement specimens.

The total concentration of urea hydrolyzed and treatment days during each calcium pulse between the MICP, EICP, ENICP, ENFICP, and MEICP specimens are shown in Table 3. The first attempt at making MICP (1st try) specimens resulted in higher total urea hydrolyzing due to the extra injections. This is why a second set of MICP specimens (2nd try) were developed and tested. During the second injection process, the system became clogged and specimens were terminated before the total mass of urea hydrolyzed was the same.

On average, it was measured that the ENICP specimens converted 11.7 ±1.4 g/L per pulse and the MICP specimens converted 9.0 ± 1.0 g/L of urea per calcium pulse for 2.5 cm x 5 cm specimens. EICP, MICP-1 (1st try), MICP-2 (2nd try), MEICP, ENICP and ENFICP specimens converted 12.7 ± 3.4 g/L, 9.9 ± 3.6 g/L 9.5 ± 2.5 g/L, 2.9 ± 4.5 g/L, 9.8 ± 4.8 and 9.6 ± 4.9 g/L per pulse, respectively for 5 cm x 10 cm specimens.

Table 3. Urea hydrolyzed during calcium pulses cylindrical testing.

Reactor	Biocement	Total Urea Hydrolyzed (g/L)	# of Calcium Pulses	# of days for treatment
2.5 cm x 5 cm	ENICP	340 ± 1.5	29	11
	MICP	361 ± 1.1	40	16
	EICP	340 ± 3.4	27	7
	MICP-1(1st try)	367 ± 3.6	40	9
5 cm x 10 cm	MICP-2 (2nd try)	332 ± 2.5	35	7
	MEICP	84* ± 4.5	29	7
	ENICP	341 ± 4.8	35	7
	ENIFICP	337 ± 4.9	35	7

* The urea hydrolysis results for the MEICP specimens do not seem to reflect the calcium precipitation actually achieved or the result that the strength of the MEICP specimen was equivalent to the MICP specimens. One possibility was there could be interferences in the Jung assay with the combination of JBM and microbes that was not observed with the urease enzymes sources on their own.

It was decided to increase the number of calcium pulses in the microbial specimens until the overall concentration of urea converted was approximately equal to the enzyme specimens as described in section injection and fluid sampling section (approximately 340 g/L).

Compression Strengths

Compression strengths of Type I, well cement and fine cement cylindrical specimens were measured at 7-, 14- and 28-day according to ASTM Standard C39. Peak stresses were calculated by dividing the peak measured load by the cross-sectional area of the specimen to obtain the compressive strength (Eq. 2).

$$\sigma = P/A \qquad \text{(Eq. 2)}$$

Where: σ = compressive strength in MPa or [psi], P = total maximum load N or [kip] and, A= area of loaded surface mm^2 or [in^2].

2.5 cm x 5 cm specimens

Compression strengths of the cement samples at 7, 14, and 28 days are shown in Table 4 and Figure 15. The ENICP specimens that received 29 calcium pulses over the course of 11 days exhibited 77% and 66% of the compressive strengths of the 28-day well-cement and Type I cement. The strength of the 28-day fine cement specimens reached 58% of the ENICP specimens. MICP specimens that received 40 calcium pulses over the course of 16 days were 32%, 28% and 72% of the 28-day strengths of the well-cement, Type I cement and fine cement mortars, respectively. Strengths at 28-days were lower than 14-day strengths for cement specimens. The decreased 28-day compression strengths compared with those measured after 14 days was not expected for the cement specimens. These reduced strengths could be the result of increased variability for the smaller specimen size and/or the unavailability of ASTM loading caps and neoprene pads for 2.5 cm x 5 cm cylindrical specimens.

Table 4. Compression strengths of three types of 2.5 cm x 5 cm cement and two types of 2.5 cm x 5 cm biocement

	Average Compression Strength (MPa)		
Cement	Day 7	Day 14	Day 28
Well Cement	11.0 ± 1.1	26.0 ± 2.7	21.1 ± 4.1
Type I	21.4 ± 5.0	26.8 ± 2.7	24.0 ± 5.8
Fine Cement	12.2 ± 2.6	19.6 ± 2.5	9.5 ± 3.1
MICP	6.8 ± 2.3		
ENICP	16.3 ± 2.4		

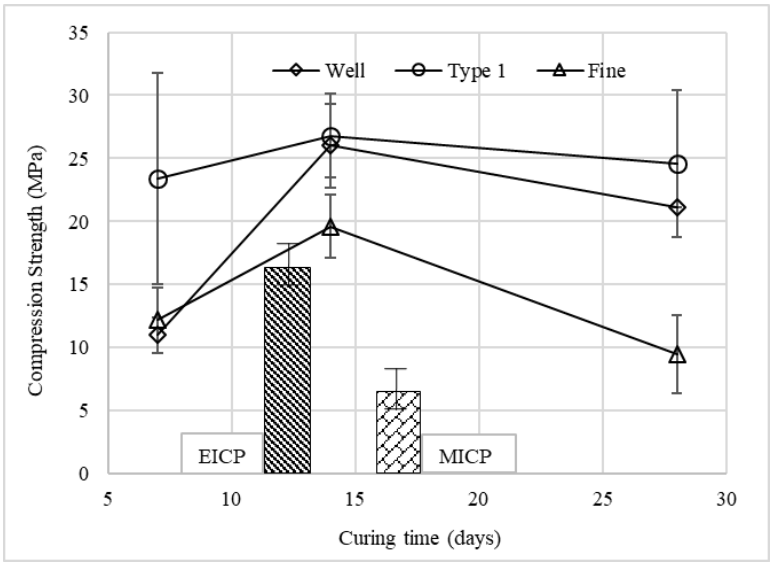

Figure 15. Average compression strength vs. age (days) of three types of cement. The ENICP and MICP specimens strengths shown were tested after the termination of injection after 11 and 16 days, respectively.

Representative fracture patterns of the 2.5 cm x 5 cm cement and biocement specimens can be seen in Figure 16. The three cement specimens failed with columnar vertical cracking through both ends, which is characteristic of a tensile splitting failure caused by the Poisson effect. The failure of the ENICP specimen was similar and included a single columnar vertical crack down the center with some bond separation between the calcium carbonate and sand particles. The MICP specimen did not develop compressive stresses large enough to cause splitting failure; the bonded sand particles crumbled as the force was applied.

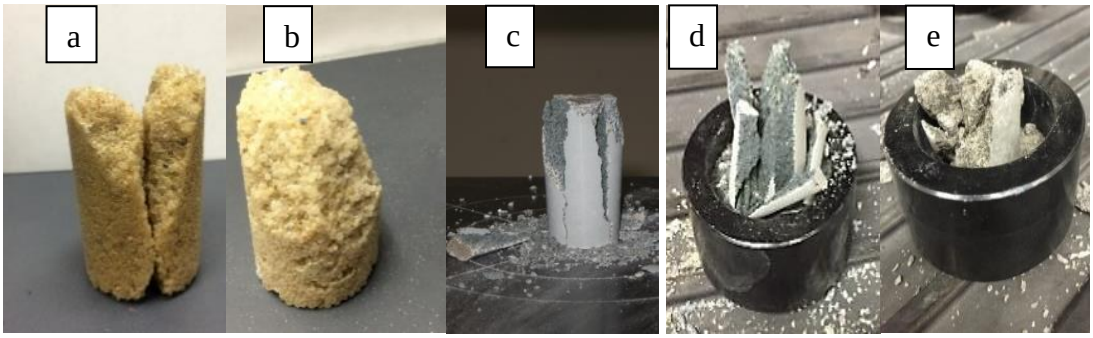

Figure 16. Fracture patterns for 2.5 cm x 5 cm specimens. (a) ENICP, (b) MICP, (c) fine, (d) well and (d) Type I cement

The biocement produced from the MICP had weak spots near the inlet of the flow-through reactor system which became failure planes when the specimens were removed from the molds. This observation contrasted previous experiments in the laboratory (data not shown since compression strength testing was not performed on those specimens) in which microbe

specimens were more strongly bonded and enzyme specimens crumbled during the removal from the PVC molds and further handling.

One reason for the enzyme specimens exhibiting greater compressive strength than the microbe specimens could be the addition of the nutrient broth (Beckton Dickinson) into the media that was used for both microbe and enzyme samples. In the previous work, the nutrient broth was not added to the enzyme promoting solutions. A hypothesis is that the proteins, carbohydrates, and other organics present in the biofilm in MICP might alter the material properties of the bio-cement. A similar hypothesis might be made with the presence of the proteins, carbohydrates and organics present in the nutrient broth. The 5 cm x 10 cm specimens experiment was performed to explore the role of additives to the bio-cements in altering material properties.

5 cm x 10 cm specimens

Comparison of well cement, Type I cement and fine cement (mixed according to ASTM) strengths at 7, 14, and 28 days are shown in Table 5 and Figure 17. Fine cement strength at 28 day exhibited 51% and 47% of the 28 day well cement and Type I cement specimens.

Table 5. Comparison of well cement, Type I cement and fine cement

	Average Compression Strength (MPa)		
Cement	Day 7	Day 14	Day 28
Well Cement	13.48 ± 0.8	22.03± 5.2	36.2 ± 1.0
Type I	26.02 ± 3.5	30.17 ± 5.3	39.3 ± 0.8
Fine Cement (ASTM)	10.8 ± 0.2	16.76 ± 0.5	18.34 ± 0.3

MICP-1, MEICP, MICP-2, ENICP, ENFICP and EICP specimens reached 77%, 46%, 42%, 38%, 19% and 16% of fine cement (injected) specimens. The ENFICP specimens had smaller compression strengths than specimens without fibers which is unlike results of similar study by Li et al. [108]. Unlike the 2.5 x 5 cm specimens, the average compression strength of ENICP cylinders was not larger than MICP.

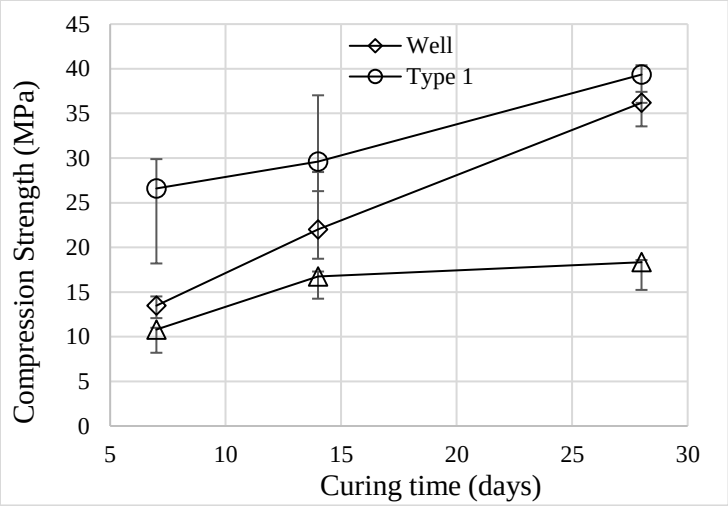

Figure 17. Average compression strength vs. age (days)

Compression strengths of fine cement (injected) and biocement specimens are shown in Table 6 and Figure 18. Only fine cement (injected) was compared with biocement specimens because Type I and well cement are commonly used as materials to construct wells but not sealing leakage pathways which was the objective of the development of the biocementing materials.

Table 6. Compression strengths of fine cement (injected) specimens at 28 day and biocement specimens

Cement	Average Compression Strength
Fine Cement	16.64 ± 2.85
MICP-1	12.73 ± 1.59
MEICP	7.64 ± 2.22
MICP-2	6.98 ± 3.97
ENICP	6.36 ± 3.00
ENFICP	3.17 ± 0.56
EICP	2.73 ± 0.78

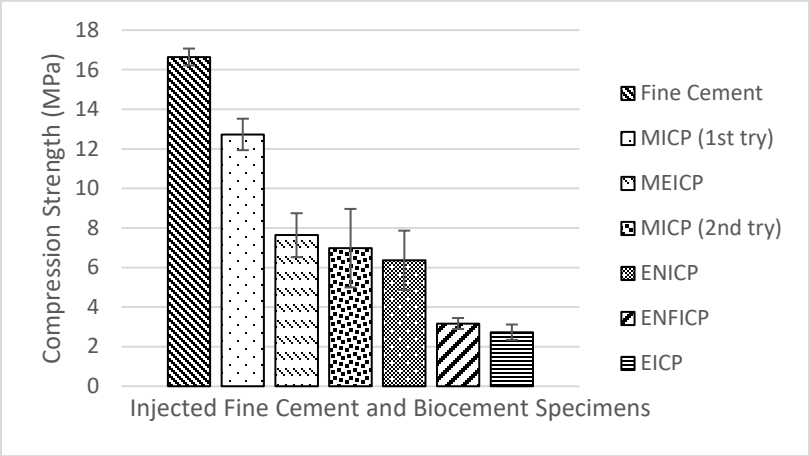

Figure 18. Average compression strength of fine cement (injected) and biocement specimens.

When the medians or means are ranked, there is a notable progression in strength by treatment condition that appears substantial for cement and biocement strengths. However, when subjected to statistical tests, certain samples did not perform significantly different than others. Figure 19 shows which treatments were not significantly different than others ($\alpha = 0.05$). Any group of treatments having the same letter above the box plot were not significantly different. Groups of treatments not sharing the same letter were significantly different. For example, MICP-1 specimens are not significantly different than fine cement specimens. However, enzyme induced specimens are significantly different than fine cement and MICP specimens.

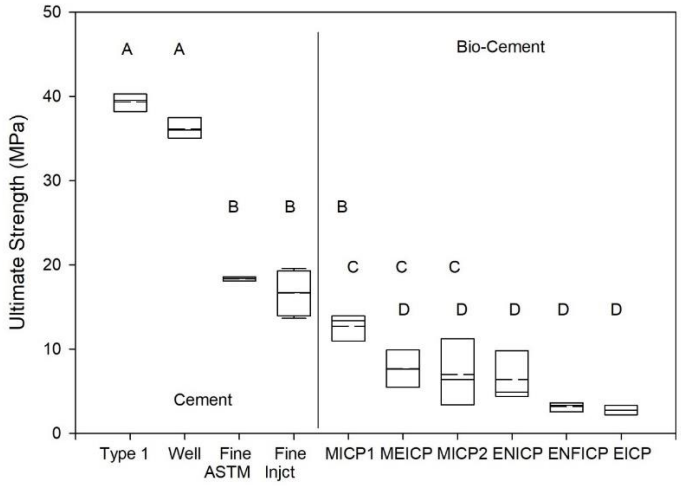

Figure 19. Statistical analysis for biocement and cement specimens

Representative fracture patterns for 5 cm x 10 cm cement and biocement specimens are shown in Figure 20 and Figure 21. Fine cement specimens (both ASTM and injected) had diagonal fractures with no cracking through the ends. The cracks occurred in the middle of well cement specimens, while Type I specimens had a well-formed cone shape. Two of the three EICP specimens were damaged at the top during the mold removal process. The EICP specimens

crumbled during the strength testing; they did not display a well-defined fracture pattern. ENFICP and ENICP specimens were not as crumbly as EICP specimens from the outside. However, during testing, they showed similar crumbling behavior as EICP specimens. MICP-1 specimens had side fractures at the top or bottom. MICP-2 and MEICP specimens showed similar fracture behaviors as MICP-1 specimens.

Figure 20. Fracture patterns for 5 cm x 10 cm specimens. From left to right: Type I cement, well cement and fine cement (ASTM) specimens

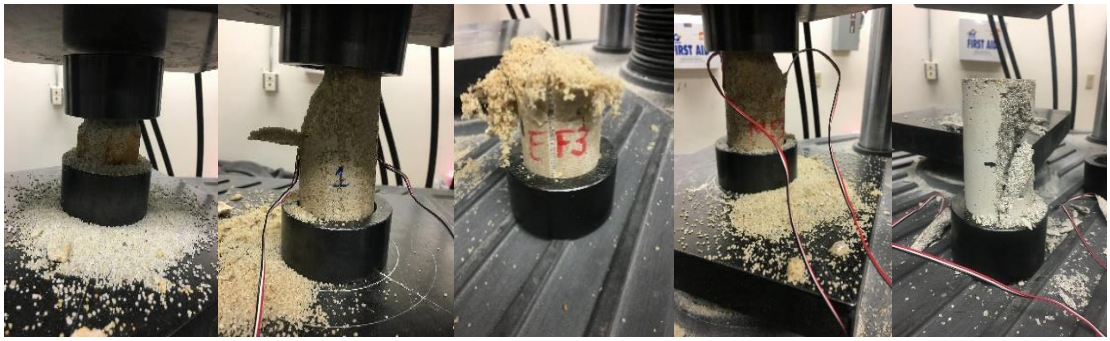

Figure 21. Fracture patterns for 5 cm x 10 cm specimens. From left to right: EICP, MICP-1, ENFICP, MEICP and fine cement specimen

<u>$CaCO_3$ vs Strength</u>

A plot of the percentage of $CaCO_3$ precipitated and compression strength for the biocement specimens were compared to the investigation by others [37, 109-112](Figure 22). These calcium carbonate mass percentage results fall into the range of the specimens analyzed. A trend of increasing strength for larger percentages of $CaCO_3$ precipitated generally observed in the data presented from others was also observed for MICP-1 specimens. One general difference to note is the larger compression strengths measured for biocement specimens prepared in this study compared to reported values at similar calcium carbonate percentages in other studies. One hypothesis for the increase in strength is that the addition of the nutrient broth in the biocement specimens may have positively impacted the strength of the materials. A study by van Paassen et al.[37] also showed increased strength and calcium carbonate content compared to other MICP specimens reported in the literature that were promoted with nutrient broth (biocement promoting solutions section). In addition, the number of injections were greater in these experiments. For example, in van Paassen et al. (2010), 10 injections were performed over 16

days. Park et al. (2014) mixed the JBM solution with the sand only once. For this study, 29 injections for EICP, 40 injections for MICP-1, 35 injections for MICP-2, 29 injections for MEICP, 35 injections for ENICP and ENFCIP were used, which results in more substrate available to react over a longer period of time. Increased strengths were observed when more pulses over a longer period of time were used.

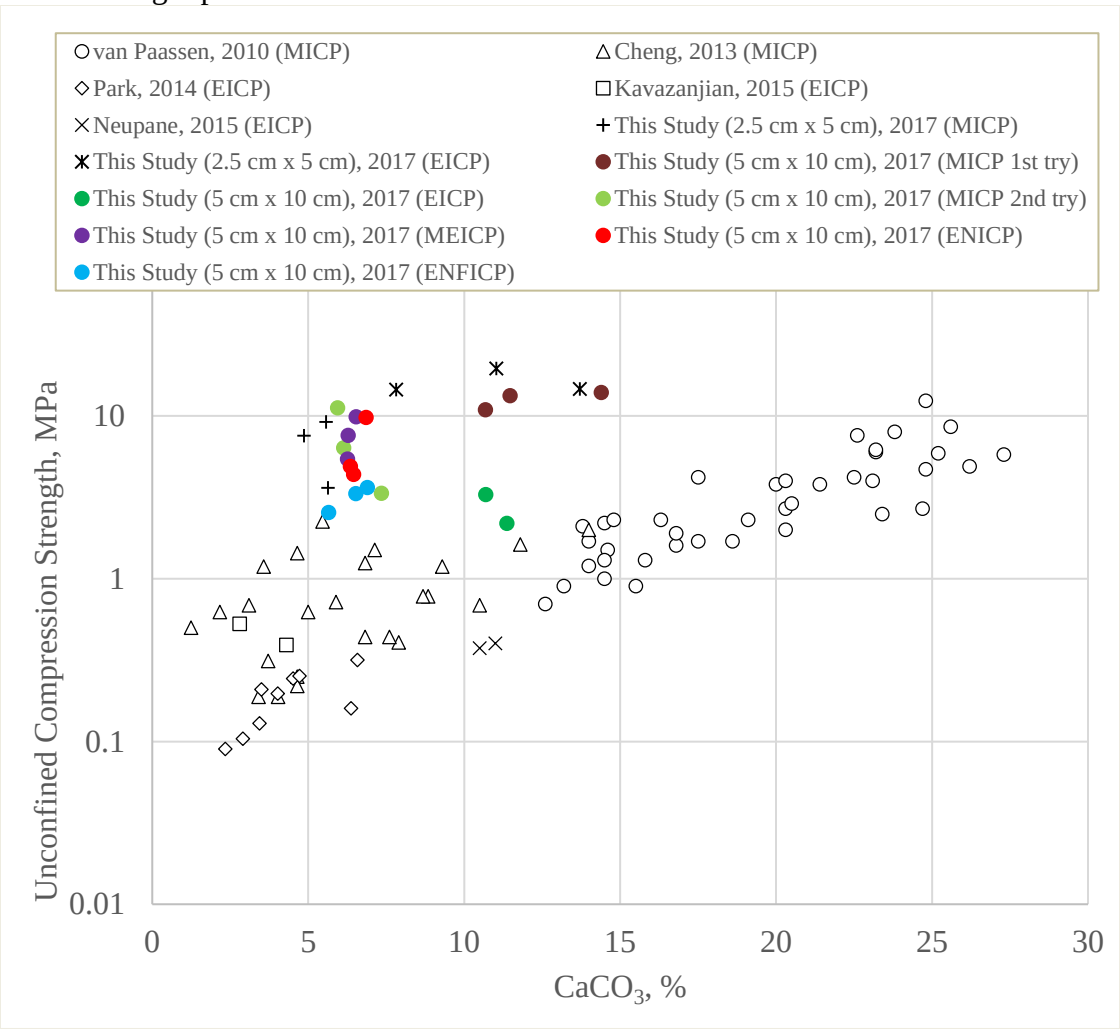

Figure 22. Mass of $CaCO_3$ per mass of sand expressed as percentage plotted against the measured compression strength.

The only statistically significant difference in $CaCO_3$ content is between 5 cm x 10 cm MICP-1 specimens, and 2.5 cm x 5 cm MICP specimens. 2.5 cm x 5 cm; ENICP, 5 cm x 10 cm; EICP, ENICP, MICP-2, ENFICP and MEICP specimens were not significantly different than each other.

Modulus of Elasticity

Strain gages were installed on selected 28-day fine cement (ASTM and injected), MICP, MEICP, ENICP, and ENFICP specimens. These specimens were subsequently tested to determine their modulus of elasticity. National Instruments data acquisition with LabVIEW software was used to

record data from the experiments. The load was applied continuously at a rate of 1 mm/min [0.05 inches /min] until failure occurred. The modulus of elasticity was calculated by Eq. 3 (ASTM C469).

$$E = (S_2 - S_1) / (\varepsilon_2 - 0.000050) \qquad \text{(Eq. 3)}$$

Where: E = chord modulus of elasticity, MPa [psi], S_2 = stress corresponding to 40 % of ultimate load, S_1 = stress corresponding to a longitudinal strain, and ε_2 = longitudinal strain produced by stress S_2. In order to exclude the fluctuations (noise) at the beginning of tests, 0.00005 was subtracted from longitudinal strain as required by ASTM.

Average elastic moduli for each type of specimen is shown in Table 7 (with average compression strengths shown for reference), and the average stress-strain response for all specimens are plotted in Figure 23. Concrete materials made with Portland cement are known to have larger moduli of elasticity for higher compression strengths. A similar trend was observed for the ENICP/ENFICP and MICP specimens, however the opposite trend was observed for the fine cement specimens, produced by injecting and mixing.

Table 7. Modulus of elasticity values of cement and biocement specimens

Cement	Average Modulus of Elasticity (MPa)	Compression Strengths (MPa)
MICP-1	18,475 ± 482	12.7 ± 1.6
ENICP	17,316 ± 1430	6.4 ± 3.00
MEICP	16,623 ± 915	7.6 ± 2.2
ENFICP	15,080 ± 1831	3.2 ± 0.6
MICP-2	14,224 ± 3927	7.0 ± 3.9
Fine Cement (injected)	14,223 ± 223	16.6 ± 2.9
Fine Cement (ASTM)	12,084 ± 384	18.3 ± 0.3

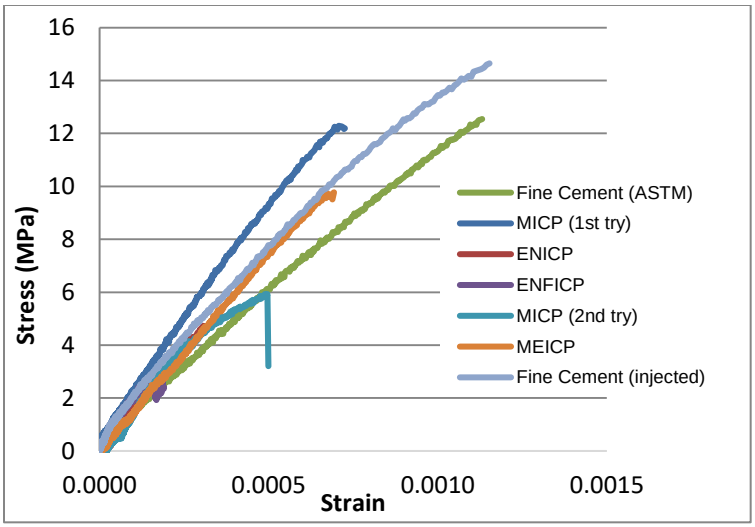

Figure 23. Representative stress-strain diagrams for the biocement and fine cement specimens.

Referring to Figure 23, the largest moduli of elasticity (stiffest/steepest response) was measured in the MICP-1 specimens and the smallest stiffnesses were measured in the two fine cement specimens. Reduced stiffness of the fine cement specimens were accompanied by increased strengths. A similar trend was not observed for biocement specimens. Even though there are substantial observational differences in the average moduli, the only statistically significant difference is between MICP-1 and Fine Cement (ASTM) specimens. The ENICP, MEICP, ENFICP, MICP and Fine Cement (injected) specimens were not significantly different than each other.

Image Analysis

A Scanning Electron Microscope (SEM) was used to observe the surface topography and composition of the EICP, MICP, ENICP and ENFICP specimens. Both 2.5 cm x 5 cm and 5 cm x 10 cm specimens were investigated in the image analysis. The MICP samples were observed to have bonds between the particles as shown in Figure 24(d). The ENICP samples appeared to have bonds not only located in the regions between the particles, but also distributed across the sand surface, as shown in Figure 24(b). Biofilm (microbes attached to the sand surface in MICP treatments) may act as a template for the mineral to initiate on the surface of the sand in contrast to the JBM suspension, which may stay more freely suspended in the fluid, resulting in precipitation predominately occurring in the liquid phase followed by settling out of the precipitates. Still, there was a significant amount of calcite formation bridging sand particles within the ENICP specimens produced, as seen in Figure 24(b). Similar bridges can be seen in the MEICP specimens shown in Figure 24(c). Unlike the sand grains, most of the fibers in the ENFICP specimens were partially coated as shown in Figure 24(a).

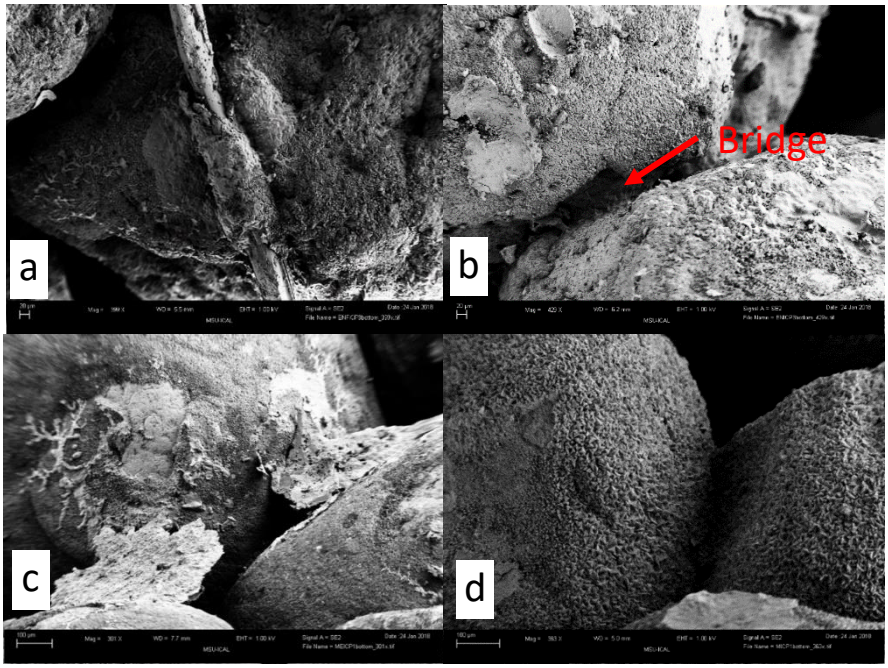

Figure 24. SEM images of 5 cm x 10 cm (a) ENFICP (b) ENICP (c) MEICP and (d) MICP specimens.

The images shown in Figure 25 ENICP reveal a more consolidated $CaCO_3$ coating on the sand grains as can be seen in Figure 25(a). Larger number of cavities were observed in EICP specimens (Figure 25(b)) and it was hypothesized that they might have contribution to the lower strength, however that has not been confirmed.

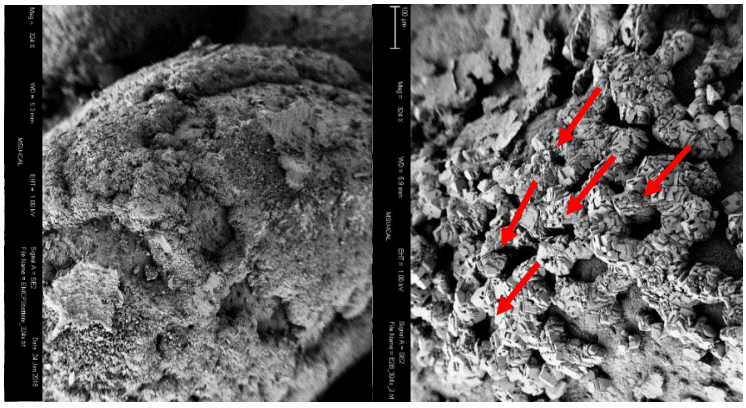

Figure 25. Cavities in (a) ENICP and (b) EICP specimens

Conclusions (Conclusions)

The strength of two different 2.5 cm x 5 cm biocement specimens (MICP and ENICP), and strength and moduli of elasticity of five different 5 cm x 10 cm biocement specimens (MICP, MEICP, EICP, ENICP and ENFICP) were compared with three types of cement mortars (well-, fine- and Type I cement). The plant-based source was from jack bean and the microbial enzyme source was *Sporosarcina pasteurii*. Influence of fibers and nutrient broth were investigated for

enzyme specimens. Fine cement (injected) specimens were made using the same volume of sand as the biocements and were prepared using a water-to-cement ratio of 0.63. Compression and modulus of elasticity tests were performed in triplicate on the cylindrical specimens for each material. Based on the experimental work presented here, the following observations and conclusions were made:

- For 2.5 cm x 5 cm specimens, compression strengths of the ENICP specimens were 77% and 66% of the compressive strengths of the 28-day well- and Type I-cement mortars, respectively. The ENICP specimens were over two times stronger than the fine cement specimens. MICP specimens were 32% and 27% of the 28-day strengths.
- For 5 cm x 10 cm specimens, compression strengths of MICP-1, MEICP, MICP-2, ENICP, ENFICP and EICP specimens reached 77%, 46%, 42%, 38%, 19% and 16% of the 28-day injected fine cement specimens.
- The biocement specimens with fibers (ENFICP) had smaller compression strengths than specimens without fibers.
- All E(N, NF, I)CP specimens had statistically significantly lower strength than all MICP-1 specimens.
- The addition of nutrient broth to the enzyme specimens (ENICP) resulted in increased compression strengths compared with specimens without nutrient (EICP). The higher strengths measured in the ENICP specimens compared to EICP specimens can be due to a more consolidated surface of $CaCO_3$, leading to more connections between sand particles.
- The average modulus of elasticity of ENICP was 17,316 ± 1,430 MPa with 8.3 ± 1.8% $CaCO_3$ content (g/g sand) and was approximately 30% larger than the average modulus measured for the fine cement specimens. Increased moduli of elasticity were measured for increased strengths for the MICP, ENICP, and ENFICP specimens.

It is recognized that the statistical significant differences between the specimens is difficult because of the small number of replicates. However, results of this investigation suggest that UICP specimens can be produced with similar stiffness of fine cements and strengths of these UICP specimens can be as high as 77% of the fine cement specimens. In addition, depending on the nutrients present or the number of injections of biocementing promoting solutions, different material properties might be achieved. The improved characteristics of these environmental friendly materials have the potential for more efficient use in subsurface applications such as in enhanced oil recovery and hydraulic fracturing operations.

Future research should include investigations of different fiber lengths and types for both enzyme and microbe specimens. Future studies also should aim to explore the role of additives including nutrient sources to the EICP and MICP produced cements to alter material properties. Methods to prepare more consistent specimens should be examined and studies should be planned to investigate impacts to the material properties in the presence of chemistries, temperatures and pressures conditions typically found in the subsurface.

Section Two: Scale-Up Experimental Efforts

In this section, we describe the experiments that were used to scale up injection strategies to promote biomineralization in porous media at the field scale. This was important because in the second and third field test at the Rexing well in Indiana, the fracture in the wellbore cement was allowing fluids to flow into a sandstone formation approximately 50 feet above the targeted injection zone. Therefore, methods were needed that could not only impact potential fractures in cement, but also to reduce permeability in large rock formations. Larger volumes of microbes and urea calcium solutions were necessary. Methods of growing the desired microbes in non-sterile conditions needed also to be developed. To accommodate larger injection volumes, less expensive sources of urea and calcium needed to be identified and tested to ensure economic feasibility in field applications. As such, two representative sand pack reactor systems were designed to develop scaled-up cell culturing protocols and injection methods and to study the distribution of mineral in the model sand pack. Mineralization was promoted in both a sand annulus (radially around a mock wellbore) and in sand columns. In the case of the sand annulus, an NMR wellbore logging tool was used to monitor the change in porosity as the biomineralization progressed over the course of several days. In the case of the sand column experiment, permeability was monitored by assessing the changes in flow rate and pressure as the biomineralization sealed the pore spaces of the sand and at the end of the experiment the distribution of calcium was assessed. These experiments resulted in the finalized injection strategy for both of the field tests performed at the Rexing well (described in section 3.2 and 3.3). This section describes the efforts used to meet the objectives as described in the proposal:

Objective 1: After thorough laboratory testing of MICP sealing, develop a field test protocol for effective MICP placement and control.
Objective 2: Prepare for and conduct an initial MICP field test aimed at sealing a poor well cement bond.
Objective 3: After thorough analysis of the results from the first field test, conduct a second MICP test using improved MICP injection methods.

Section 2.1 is adapted (with permission from ACS- see appendix B) from the following manuscript:

- Kirkland, CM, Zanetti, S, Grunewald, E, Walsh, DO, Codd, SL, Phillips, AJ. (2017) Detecting microbially induced calcite precipitation (MICP) in a model well-bore using downhole low-field NMR Environmental Science and Technology, 51 (3): 1537–1543 http://pubs.acs.org/doi/abs/10.1021/acs.est.6b04833

Section 2.2 is adapted from data reported in quarterly reports.

Section 2.1 Detecting microbially-induced calcite precipitation (MICP) in a model well-bore using downhole low-field NMR

Abstract (Abstract)

Microbially-induced calcite precipitation (MICP) has been widely researched recently due to its relevance for subsurface engineering applications including sealing leakage pathways and permeability modification. These applications of MICP are inherently difficult to monitor non-destructively in time and space. Nuclear magnetic resonance (NMR) can characterize the pore size distributions, porosity, and permeability of subsurface formations. This investigation used a low-field NMR well-logging probe to monitor MICP in a sand-filled bioreactor, measuring NMR signal amplitude and T_2 relaxation over an 8-day experimental period. Following inoculation with the ureolytic bacteria, *Sporosarcina pasteurii*, and pulsed injections of urea and calcium substrate, the NMR measured water content in the reactor decreased to 76% of its initial value. T_2 relaxation distributions bifurcated from a single mode centered about approximately 650 ms into a fast decaying population (T_2 less than 10 ms) and a larger population with T_2 greater than 1000 ms. The combination of changes in pore volume and surface minerology accounts for the changes in the T_2 distributions. Destructive sampling confirmed final porosity was approximately 88% of the original value. These results indicate the low-field NMR well-logging probe is sensitive to the physical and chemical changes caused by MICP in a laboratory bioreactor.

Introduction

Biofilms form when bacteria secrete a matrix of extracellular polymeric substance (EPS), attaching themselves to solid surfaces in colonies akin to multicellular organisms and buffering their micro-scale environment.[113] Bacterial biofilms are known to induce metal corrosion,[114] cause persistent infections,[115] treat wastewater,[116] or remediate contaminated groundwater.[117] When composed of ureolytic microbes, biofilms can also induce calcite precipitation,[118] a process referred to as biomineralization or microbially-induced calcite precipitation (MICP). Many strains of bacteria found naturally in soil and groundwater are ureolytic, meaning they can hydrolyze urea for energy and a source of nitrogen.[119] *Sporosarcina pasteurii*, the ureolytic bacteria used in this experiment, forms a thin biofilm in porous media[120] where the EPS matrix, a 3-dimensional diffusion-limited hydrogel, can either facilitate or inhibit MICP over microscales. The organic molecules comprising the EPS matrix restrict mass transfer, creating localized chemical gradients within the hydrogel structure.[118] Ca^{2+} ions are not used in metabolic processes and accumulate near cell surfaces where ureolysis produces an alkaline environment. Thus, the microbial biofilm matrix provides nucleation sites for calcite precipitation.[2] In porous media, the precipitated calcite binds together media grains and fills pore spaces.[8]

MICP has engineering applications[1] that include soil stabilization[8, 37] and subsurface barriers,[50] sealing of cap rocks and well-bore regions,[40, 42, 121] and limestone and concrete remediation.[2] Many of these beneficial applications of MICP occur in the subsurface, raising the question of how the process can best be monitored spatio-temporally. Nuclear magnetic resonance (NMR) is commonly used non-destructively and non-invasively to characterize the pore size distributions, porosity, and permeability of subsurface geologic formations.[122] These are the same physical properties affected by MICP, indicating that NMR well-logging tools may have potential for

monitoring subsurface engineering applications of MICP. This study used a low-field NMR well-logging tool designed for subsurface hydrogeologic investigations[123] to detect changes in NMR signal response indicative of MICP in the pore spaces of sand-filled radial-flow bioreactor.

Background

There are limited examples in the scientific literature where NMR methods have been applied to the study of biomineralization in porous media relevant for engineering applications.[120, 124] These previous studies have used high field strength magnetic resonance imaging (MRI) along with other NMR methods to probe hydrodynamic properties of biomineralization in model porous media systems. Fridjonsson *et al.*[120] used high-field NMR to measure changes in hydrodynamic dispersion resulting from MICP in model porous media to compare flow dynamics between systems influenced by either solid precipitates or a biofilm matrix. The authors used a combination of NMR displacement measurements, relaxation mapping, MRI, and microscopy methods. Sham *et al.*[124] used MRI and NMR flow measurements on both a model bead pack and a Bentheimer sandstone rock core to examine structure and transport properties of each system following MICP. The authors report a reduction of 3.7% in absolute porosity in the bead pack, which correlated to a 98% reduction in permeability. In the sandstone, a 7.2% reduction in absolute porosity yielded a 96.5% reduction in permeability. In both systems, preferential fouling of the inlet region of the column was observed.

The low-field NMR well-logging tool used in this study (Javelin JP350, Vista Clara, Inc., Mukilteo, WA) is sensitive to biofilm growth in the pore spaces of a sand-filled bioreactor[125] and in the subsurface soil of an engineered field testing site.[126] In both of these studies, biofilm growth caused enhanced relaxation with T_2 relaxation times decreasing by approximately 40 – 60%.

These previous studies show 1) NMR methods are useful for analyzing changes resulting from MICP in porous media and 2) the well-logging tool is sensitive to small changes over time in the micro-scale pore environment. To our knowledge, field scale low-field NMR instruments have not been applied to the measurement or monitoring of MICP. In the current study, $CaCO_3$ precipitation was expected to change the NMR signal response by reducing the liquid fraction from which the signal is obtained, causing a decrease in signal amplitude over time as the pores accumulate calcite. MICP will also change the pore sizes and mineral surface of the porous media, thereby influencing the signal relaxation response. A correlation between the signal response and reduction of porosity due to MICP may indicate the use of a NMR well-logging tool as a sensor for biomineralization in field applications where optical or destructive monitoring methods are not possible. This study represented a first step toward that end by demonstrating that a NMR well-logging tool is sensitive to MICP.

NMR Theory

The NMR well-logging tool is sensitive to the hydrogen protons in water, called ‘spins,’ such that the behavior of the NMR signal over time is related to the various micro-scale water environments in the surrounding formation. The tool measures 1.37 m long and 8.9 cm in diameter and is designed to be lowered into small-diameter cased or uncased borehole wells[123] The dual frequency probe used in this experiment operates at approximately 250 and 300 kHz,

and is composed of an array of permanent magnets and radio-frequency (RF) induction coils.[123] The permanent magnets establish a static magnetic field, $\mathbf{B}_0$, along the direction of the borehole, where the field strength depends on the radial distance from the tool. The RF pulses produce two mm-scale cylindrical excitation shells at radial distances of 17-19 cm from the probe center and in the middle of the reactor's sand annulus. The excited shells are 50 cm in height. Only spins in these two excitation shells contribute to the measured NMR signal response, which is averaged over all the spins in each shell.

The initial amplitude of the NMR signal is proportional to the amount of water in the excitation shell and reflects the volumetric water content, or porosity, of the porous media. The NMR signal amplitude decreases when water is displaced by mineral formation in the pores. The observed decay rate reflects spin-spin, or T_2, relaxation, which occurs as protons interact with each other in the transverse plane. These interactions cause a dephasing of spin coherence and signal attenuation. In geologic materials, the observed T_2 relaxation rate comprises the bulk relaxation rate of the pore fluid, $\frac{1}{T_{2B}}$, the surface relaxation rate, $\frac{1}{T_{2S}}$, related to interactions between the fluid and the pore walls, and the diffusion relaxation rate, $\frac{1}{T_{2D}}$, related to diffusion of fluids within pores due to inhomogeneities in the local magnetic field (Equation 2).[127, 128]

$$\frac{1}{T_2} = \frac{1}{T_{2B}} + \frac{1}{T_{2S}} + \frac{1}{T_{2D}} \quad [2]$$

At the low magnetic field strength used in this study, the experimental parameter of the echo spacing, t_E, can be selected to make the influence of diffusion relaxation, T_{2D}, sufficiently small to be neglected. [125, 128] For the current study, changes in the fluid properties of the pore liquid, such as viscosity, are not expected be a significant factor in the overall change of the system T_2 relaxation time.[120] The influence of changes in T_{2B} can therefore also be neglected. Changes in surface relaxation, T_{2S}, are expected to dominate changes in the observed T_2 of this experimental system.

The low-field NMR signal response in most saturated natural geologic media is dominated by surface relaxation.[127, 129] Surface relaxation occurs as excited spins approach and interact with the pore walls. Thus, the rate of surface relaxation is most strongly related to pore size and the mineral surface of the solid matrix. Surface relaxation occurs faster in small pores with a high surface-area-to-volume-ratio because the diffusing water molecules are more likely to interact with the grain surface. The surface relaxation rate also depends on the propensity of the surface for inducing relaxation, a characteristic referred to as surface relaxivity, ρ. Greater concentrations of paramagnetic ions like Fe^{3+} and Mn^{2+} produce higher magnitudes of ρ and faster relaxation rates.[130, 131] In heterogeneous materials with a range of pore sizes or variable ρ, there may be a distribution of relaxation rates making up the bulk response. Thus, an Inverse Laplace Transform yields a decay-time distribution that can be interpreted as a distribution of pore environments.

In our experiments, we expect MICP to have several combined influences on the NMR response (Figure 26). First, we expect that growth of calcite within the pore space will reduce the total porosity and water content. We also expect the growth of $CaCO_3$ to influence the observed

relaxation rate due to changes in mineralogy and pore size.[132-134] The quartz sand used in this study is coarse-grained and contains small percentages of paramagnetic species including iron oxide (Fe_2O_3) at a mean weight percent of 0.04 (2095 Granusil® silica sand, Unimin Corp., Ottawa, MN). We expect that $CaCO_3$ forming on the quartz grain surfaces will decrease the total macro-pore dimension which could drive faster relaxation rates. On the other hand, $CaCO_3$ precipitating on the grain surface may shield water from the paramagnetic ions on the sand, thus decreasing the average ρ of the grain surface. A lower average ρ would tend to decrease the surface relaxation rate in the macro-pores, resulting in longer overall T_2. Further, the $CaCO_3$ may form microcrystalline structures that incorporate significant micro-porosity of nanometer scale. We expect water in the very small geometry of these micro-pores to exhibit very short relaxation times. Thus, we anticipate these changes in the pore structure concurrent with MICP will manifest themselves as multiple changes to the NMR T_2 relaxation time distribution. These observed changes are expected to indicate which mechanism dominates in the bioreactor where there exists a particular initial pore size distribution and surface minerology.

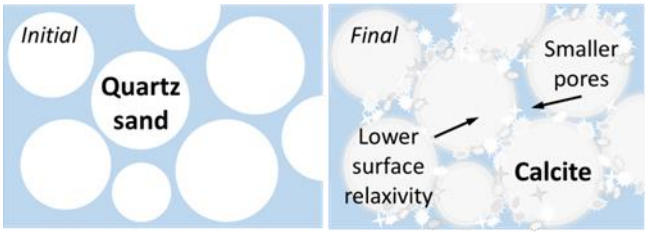

Figure 26. The production of calcite on the surface of a sand grain has the potential to influence not only the pore sizes between the grains, but also the surface properties that may also impact the measurement of surface relaxivity.

Materials and Methods (Experimental Methods)

Bioreactor

The radial flow bioreactor is designed to model the near well-bore environment and consists of four concentric polyvinyl chloride (PVC) pipe sections sealed with grooved top and bottom plates (Figure 27). The reactor is the same as was used in a previous study to detect biofilm growth in sand using the same NMR logging tool.[125] In the current experiment, the height of the reactor was 50 cm. The inner and outer pipes are solid while the two inner pipes are slotted to allow radial flow through the sand annulus between them. The inner and outer annuli are the influent and effluent reservoirs, respectively. The sand annulus measures 7.6 cm wide and was filled with 1 mm nominal quartz sand (2095 Granusil® silica sand, Unimin Corp., Ottawa, MN). The liquid volume of the reactor is approximately 30 L, including the sand pore volume and influent and effluent reservoirs.

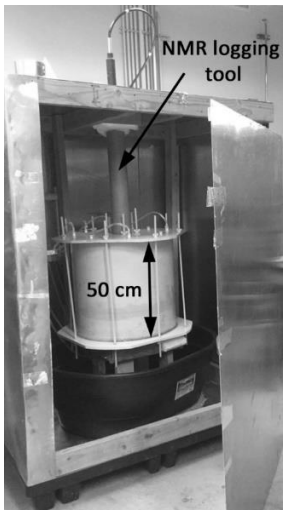

Figure 27. The radial flow bioreactor and NMR logging tool were housed in a Faraday cage to reduce detection of electromagnetic noise from the laboratory.

Media and Injection Strategy

Two kinds of substrate media were used in this study, a bacterial growth medium (growth medium) and a calcite mineralization-promoting medium (calcium medium). Both were urea- and yeast extract-based (1 g/L yeast extract (Arcos Organics, Gheel, Belgium), 20 g/L urea, 1 g/L NH_4Cl, and 24 g/L NaCl). The calcium medium contained an added 49 g/L $CaCl_2 \cdot 2H_2O$. Commercial-grade chemicals were used for urea (Urea Fertilizer, Espoma, Millville, NJ), calcium chloride (various brands of commercial ice melt), and sodium chloride (Morton Table Salt, Chicago, IL). Media were mixed just prior to use in a non-sterile manner using tap water.

A pulsed-flow injection strategy promoted an even distribution of $CaCO_3$ precipitation by balancing reaction and transport rates.[52] Each 30 L pulse of substrate was pumped at a flow rate of 1 L/min, producing a pore velocity of approximately 0.4 cm/min and ensuring that the fresh substrate would penetrate the full width of the sandpack. Calcium medium was injected four times per day during the biomineralization phase Days 4 – 7. A 2-hour batch reaction period (no flow) followed each injection of calcium medium. One pulse of growth medium was injected each evening to stimulate the bacteria for the following day's calcium medium injections. A 10 L brine rinse (24 g/L NaCl) was injected into the reactor first each morning to reduce mixing of the two substrate media in the influent reservoir and minimize clogging of the slotted pipe.

Bacterial Culture

The bacteria used in this experiment, *Sporosarcina pasteurii* (ATCC 11859), formerly known as *Bacillus pasteurii*, is widely used in laboratory experiments related to urea hydrolysis and biomineralization.[1] *S. pasteurii* is a non-pathenogenic natural soil organism capable of producing relatively large amounts of the urease enzyme needed to catalyze urea hydrolysis.[1] For the inoculum, one mL of frozen stock of *S. pasteurii* was cultured in 100 mL of growth medium on a shaker table at 150 rpm for 24 hours. The 100 mL culture was then added to 10 L fresh growth medium and mixed on a stir plate at 1150 rpm for 24 hours. Finally, the 10 L culture was added to 20 L of fresh growth medium and mixed as before to produce a final

inoculum volume of 30 L. No attempt was made to maintain a monoculture in the inoculum or in the reactor.

The reactor was inoculated by first injecting 5 L of fresh growth medium to condition the reactor at a flowrate of 1 L/min, followed by the 30L inoculum. An additional 5 L of fresh growth medium was injected last. Bacteria were allowed to attach to the sand for approximately 15 hours with no flow before the first injection of calcium medium. There was no calcium present in the reactor during the 3-day control period or during inoculation. The initial period was used as the control. Note that previous experiments have shown no permeability reduction was achieved when urea and calcium containing solutions were injected into glass bead filled columns that were not inoculated with ureolytic microbes.[135]

NMR Measurements

Low-field NMR measurements typically consist of repeated scans which are stacked and averaged to reduce noise in the data. In this study, two experiments were conducted sequentially and together constitute one CPMG scan for measurement of T_2 relaxation. Experiment 1 collects T_1-weighted fast-decaying signal (t_E=1.3ms, T_r=800ms, 54 echoes, 360 averages). Experiment 2, on the other hand, collects the signal from spins with longer relaxation times (t_E=1.3ms, T_r=5000ms, 334 echoes, 60 averages). All NMR measurements were collected under no flow conditions. Measurements during the control period, Days 1 – 3, consisted of 24 CPMG scans. Three (3) CPMG scans were stacked and averaged for each daily measurement during the biomineralization phase, Days 4 – 8, because of the timing of repeated substrate injections on a 2-hour cycle. Data presented here was collected with a noise level of approximately 1.4%.

As only one tool was available on loan for a limited period, it was not possible to run replicate experiments. However, previous work with this tool[21,22] has allowed multiple experimental runs whilst monitoring biofouling in both a sand pack and in the subsurface. The tool's performance has been consistent and repeatable.

Sampling

Influent and effluent samples were collected for each injection of brine, calcium medium, and growth medium and analyzed using methods described in Section 1.1. After the final measurement on Day 8, the reactor was drained and destructively sampled. The outer pipe was cut away in sections, leaving the biomineralized sand annulus exposed for sampling (Figure 28). Twenty-four (24) cores were collected: 2 radial cores of approximately 1-inch diameter (2.5 cm) and 3 inch length (7.5 cm) at each of 3 depths were sampled in 4 orthogonal directions. Each core sample was divided into 3 subsamples which were then weighed and subjected to nitric acid digestion to remove the solid precipitates. The liquid was extracted for calcium content analysis by ICP-MS using an Agilent 7500ce (Santa Clara, CA) with a collision cell (helium mode) and a certified environmental calibration standard from CPI International (product number 4400-12 1116NCO2). Additionally, micrograph images were acquired using a Zeiss Supra 55VP scanning electron microscope (Zeiss, USA). Biomineralized sand samples from the reactor and control sand samples were sputter coated with iridium and high-resolution images were taken at 1.0 kV at a working distance of 3-4 mm.

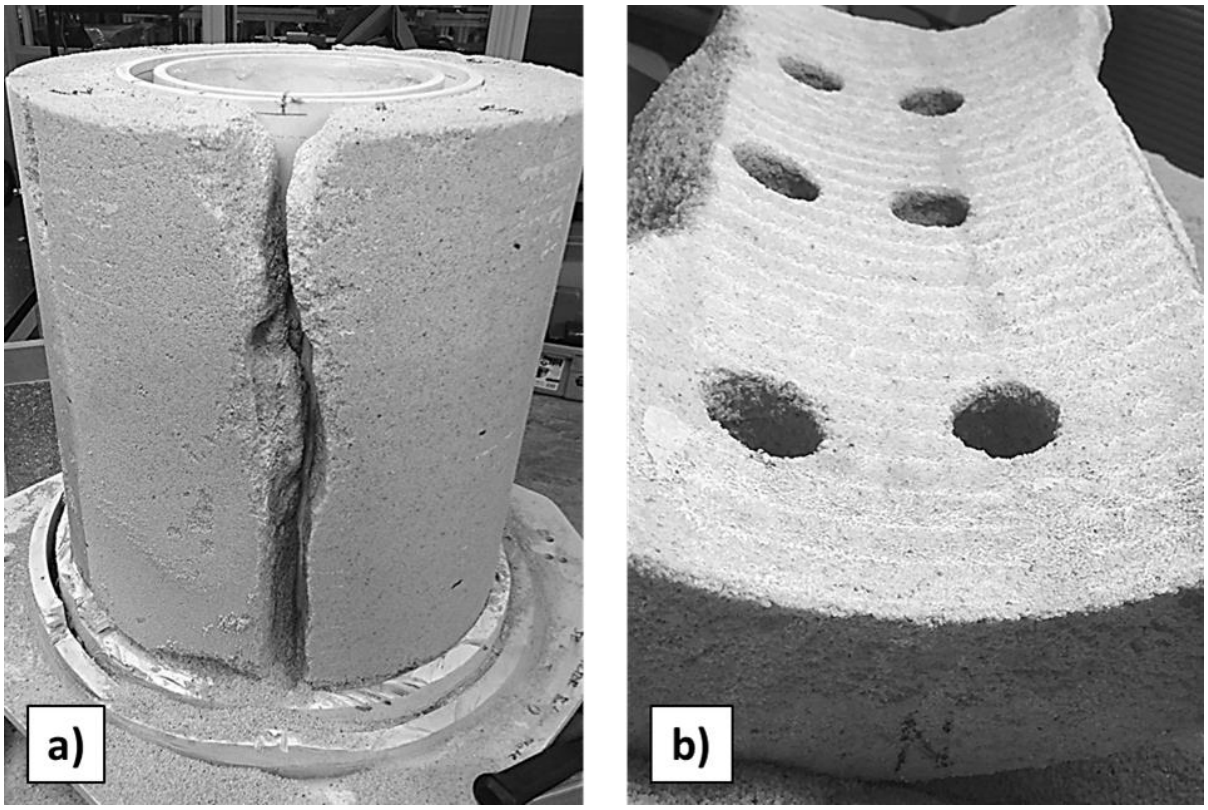

Figure 28. The biomineralized sand annulus was destructively sampled to quantify CaCO3 precipitation. a) The outer pipes of the bioreactor were cut away to expose the biomineralized sand annulus. A saw was used to cut the annulus into quarters, producing the large crack shown here. b) Six radial core samples were collected from each quarter.

Results and Discussion (Results and Discussion)

The influence of $CaCO_3$ precipitation on the NMR signal response is reflected in the daily signal decay curves and resulting T_2 distributions where significant changes were observed over time. Representative data, collected on Days 2, 4, 6, and 8, are presented in Figure 29; the top panel shows fits to recorded signal decay curves, and the bottom panel presents the T_2 distributions for those decay curves. First, we will address the change in water content which corresponds to a drop in the porosity of the sandpack. Then we will discuss the relaxation distributions, which give insight to changes in the relaxation mechanism.

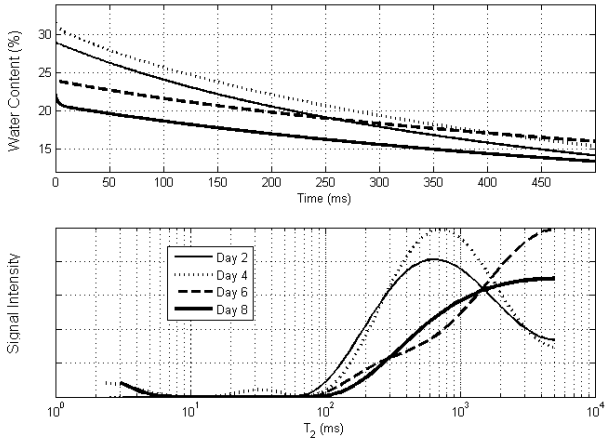

Figure 29. Signal decay curves (top) and the corresponding T2 distributions (bottom) are shown with each curve representing a day. Day 2 occurred during the control period. Inoculation occurred on Day 3 (not shown). The calcium media injections occurred between Day 4 – 7. The Day 8 data was collected prior to flushing the reactor with brine and destructively sampling. Both graphs show fits to the raw data.

Water Content and Porosity

Decreasing signal amplitude over time is an indication of $CaCO_3$ precipitation, since $CaCO_3$ will displace water in the pore volume. During the control period the initial porosity indicated by the NMR-measured total water content was approximately 30% which is slightly less than the 35-39% expected from a sand pack with relatively uniform grains. The observation of entrained air leaving the system after the first flow pulse following inoculation, and the subsequent increase in the water content signal on Day 4, leads us to conclude that the sand pack was not fully saturated during the control period. This also explains why the measured water content value of ~30% is less than the expected value of 35-39%. The NMR-measured total water content in the reactor decreased to approximately 76% of its original value between the control period (Day 2 data) and the end of the biomineralization phase on Day 8 (Figure 29, top panel, and Figure 30). This reduction in total water content indicates that the pore volume within the reactor decreased significantly during the biomineralization phase. If we consider Day 4 to represent full saturation, then the NMR-estimated porosity reduction is 70% of the initial value, indicating the sensitivity of the NMR measurement to partial saturation.

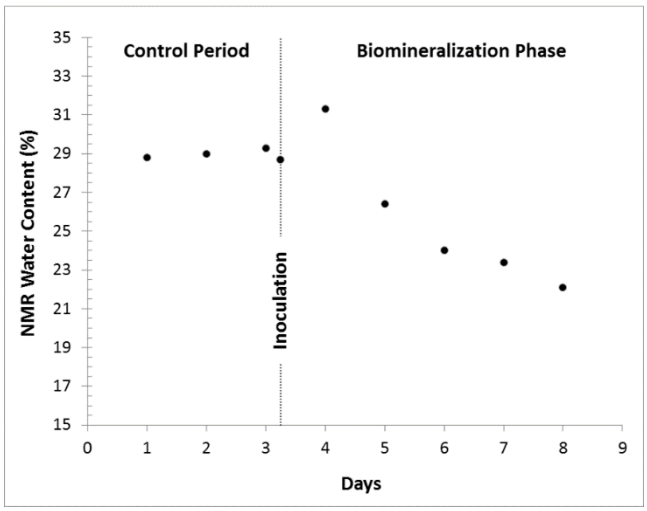

Figure 30. The measured total water content in the radial flow reactor decreased from approximately 29% during the control period Days 1-3 to approximately 22% by Day 8. Note that the increase on Day 4 is real and well outside expected error bounds. The increase follows the observation of entrained air leaving the bioreactor, indicating the desired fully saturated state may not have been obtained until after the control period.

$CaCO_3$ formation was confirmed by scanning electron microscopy (SEM). There appeared to be a relatively uniform $CaCO_3$ coating on the sand samples viewed with SEM. Figure 31 shows an SEM micrograph showing the crystals formed on a grain of sand from the reactor (a) and the surface of a control sand grain (b). The surface of the $CaCO_3$ -encrusted sand reveals micro-scale cavities and pores between crystals. No bacteria were visible in the sand samples viewed with SEM; it is most likely that the cells are entombed within the crystals.

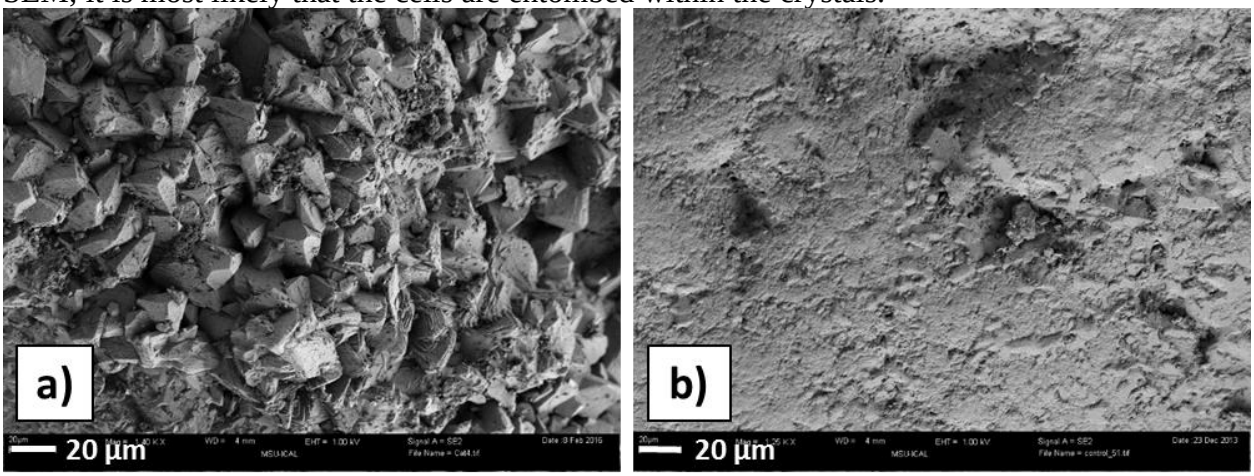

Figure 31. SEM image of a) CaCO3 crystals attached to a grain of sand from the reactor following 4 days of MICP and b) control sand without CaCO3. Scale bar is 20 µm. Note that the CaCO3 crystals completely cover the sand surface and the sand is not visible in (a), whereas in (b) the smooth sand surface is observed.

Several methods were applied to estimate the volume of $CaCO_3$ formed in the reactor in order to independently determine the reduction in pore volume achieved. These methods include a mass balance on urea, ICP-MS detection of Ca^{2+}, and gravimetric methods. An initial porosity estimate of 37%, typical for the sand in the reactor, was used in these calculations. Because the reactor was not fully saturated during the control period, the total porosity is greater than the NMR water content. The results of these three methods are in good agreement with each other and support the NMR data showing a significant pore volume reduction due to calcite precipitation. Mass balance on urea: Influent and effluent samples of each pulse of media were analyzed using the Jung Assay[136] to quantify the urea content. A mass balance on urea showed that approximately 4.2 kg of urea was consumed within the reactor, stoichiometrically producing approximately 6.9 kg of calcite. This mass of calcite would occupy at maximum approximately 15% of the pore space in the sand annulus. Since $CaCO_3$ also formed in the tubing and on the reactor walls, we consider the urea mass balance method to provide an approximation of the upper bound of $CaCO_3$volume. ICP-MS: ICP-MS was used to measure the concentration of Ca^{2+} in the acid extraction liquid from 24 samples of biomineralized sand from the reactor. A mean value of 9.36 g/L Ca^{2+} was obtained with a sample standard deviation of 1.89 g/L, which equates to an average total mass of 6.3 kg $CaCO_3$ within the sand. The ICP-MS data translates to an average pore volume reduction of approximately 12% (+/- 2.4%). Gravimetric method: The 24 sand samples were also weighed before and after the acid digestion removed the precipitate, resulting in an average mass of calcite of 63.6 mg $CaCO_3$/g sand with a sample standard deviation of 13 mg/g. By this method, the average total mass within the sandpack was 5.5 kg calcite. The gravimetric method indicates that approximately 11% (+/- 2.2%) of the pore space in the sand annulus was occupied by $CaCO_3$at the end of the experiment. Unlike the mass balance method, ICP-MS and gravimetry account only for $CaCO_3$ attached to the sand. On the basis of these complementary and independent methods, we estimate that $CaCO_3$ occupied approximately 11 – 12% of the pore space in the sandpack by Day 8 of the experiment.

This estimated porosity reduction is significantly higher than those previously reported in other NMR/MICP studies.[120, 124] The pulsed flow injection strategy used here promotes relatively uniform $CaCO_3$ precipitation, as evidenced by the small standard deviation of the samples collected from the reactor. The uniform calcite precipitation implies spatially uniform porosity reduction. Consequently, only an insignificant reduction in permeability was observed in this study.

Compared to the methods described above which found final porosity to be approximately 88% of the original value, NMR measurements of water content overestimate the porosity reduction achieved. Final NMR water content was 76% of the initial value, or 70% of the Day 4 value. The overestimation can be attributed to carbon dioxide (CO_2) gas production inside the reactor. The excess CO_2 produced by microbial oxidation of the yeast extract in the substrate can be trapped in the reactor pore spaces, displacing water and reducing signal amplitude without changing the pore geometry. Gas formation was also observed in previous NMR studies of MICP.[120, 124] Furthermore, signal decaying in the interval before the first echo acquisition will underestimate the water content and may explain in part the NMR overestimation of porosity reduction.

Relaxation

The tall initial peak (Day 2 data) in the bottom panel of Figure 29, centered about approximately 600-700 ms and associated with water in large pores, first increases then decreases in amplitude over time as the biomineralization phase proceeds. At the same time, there is an increase in both the occurrence of very fast T_2 relaxation times less than 10 ms, and an increase in the proportion of spins experiencing very long relaxation times, greater than 1000 ms. At the left-hand limit of the T_2 distribution (Figure 29, bottom), the NMR logging tool cannot capture NMR signal that decays faster than the measurement echo time (t_E=1.3ms). We note that since the time of this study, the echo time of the Javelin tool has been reduced to 0.7 ms. At the right of the distribution, signals with T_2 between 1-5 s are not tightly resolved on the T_2-axis because the signal is sampled only to 500 ms. However, the amplitude of these long signals is accurately measured (Figure 29, top). By Day 8 of the experiment, the mean log T_2 time of the distribution had increased to greater than 1000 ms from approximately 650 ms during the control period.

The data shows that T_2 relaxation in the macro-pores of the sandpack is more significantly affected by the reduction in ρ than by the decrease in the macro-pore dimension. As seen in the SEM images (Figure 31a), the $CaCO_3$ crystals are on the order of 10^1 μm thick. In a large pore on the order of 10^2 μm in diameter, there is a relatively minor change in pore dimension due to calcite precipitation. On the other hand, the relatively thin and uniform coating of $CaCO_3$ crystals is sufficient to minimize molecular interactions between the pore fluid and paramagnetic species on the sand, making the surface much less likely to induce relaxation. The combination of a large change to ρ and a small change to the pore size explains the lengthening of the overall mean log T_2 relaxation time. At the same time, $CaCO_3$ precipitation also creates micro-pores between and within the crystals. In these pores, the pore size effect dominates and T_2 relaxation occurs rapidly for the small population of spins within the crystals.

Previous NMR/MICP studies reporting the opposite[124] or no relaxation effect[120] are not at odds with this interpretation of the data. Both previous studies used smaller diameter (~100 – 250 μm) model porous media (borosilicate or polystyrene beads, respectively) with a low initial ρ and small initial pore size, where we would expect more potential influence from a change in the pore geometry than from a reduction in ρ. We expect if $CaCO_3$ precipitation had continued to progress in the current experimental system, the reduction in the macro-pore dimension would eventually become the dominate influence, driving relaxation times to decrease. Thus, the potential complexity of the relaxation response leaves open the possibility of different relaxation signatures in other porous materials where pore sizes or surface properties are more heterogeneous.

Conclusions

Our results show that changes in NMR signal response due to MICP include 1) a decrease in signal amplitude over time, indicating a reduction in porosity, and 2) a lengthening of the overall T_2 relaxation time in the quartz sand of the bioreactor. NMR measured water content in the reactor decreased to approximately 76% of the initial value, which corresponds well to the measured reduction in porosity to approximately 88% of the typical initial value. The extent of the decrease in porosity, and the corresponding minimal change in permeability, is related to the pulsed-flow injection strategy employed to achieve the MICP. T_2 relaxation distributions

bifurcated from a single mode centered about approximately 650 ms during the control period into a very fast decaying population (T_2 less than 10 ms), associated with water in the porous $CaCO_3$, and a larger population with relaxation times greater than 1000 ms, corresponding to the bulk water in the large crystal-coated pores. Slower relaxation is caused by $CaCO_3$ crystals on the mineral surface of the macro-pores shielding paramagnetic species from the pore fluid, reducing ρ of the pore. In the $CaCO_3$ micro-pores, the pore size effect dominated and enhanced relaxation. Future work will evaluate the NMR signal response to MICP in natural soils and porous rock where surface relaxivity and pore sizes are more heterogeneous. This study demonstrates that a NMR well-logging tool is sensitive to MICP and has potential as a sensor for biomineralization in field applications where optical or destructive monitoring methods are not possible.

Section 2.2 Preparing for the second and third field demonstration at the Rexing #4 well using a sand column experiment

Introduction

The Rexing #4 well, located near Owensville, IN, has historically been used to sweep residual oil to production wells until injection pressure was recently lost. Subsequent well logging measurements suggested that rather than entering the target formation, injectate was traveling up the well bore through defects in the well cement to a sandstone thief zone approximately 30-50 feet above the target formation. The goal of the field demonstration project at the Rexing #4 well was to use MICP to reduce permeability in the thief zone sand and cement defect to restore injection pressure.

Materials and Methods (Experimental Methods)

Laboratory-scale study

Prior to the field demonstration in Indiana, a laboratory study was designed to model the field conditions and establish experimental protocols. The lab-scale reactor consisted of i) two sand columns to model the target injection formation (a low permeability sandstone) and the thief zone (a higher permeability sandstone); ii) a fracture fixture to model the well cement defect; and iii) a pumping reservoir where media solutions were diluted and pumped into the system to model the wellbore injection methods applied in the field (Figure 32).

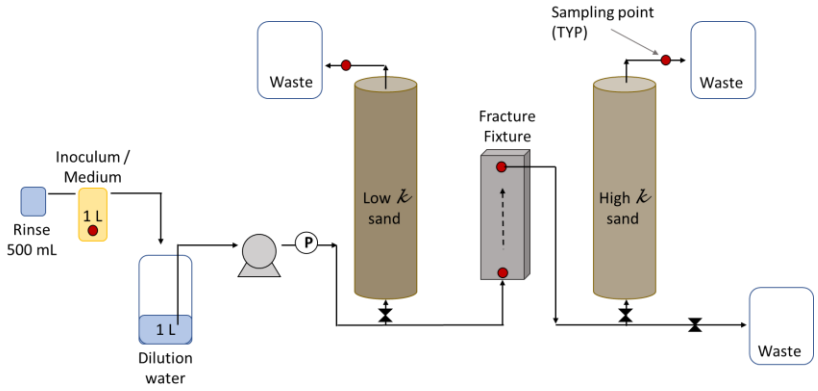

Figure 32. Schematic of the laboratory-scale reactor used to model the Rexing field demonstration.

Results and Discussion (Results and Discussion)

After 10 pulses of *Sporosarcina pasteurii* inoculum and 19 pulses of calcium medium, injection pressure exceeded system limits and the experiment was ended. Effluent from the sand columns generally showed very little remaining urea since it was presumably hydrolyzed during preceding batch periods. The flow–pressure ratio of the system, defined as the flow rate (mL/min) divided by pressure (psi), decreased from 95.5 to 0.98 mL/min/psi, a reduction of two orders of magnitude over the four days of the experiment (Figure 33).

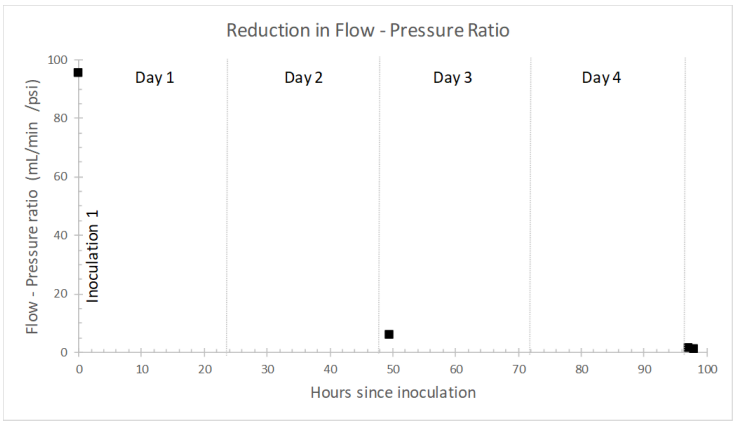

Figure 33. The ratio of flow to pressure in the lab-scale reactor, an indication of the system permeability, decreased by two orders of magnitude over 4 days of inoculum and calcium medium injection.

The majority of the mineral formation occurred in the higher permeability sand, the model for the thief zone sandstone formation at the Rexing #4 well. It appeared that the sand grains were coated with mineral precipitation when observed by SEM and that the sand was cemented together with the mineral precipitates (Figure 34). These laboratory efforts mimicked the design of the first Rexing #4 well field injection strategy where it was planned to use pulsed injection with a bailer delivery method.

Figure 34. Left, Calcium carbonate-like minerals were observed to coat the sand grains and appeared to also bridge the gaps between the sand grains (red arrow), right, only the high permeability column was observed to be cemented together whereas the low permeability column was crumbly with loose sand and did not stay intact after the PVC pipe was cut.

Conclusions (Conclusions)

The sand column experiment resulted in knowledge that was applied to the injection strategies at the Rexing field experiment. For example, we learned that the high permeability sand could be successfully sealed to reduce porosity and permeability with urea fertilizer and calcium chloride ice melt as the chemical sources.

Section Three: Field Scale Experimental Efforts

Section three of this final report contains information about the characterization of two wells (Gorgas well in Alabama and the Rexing #4 well in Indiana) used for our three field experiments as well as the methods used and data collected during the field experiments. Lessons learned and methods developed from the laboratory efforts highlighted in Section One and Two were modified and adapted to fit the field scale. In subsection 3.1 we describe the efforts to seal an identified channel in the cement annulus of the Gorgas # 1 well which was located at the Gorgas Power Plant near Parrish, Alabama. The channel was located in the region between 1020 (311m) and 990 feet (302 m) below ground surface. The treatment with biomineralization resulted in the sealing of the channel (no fluid could be injected) and a noticeable increase in solids in the region of the channel as observed in the cement bond logs. The second and third field demonstrations (subsections 3.2 and 3.3) were conducted in the Rexing #4 well in southern Indiana. The well was a water injection well used to inject water for sweeping oil from an oil-bearing formation. Failure of the well cement allowed injected fluids to travel through the cement fractures to a thief zone about 50 feet (15m) above the targeted oil-bearing zone. Biomineralization treatment was conducted in two separate deployments. The first deployment utilized a bailer delivery method to deliver fluids downhole, and the second deployment used a continuous injection method to restore desired injection pressure. The last subsection summarizes and highlights the design, construction, and modifications made to a mobile laboratory that was constructed to assist in the field demonstrations and advance the technology readiness level of the sealing technology. These successful field demonstrations and the mobile laboratory construction complete the tasks/objectives of the proposal:

Objective 1: After thorough laboratory testing of MICP sealing, develop a field test protocol for effective MICP placement and control.
Objective 2: Prepare for and conduct an initial MICP field test aimed at sealing a poor well cement bond.
Objective 3: After thorough analysis of the results from the first field test, conduct a second MICP test using improved MICP injection methods.

Section 3.1 is adapted (with permission from Elsevier-see appendix A) from the following published paper:

- Phillips, AJ, Troyer, E, Hiebert, R, Kirkland, C, Kirksey, J, Rowe, W, R, Gerlach, R, Cunningham, A, Esposito, R, Spangler, L. (2018) Enhancing wellbore cement integrity with microbially induced calcite precipitation (MICP): a field scale demonstration *Journal of Petroleum Science and Engineering*, 171: 1141-1148 https://www.sciencedirect.com/science/article/pii/S0920410518306788

Section 3.2 is adapted from the following submitted but not yet published paper:

- Kirkland, C, Thane, A, Cunningham, A, Gerlach, R, Hiebert, R, Kirksey, J, Spangler, L, Phillips, AJ. Improving waterflood efficiency using microbially-induced calcium carbonate precipitation (MICP): a field demonstration (Submitted July 2019 Journal of Petroleum Science and Engineering, #PETROL17950, In revision)

Section 3.3 is adapted from the following manuscript in preparation:

- Kirkland, C, Thane, A, Hiebert, R, Hyatt, R, McCloskey, J, Kirksey, J, Gerlach, R, Cunningham, A, Spangler, L, and Phillips, AJ. MICP in the field: continuous injection to reduce permeability and enhance wellbore integrity

Section 3.4 is adapted from the following manuscript in preparation:

- Phillips, AJ, Kirkland, C, Hyatt, R, Hiebert, R, Gerlach, R, Cunningham, A, and Spangler, L. Design of a novel mobile laboratory for implementing engineered mineralization projects in field settings

Section 3.1 Enhancing wellbore cement integrity with microbially induced calcite precipitation (MICP): a field scale demonstration

Abstract (Abstract)

The presence of delaminations, apertures, fractures, voids and other unrestricted flow channels in the wellbore environment substantially reduces wellbore integrity. Compromised cement may cause a loss of zonal isolation leading to deleterious flow of fluids between zones or to the surface with multiple potential negative impacts including: loss of resource production, reduction of sweep efficiency in EOR operations, and regulatory non-compliance. One potential solution to enhance wellbore integrity is microbially induced calcite precipitation (MICP) to plug preferential flow pathways. MICP is promoted with micrometer-sized organisms and low viscosity (aqueous) solutions thereby facilitating fluid transport into small aperture, tortuous leakage flow paths within the cement column. In this study, MICP treatment of compromised wellbore cement was demonstrated at a depth interval of 310.0 - 310.57 meter (1017-1019 feet) below ground surface (bgs) using conventional oil field subsurface fluid delivery technologies (packer, tubing string, and a slickline deployed bailer). After 25 urea/calcium solution and 10 microbial (*Sporosarcina pasteurii*) suspension injections, injectivity was reduced from the initial 0.29 cubic meters per hour (m^3/h) (1.28 gallons per minute (gpm)) to less than 0.011 m^3/h (0.05 gpm). The flow rate was decreased while maintaining surface pumping pressure below a maximum pressure of 81.6 bar (1200 psi) to minimize the potential for fracturing a shale formation dominant in this interval. The pressure decay immediately after each injection decreased after MICP treatment. Comparison of pre- and post-test cement evaluation logs revealed substantial deposition of precipitated solids along the original flow channel. This study suggests MICP is a promising tool for enhancing wellbore cement integrity.

Introduction

According to the 2003 *Oil Field Review* report, since the earliest gas wells were drilled the escape of hydrocarbons to the surface has been a significant challenge. The gas migration leads to sustained casing pressure (SCP) or sustained annular pressure (SAP) which indicates there is hydraulic communication between the formation and the annulus because of inadequate zonal isolation. The causes of SCP can be improper cement slurry design or damage to the primary cement after setting. According to the report, of the 15,500 producing, shut-in, or abandoned wells in the Gulf of Mexico, 43% of them have reported SCP and the problems only increase with the age of the well. Data from the United States Mineral Management Service cited in the report suggested that a 15 year old well has a 50% chance of a SCP problem[137].

Wellbore cement integrity

The primary purpose of wellbore cement is to provide zonal isolation critical for safe and effective operation of both production and injection wells. The presence of delaminations, apertures, fractures, voids and other unrestricted flow channels in the wellbore environment substantially reduces wellbore integrity. Compromised cement can cause lost zonal isolation leading to deleterious flow of fluids between zones or to the surface. Potential negative impacts of compromised wellbore cement include potential damage to drinking water aquifers, leakage of greenhouse gases (e.g. methane) to the atmosphere, reduction of sweep efficiency in enhanced

oil recovery (EOR) operations, regulatory non-compliance, and failed mechanical integrity testing (MIT) necessary prior to plug-and-abandonment. Maintaining wellbore cement integrity is important to geothermal production, unconventional oil and gas, gas storage, or enhanced oil recovery wells [72, 73, 138-140].

Alternative sealing technologies

A common method for repairing wells with compromised integrity is the use of cement, in particular fine cement[15, 16], that can be injected into gaps as small as 120 µm. The success rate of squeezing cement to fix leaks may be less than 50% due to the difficulties in getting cement to the proper locations [141]. Additional research is being performed to assess the use of gels, epoxies and nanocomposite materials that may be able to access smaller aperture fractures [75, 76]. These novel materials may have additional considerations for use in repairing wells including 100 times higher viscosity than that of the MICP promoting sealing solutions. Higher viscosity fluids require increased pumping pressures to deliver the materials, potentially limiting the gap configurations that can be accessed. A comprehensive review of different methods to repair well integrity was not conducted, but a few options are compared in Table 8.

Table 8. Emerging Technologies used to Repair Leaking Oil & Gas Wells

Technology	Maturity	Smallest fracture penetrated	Initial Viscosity	References
Micro-cements	Field utilization	120-150 µm	250 cP	[142]
Ultrafine cementitious grout	Some field data	150 µm	16-40 cP	Product Data Sheets
Gels and epoxies	Research & development and some field data	5-50 µm	80-500cP Depends on temperature	[143] and Product Data Sheets
Nanocomposite Materials	Research	< 1 µm to 13 µm	200 cp	[142]
MICP	Research and field demonstration	2-5 µm	1-3 cP	[42]

Microbially Induced Calcite Precipitation (MICP)

While wellbore cements and ultrafine cements continue to be developed, there is an obvious need for novel technologies that can be delivered via low viscosity fluids thereby improving the ability to plug small aperture leaks such as fractures or delaminations at interfaces. MICP, as discussed in detail below, utilizes micrometer-sized organisms and low viscosity (aqueous) solutions thereby facilitating fluid transport into small aperture flow channels within cement. Data from mercury intrusion porosimetry performed on biomineralized sandstone cores suggested pore spaces in the size range of 6-16 µm were most impacted by biomineralization treatment[42, 144]. Conceivably, since the microbe itself is in the size range of 1-5 µm, the aperture of fractures that can be

impacted by MICP treatment is only limited by the ability of the microbe to be transported into the fracture. These are smaller pore spaces than those accessible with cement-based technologies, which may be due to the higher viscosity of cement/water mixtures, compared to in biomineralization promoting solutions [78, 144].

While the MICP treatment may have the advantage of sealing small aperture fractures and can be placed in channeled cement with water-based solutions, it is not without risk. For example, if fractures in the treatment zone extend to functional aquifers then there could be a risk of urea (a nitrogen source) impacting groundwater. This risk could be mitigated by carefully controlling the placement of the fluids, for example, only adding the volume estimated in the wellbore cement channeled region. In addition, the risk of injecting microbes can be mitigated by using different sources of the enzyme. Some additional sources include inactivated microbes, which contain active enzymes in their cells, using enzymes directly (plant or extracted from microbial cells), or by promoting the entombment of the microbes at the end of the MICP sealing process, which would result in trapping of the microbes, reduced microbial transport, and likely inactivation over time [80].

MICP Fundamentals

As descried in previous sections, MICP is proposed for a number of engineering applications and is promoted by the urease enzyme to create conditions favorable for precipitation of calcium carbonate. While many studies related to MICP have been reported on a laboratory scale only a few have been performed on a field scale. These studies include the use of MICP to promote urea hydrolysis and calcite precipitation in groundwater, (Fujita *et al.*, 2008) improving the geotechnical quality of soils [37, 145] and promote fracture sealing 25 m below ground surface in the fractured dacite[43]. Recently, we described a study where MICP was used to seal a hydraulic fracture in a sandstone formation 340 m below ground surface[40]. The MICP study described here utilized *Sporosarcina pasteurii,* ATCC 11859.

Materials and Methods (Experimental Methods)

Site Characterization

The MICP sealing field demonstration was performed inside a 24.4 cm (9.625 inch) diameter well located on the William Crawford Gorgas Electric Generating Plant (Alabama Power, Southern Company) near Jasper, Alabama, USA (hereafter referred to as "Gorgas". This well was drilled as part of the Department of Energy effort to characterize geologic formations suitable for carbon sequestration. The well was used in a previous MICP experiment located at 340 m below the ground surface which focused on sealing a hydraulic fracture in a sandstone formation. This well has been used for testing purposes and could be described as shut in with plans to plug and abandon the well as soon as the testing projects are completed. Additional details of the well and site can be found in Phillips et al. (2016). The target zone for our current field study was at a depth where the wellbore cement was channeled approximately 310 m below ground surface.

Cement Evaluation Log and Sidewall Coring.

The region of compromised cement was identified through the use of an ultrasonic imaging tool (USIT) provided by Schlumberger. The USIT, which was lowered into the well on a wireline, provided a continuous image of the quality of the cement bond at the cement-casing interface.

Ultrasonic cement imaging log (IBC® Schlumberger) results, shown in Figure 35, suggested that cement in the vicinity of 310 m (1017 feet) bgs appeared to contain solids but was dominated by a liquid filled channel above which very few solids were present.

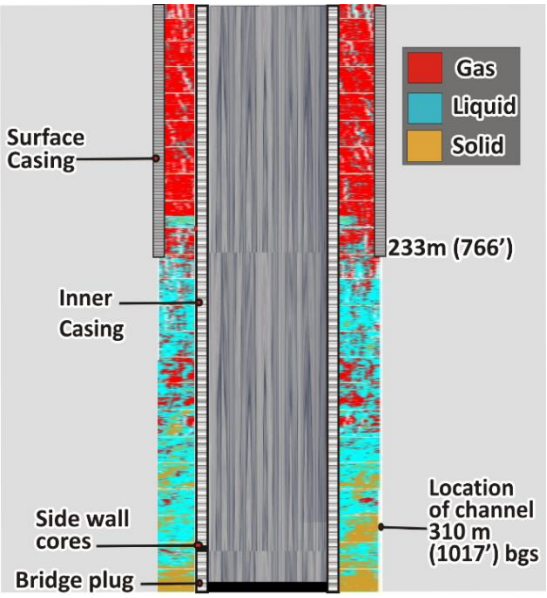

Figure 35. This ultra-sonic cement imaging log suggests that the region near 310.0 m (1017 feet) bgs was favorable for an MICP sealing demonstration as a channel was shown to exist in the cement behind the casing. In this figure, the behind-the-casing environment of the wellbore is color coded by the fluid or solid detected. Red = gas, blue = liquid and tan = solid. In the region of 310 m below ground, both solids and liquids were detected with channels present. The sidewall cores obtained were located at 310.0, 310.3, and 310.9 m (1017, 1018 and 1020 feet) bgs.

To access this zone, three side wall cores were drilled at elevations 310.0, 310.3, and 310.9 m (1017, 1018 and 1020 feet) bgs. The coring device was lowered via wireline to the elevation chosen for coring then activated. Figure 36a shows that the sidewall core recovered from 310.0 bgs consisted of steel casing and good quality cement. The fracture transecting the core could possibly serve as a channel for flow of injected fluids. However, this cannot be confirmed as the fracture could have also occurred during the drilling of the core. This core sample did not extend into the surrounding shale formation. Figure 36b shows the core recovered from the elevation 310.3 m (1018 feet) bgs. This core consisted of steel casing, good quality cement, and dense black shale. A third core (not shown), drilled at elevation 310.9 m (1020 feet) bgs, penetrated the steel casing into a region devoid of cement, and no cement or shale was recovered. It was assumed that this core accessed the channel and was the target for subsequent MICP sealing.

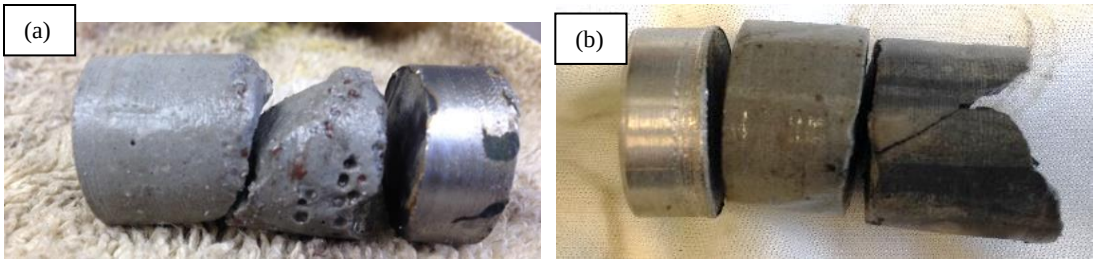

Figure 36. December 2015 (a) Sidewall core consisting of steel casing and fractured, good quality cement recovered from elevation 310.0 m (1017 feet) bgs. (b) Sidewall core, consisting of steel casing, cement, and dense shale recovered from elevation 310.3 m (1018 feet) bgs. A third coring at elevation 3120.9 m (1020 feet) bgs exposed a void in the cement behind the casing. No cement or shale was recovered.

MICP Field Demonstration Design

The objective of the MICP field experiment was to demonstrate that MICP treatment can improve the integrity of compromised wellbore cement along the target elevation interval. The experimental procedure included: 1) creation of an access point through the casing to deliver fluids, 2) injection of microbial suspensions that attach to surfaces of the channel casing and cement interface, 3) injection of calcium-containing solutions that promote mineralization, and 4) assessing the degree of cement channel plugging by monitoring the relationship between injection flow rate and pressure. Conceptually the MICP seal grows *in-situ* from the surfaces of the cement and casing interfaces into the cement channel(s) until fluids can no longer be injected without exceeding the threshold fracture pressure of the surrounding formation (Figure 37).

Collaborators on this field test included the Center for Biofilm Engineering at Montana State University (CBE/MSU), Southern Company (SC), Schlumberger Carbon Services (SLB), Loudon Technical Services (LTS), and Montana Emergent Technologies (MET). CBE/MSU together with MET designed the field test protocol, oversaw testing and analyzed results. SC provided access to the well and coordinated field operations with SLB; SLB, MET, and LTS provided field oversight, coordinated equipment and subcontractors for the field work, and helped with the analysis of the results. All collaborators actively participated in decision-making and evaluation for each stage of the project. CBE/MSU, MET, and SLB moved on-site, received rental equipment and chemicals, and began cultivating microbes. Pumps, surface tubing, sampling equipment, mobile chemical testing laboratory, and the microbial laboratory were all set up as SLB mobilized equipment including the slickline unit and workover rig and crew. This project integrated expertise from practitioners (SC, SLB, and Shell) with experimental research and development (MSU/CBE, MET) to successfully complete the demonstration and thoroughly evaluate the field injection protocol, field delivery system, and effectiveness of the biomineralization sealing process.

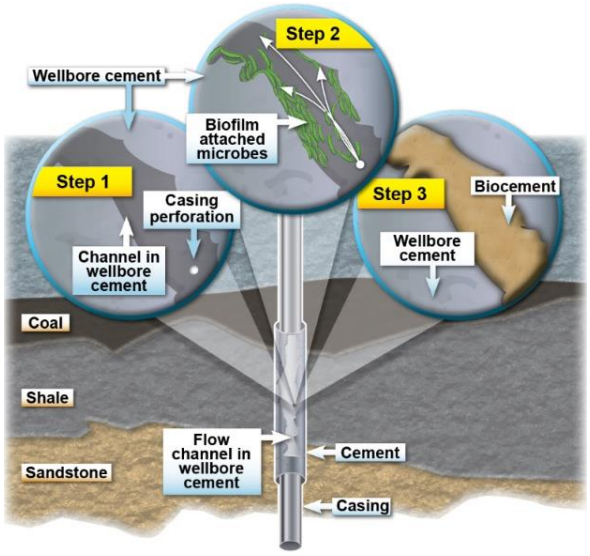

Figure 37. Biomineralization promoting fluids are injected into the channel where a mineral seal forms to limit further fluid injection.

Preparation of Microbes. Filtered (0.2 µm bottle top filter Fisher Scientific, NJ, USA) BHI+ Urea medium (37 g/L BHI Becton Dickinson, 20 g/L Urea, Fisher Scientific) was prepared in 250 ml plastic screw top flasks and inoculated with a thawed glycerol stock suspension containing *S. pasteurii.* The cultures were grown overnight and then transferred to carboys (Reliance Products) containing 15L YE-medium (5 g/L Yeast Extract, Sigma Aldrich, 20 g/L urea, Potash Corp., 1 g/L NH_4Cl, BASF) for an additional overnight growth period prior to injection amendment of the subsurface. The entire carboy was placed on a magnetic stir plate in a heated (23°C) Rubbermaid tub, and the culture was allowed to grow for approximately 24 hours. No significant efforts were made to perform the carboy culturing aseptically in order to simulate a more realistic commercial application with typical oil field conditions. Overnight cultures of *S. pasteurii* were maintained throughout the demonstration. Periodic samples of the *S. pasteurii* inoculum were collected and monitored for cell concentration and purity by performing the drop plate method population assay on BHI+Urea agar plates[146]. Cultures were started and transferred daily so that several 15L (four gallon) carboys with at least 24 hour old cultures were available for inoculation each day of the experiment. The suspension had an average culturable cell concentration of $3.5x10^6$ cfu/ml at the time of injection.

Calcium-Containing Solution. The concentrated mineralization media consisted of 9 g/L yeast extract (Acros Organics, New Jersey, USA), 124 g/L as Ca^{2+} (Ice Melt, Occidental Chemical Corporation, Texas, USA) and 72 g/L urea (Potash Corporation, Illinois, USA). This solution provides the urea and calcium for biomineralization and precipitation to occur and was described as YE+.

Injection Strategy. The fracture was inoculated by injecting 3.0 gallons of overnight grown inoculum (amended with 5 g/L YE and 24 g/L urea) through the slickline bailer followed by approximately five gallons of fresh water (amended with 24 g/l NaCl). Each bailer of inoculum or concentrated growth/calcium solution was sampled and the pH, conductivity, and urea

concentrations were assessed (data not shown). A bailer on a slickline was used to deliver concentrated solutions and bacterial suspensions to the subsurface. The tubing string ran to the surface and was used to deliver brine to dilute concentrated bailer contents and deliver them into the fracture. A pulsed injection strategy was used to inject multiple microbial suspensions and calcium containing solutions over the course of four days (*Table 9*)[40, 83].

Table 9. Summary of injected fluids.

Date +time	Bailer Contents	Delivered Vol of Bailer L (Gal)	Delivered Vol of Brine L (Gal)
4/12/16 5:48 PM	Inoculum	11.36 (3)	24.2 (6.4)
4/12/16 6:16 PM	Inoculum	8.52 (2.25)	23.1 (6.1)
4/12/16 6:42 PM	Inoculum	8.52 (2.25)	23.8 (6.3)
4/13/16 11:03 AM	YE+	8.52 (2.25)	19.3 (5.1)
4/13/16 11:45 AM	YE+	8.52 (2.25)	18.9 (5)
4/13/16 12:14 PM	YE+	8.52 (2.25)	18.9 (5)
4/13/16 12:50 PM	YE+	8.52 (2.25)	18.9 (5)
4/13/16 1:18 PM	YE+	8.52 (2.25)	19.3 (5.1)
4/13/16 1:55 PM	YE+	8.52 (2.25)	19.3 (5.1)
4/13/16 2:24 PM	YE+	8.52 (2.25)	18.9 (5)
4/13/16 3:04 PM	Inoculum	8.52 (2.25)	18.9 (5)
4/13/16 3:34 PM	Inoculum	8.52 (2.25)	19.7 (5.2)
4/13/16 4:02 PM	Inoculum	8.52 (2.25)	18.9 (5)
4/14/16 10:09 AM	YE+	8.52 (2.25)	18.9 (5)
4/14/16 10:40 AM	YE+	8.52 (2.25)	18.9 (5)
4/14/16 11:11 AM	YE+	8.52 (2.25)	18.9 (5)
4/14/16 11:42 AM	YE+	8.52 (2.25)	18.9 (5)
4/14/16 12:13 PM	YE+	8.52 (2.25)	18.9 (5)
4/14/16 12:45 PM	YE+	8.52 (2.25)	18.9 (5)
4/14/16 1:16 PM	YE+	8.52 (2.25)	18.9 (5)
4/14/16 2:03 PM	Inoculum	8.52 (2.25)	18.9 (5)
4/14/16 2:34 PM	Inoculum	8.52 (2.25)	18.9 (5)
4/14/16 3:07 PM	YE+	8.52 (2.25)	36.3 (9.6)
4/14/16 3:29 PM	YE+	8.52 (2.25)	18.9 (5)
4/14/16 4:10 PM	YE+	8.52 (2.25)	18.9 (5)
4/14/16 4:39 PM	YE+	8.52 (2.25)	18.9 (5)
4/14/16 5:07 PM	Inoculum	8.52 (2.25)	17.4 (4.6)
4/14/16 5:36 PM	YE+	8.52 (2.25)	18.9 (5)
4/15/16 9:09 AM	YE+	8.52 (2.25)	18.9 (5)
4/15/16 9:48 AM	YE+	8.52 (2.25)	18.9 (5)
4/15/16 10:29 AM	Inoculum	8.52 (2.25)	18.9 (5)
4/15/16 11:14 AM	YE+	8.52 (2.25)	18.9 (5)
4/15/16 11:59 AM	YE+	8.52 (2.25)	19.3 (5.1)

4/15/16 1:17 PM	YE+	8.52 (2.25)	18.9 (5)
4/15/16 4:08 PM	YE+	8.52 (2.25)	18.9 (5)

Results and Discussion (Results and Discussion)

Initial Pressure-Flow Test Results

A packer-bridge plug system was installed to isolate the region above and below the location of the three side wall cores. Water was pumped through the sidewall core holes to establish the relationship between pressure and injection flow rate. The flow rate was chosen to be 1.89 to 2.6 L/min (0.5 to 0.7 gpm which was chosen to maintain an injection pressure below the formation fracture threshold pressure, which was estimated to be approximately 81.6 atm (1200 psi). Pressure and flow rates were recorded as a total of 469L (124 gallons) of water was injected. The water was trucked from the plant to two 2082 L (500 gallon) holding tanks where it was amended with NaCl (Mix-N-Fine, Cargill, Minnesota, USA) to 2.4% final NaCl concentration (hereafter referred to as the brine). As previously described[40], the flow rate from the Cat Model 310 (Cat Pumps, Minneapolis, MN) injection pump powered by a 5 HP 230 V motor with a variable speed drive was monitored by a Hoffer flow meter (Hoffer Inc., North Carolina, USA) with an Omega (Omega Engineering Inc., Connecticut, USA) pressure data logger to record surface pressure. The injection pump was connected to the tubing string to be able to pump brine into the subsurface.

Observations from the initial pressure-flow test suggest that the constant flow rates (first 1.89 L/min then 2.64 L/min (0.5 gpm then 0.7 gpm)) resulted in several episodes of pressure first increasing to a maximum of 78.43 atm (1153 psi), then decreasing to approximately 59.9 atm (880 psi). This behavior suggests that the injection at these pressures opened up flow channels which were more connected (and possibly wider) than the flow paths (channels) initially present. A total of 469 L (124 gallons) of brine was injected at 2.64 L/min (0.7 gpm) (177 minutes in duration), providing indication that the planned injection of MICP fluids to achieve cement sealing could be accomplished with the maximum injection pressure remaining below the assumed formation fracture threshold pressure of approximately 81.6 atm (1200 psi).

The results from the pressure-flow test were analyzed assuming that most, if not all, of the injected flow passed through a single flow channel through the wellbore cement. Based on this "single channel" assumption it was possible to estimate the equivalent channel aperture width using Cubic's law as discussed in Section 1.1. Using the pressure/flow analysis with Cubic's law we estimated a fracture aperture of 125 µm. This calculation assumes a single flow channel of width (w) equal to 40% of the circumference of the well casing or 0.31m (1.02 feet), and a length L of 9.14 m (30 feet). Given the size of the estimated aperture, this gap may be difficult to seal with micro-cements in a squeeze job (Table 8) and was thus considered an appropriate test condition for the MICP treatment technology.

MICP Treatment Results

The channel treatment experiment was performed over the course of four days during which biomineralization fluids and microbial growth media components were delivered to the target interval. Three major results were observed over the course of the experiment: 1) injectivity was

reduced, 2) the pressure falloff after shut in decreased and 3) a significant increase was observed in the percentage of solids in the channel after MICP treatment.

Injectivity. Injectivity of the fluid was significantly reduced from 0.29 cubic meters per hour (m^3/h) (1.28 gpm) to less than 0.011 m^3/h (0.05 gpm) after MICP treatment (Figure 38). The flow rate was decreased as pressure increased to remain below a maximum pressure of 81.6 bar (1200 psi), which was deemed to possibly initiate a fracture in the shale formation, which was dominant in this interval. The reduction in injectivity was attributed to the sealing of the channel which was observed in the cement bond log.

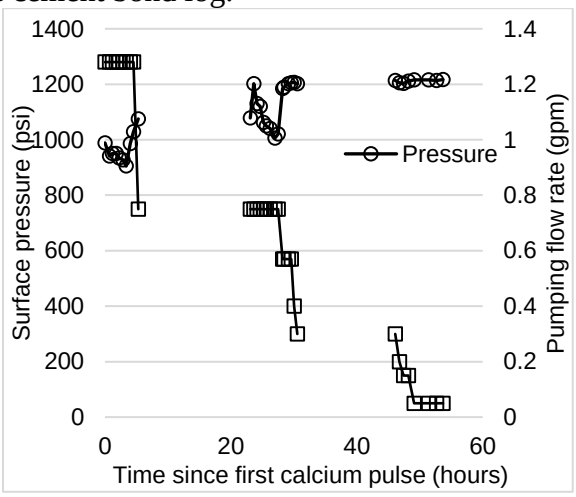

Figure 38. Pressure increase corresponding to (decreasing) injection flow rate over time during the MICP sealing demonstration. Injections were terminated when the injection pressure reached 81.6 bar (1200 psi), which was estimated to be the fracture initiation pressure for the shale formation. The corresponding injection flow rate was less than 0.011 m3/h (0.05 gpm).

Pressure Falloff. Mechanical integrity tests are used to determine whether there is a leak in the well's casing or tubing or whether there may be channels in the near wellbore environment. A well has mechanical integrity if: (1) there is no significant leak in the casing, tubing, or packer (internal mechanical integrity) and (2) there is no significant fluid movement through channels adjacent to an injection wellbore (external mechanical integrity)[147]. A series of pressure fall-off tests were performed on the final day after MICP treatment in the Gorgas well. Prior to the MICP treatment, pressure falloff was as high as 42% of the pressure decaying within 10 minutes after shut-in at 63.4 bar (920 psi). After MICP treatment on the final day of the experiment, the well was pressurized to 20.4,34.0, and 82.7 bar (300, 500, and 1200psi) and the percentage of pressure decay after 15 minutes was recorded. At 20.4 bar (300 psi) 5.1% pressure, at 34.0 bar (500 psi) a pressure decay of 7.1% and at 82.7 bar an 18% decay was observed after the 15-minute time interval. The treatment of the channel returned the well to a condition where it met the Colorado definition of a mechanical integrity for shut-in wells (the Gorgas well could be considered a shut in well) (Table 10). While this well is not in Colorado, the mechanical integrity test was only monitored for 15 minutes and not 30 minutes. Thus, it could not be determined whether the well would meet the definition of mechanical integrity for injection wells in Alabama. The definition of mechanical integrity is different between states and the type of well and while this is not a comprehensive list of all regulations, a few examples are noted (Table 10).

Table 10. Definitions of Mechanical Integrity for Different Well Types

Location or Regulatory Responsibility	Pressure (psi)	Percentage Falloff	Duration (min)	Well type
EPA	>300	3%	30	Injection (Environmental Protection Agency, 2008) [148]
Colorado	>300	10%	15	Injection, Shut-In (Colorado Oil and Gas Conservation Commission)[149]
Montana	>300	5%	15	Injection/Disposal (Montana Board of Oil and Gas Commission)[150]
Alabama	<1500	10%	30	Injection/Disposal (State Board of Oil and Gas of Alabama)[151]
Texas	>200	10%	30	Injection/Disposal (Texas Railroad Commission)[152]

Solids Increase. Wellbore cement quality in the region of interest was examined using an ultrasonic imaging tool (USIT) (Schlumberger). Briefly, the USIT uses a transducer mounted to the bottom of the tool that detects ultrasonic waves reflected from the casing interfaces. The tool has a transmitter that emits ultrasonic pulses and the rate of decay of the waves gives an indication of the cement bond at the casing interface. The transducer is mounted on a rotating stage at the bottom of the tool so 360-degree scanning can occur.

The USIT was used before and after MICP treatment to characterize the cement quality. Before sealing occurred there appeared to be an approximately 40% lack of bonded cement in the annular space (Figure 39a). The conceptual model is that there was likely a channel formed on the thin side of the annulus. This is also corroborated by the casing is not centered in the borehole at this depth in the well (data not shown). When the casing is not centralized it may be difficult for cement flow to reach the narrow side of the annular space resulting in a channel void of cement in that region.

The ultrasonic imaging tool (USIT) logs before and after MICP treatment indicated a significant increase in the solids content in the compromised cement region (Figure 39b, Figure 39c). These cement evaluation logs revealed a general narrowing of the channel observed in the cement casing interface with complete sealing observed in the region around 302m (990 feet) bgs.

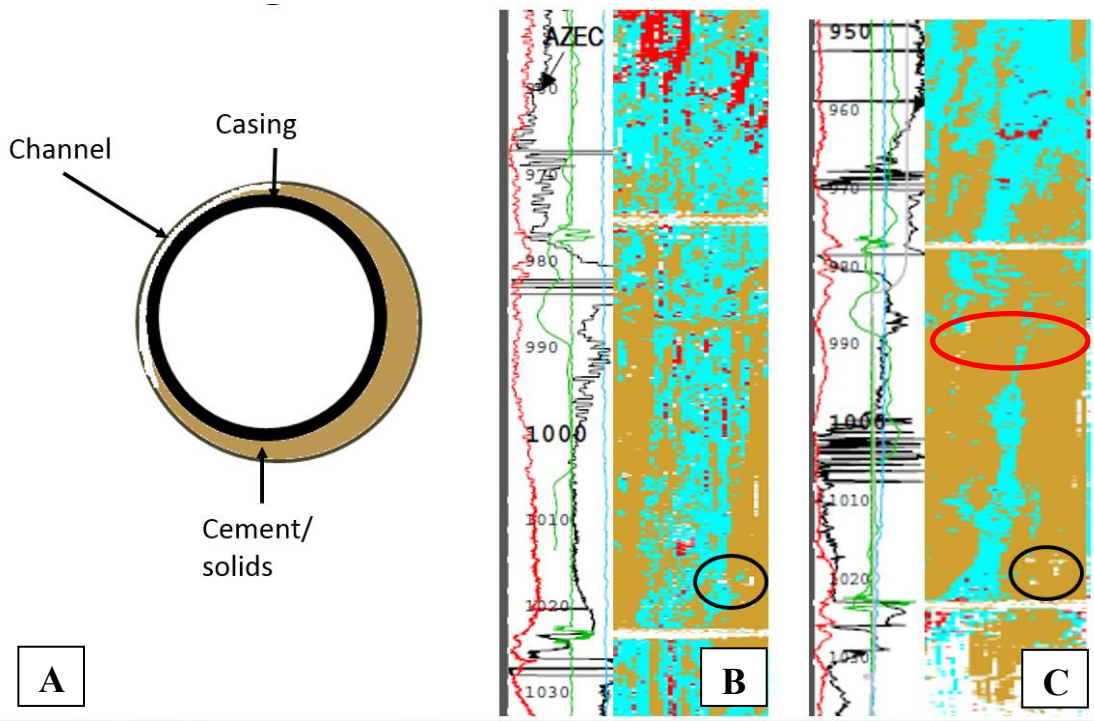

Figure 39. (A), (B), and (C). The cement bond log scanned with the Schlumberger USIT from 292.60-316.98 meters (m) (960-1040 feet) below ground surface. (A) shows the likely plan view configuration of the original flow channel at the 310.0-310.6 meter (1017-1019) foot elevation prior to MICP sealing. The casing in this depth in the borehole is not centered meaning that there could be a narrow side in the annular space, which was not completely filled with cement leaving a void. It was approximated that there could have been a gap that comprised 40% of the circumference of the casing. Panel (B) shows the cement bond log prior to MICP injection but after the side wall cores had been drilled at 310.0, 310.27, 310.6 meters (m) (1017, 1018, 1019 feet) bgs (white circles inside black ovals indicate location of core points). Panel (C) shows the cement bond log scanned after MICP treatment. Red=gas, blue=liquid, tan=solids detected in the near wellbore environment between the casing and the formation. MICP sealing resulted in a substantial increase in solid material in the 9.1m (30 foot) interval above the side wall core injection points. Note that at an elevation of about 301.75 m (990 ft bgs, red circle) the solid material appears to completely surround the casing without visible voids.

Conclusions (Conclusions)

The three lines of evidence (reduced injectivity, reduced pressure fall-off and increased solids content) offer compelling evidence that the MICP sealing field demonstration at Gorgas was successful. MICP treatment resulted in significantly reduced injectivity which corresponded to substantial deposition of precipitated solids along the originally detected flow channel and a significant reduction in pressure fall-off after the well was shut in. As the MICP treatment technology moves toward commercial application, additional research and development will be performed to further improve methods of fluid delivery and increase the depth and temperature range where the treatment can be applied.

Section 3.2 Reducing undesired subsurface permeability using microbially-induced calcium carbonate precipitation (MICP): a field demonstration

Abstract (Abstract)

Microbially-induced calcium carbonate precipitation (MICP) is an emerging biotechnology for wellbore integrity applications including sealing defects in wellbore cement and modifying the permeability of rock formations. The goal of this field demonstration was to characterize a failed waterflood injection well and provide proof of principle that MICP can reduce permeability in the presence of oil using conventional oilfield fluid delivery methods. We compared well logs performed at the time the well was drilled with ultrasonic logs, sonic cement evaluation, and temperature logs conducted after the well failed. Analysis of these logs suggested that, rather than entering the target waterflood formation, injectate was traveling through defects in the well cement to a higher permeability sandstone layer above the target formation. *Sporosarcina pasteurii* cultures and urea-calcium media were delivered 2290 ft (698 m) below ground surface using a 3.75 gal (14.2 L) slickline dump bailer to promote mineralization in the undesired flow paths. By Day 6 and after 25 inoculum and 49 calcium media injections, the injectivity [gpm/psi] had decreased by approximately 70%. This demonstration shows that 1) common well logs can be used to identify scenarios where MICP can be employed to reduce system permeability, remediate leakage pathways, and improve waterflood efficiency, and 2) MICP can occur in the presence of hydrocarbons.

Introduction

Waterflooding for secondary oil recovery

Oil and gas extraction wells are becoming increasingly common features of the landscape as hydrocarbon production expands from conventional sandstone reservoirs to unconventional reservoirs like shale and tight sand formations. In 2014, there were 1,039,000 producing oil and gas wells in the United States, compared to 735,000 in 2000 and in 2017, US oil production surpassed 10 million barrels per day (bpd)[153]. In conventional reservoirs and even under the best conditions, less than half of the original oil in place is typically extracted during primary production, the period when oil and gas flow freely from the reservoir rock due to a release of formation pressure [154, 155]. As primary production declines, oil and gas producers may employ waterflooding to promote secondary recovery. Waterflooding involves injecting water or brine into the oil-bearing formation to displace and sweep out residual hydrocarbons while also restoring formation pressure. Spatial heterogeneities in the reservoir rock and differences in fluid viscosities, however, can lead to conformance problems during waterflooding including viscous fingering, preferential flow through more permeable rock, and channel flow in fractures in well cement or the formation rock [156-158]. This field study focused on mitigating poor waterflood efficiency caused by defects in the wellbore cement. Cement defects can lead to compromised wellbore integrity, leakage pathways to functional aquifers and/or thief zones.

Wellbore cement integrity

With the increase in hydrocarbon production, comes increased concern for maintaining high water quality in aquifers above hydrocarbon-bearing strata and preventing emission of fugitive gases to the atmosphere via leaky wellbores [159]. As the well provides a direct conduit between the subsurface reservoir and the atmosphere, establishing and maintaining zonal isolation between geologic strata is vitally important for both production and injection wells. A recent study found that up to 9% of active wells drilled since 2000 in Pennsylvania, USA, have compromised cement or issues with casing integrity [160]. Moreover, waterflooding and fluid injection to improve oil recovery may exacerbate cement failure in aging wells [161].

Properly constructed (and abandoned) wells employ an impervious cement sheath between the well casing and the formation to prevent upward migration of fluids and gases. However, the cement sheath can degrade over time under the influence of thermal, geo-mechanical, and chemical stresses [20, 161-163]. Fluids can seep into fractures and channels in the cement or flow through micro-annuli between the casing and cement or between the cement and formation [21, 159, 161, 164, 165]. Depending on the nature of the cement defect and the adjacent rock formation, the fluid can migrate up the wellbore or into other rock strata.

Repairing a leakage pathway or wellbore cement defect is non-trivial. Cement squeezes are commonly used to repair larger defects. Fine cements can be injected through perforations in the casing to seal apertures as small as 120 µm before the viscosity of the cement and required pumping pressures interfere [49, 166]. According to industry estimates, up to 50% of the time, fine cement injection is not successful at sealing the leakage pathway [167]. Gels, resins, and epoxies can be used to repair smaller defects, on the order of 1-100 µm, though these technologies are in an early stage of technological development and are more expensive than fine cement [31, 49]. A major challenge in remediating wellbore leakage is proper placement of the sealing material to provide a strong and stable seal over time.

Microbially-induced calcium carbonate precipitation (MICP)

Recent research has explored how microbial metabolic processes can be harnessed to produce bio-cement consisting of precipitated calcium carbonate. Many strains of bacteria found naturally in soil and groundwater are ureolytic, meaning they produce the urease enzyme which catalyzes the hydrolysis of urea, also called ureolysis [119]. Ureolysis provides a source of nitrogen for the microbes, raises the solution pH, and produces carbonate ions. When there is also sufficient calcium to exceed saturation conditions, calcium carbonate ($CaCO_3$) precipitation can occur.

Sporosarcina pasteurii, the ureolytic bacterium used in this demonstration, attaches to rock and cement surfaces with extracellular polymeric substances (EPS), forming a biofilm [120]. $CaCO_3$ precipitation occurs in association with the microbial biofilm matrix due to the mass transfer limitations and localized chemical gradients within the hydrogel structure [118]. Additionally, the biofilm is believed to provide nucleation sites for precipitation to initiate [63, 168]. With continued injection of fresh microbial cultures and mineralization-promoting fluids, the $CaCO_3$ mineral thickens, bridging pore throats and fractures, filling voids, and sealing flow pathways.

Previous field demonstrations of MICP

Microbially-induced calcium carbonate precipitation (MICP) is being researched as an emerging technology for subsurface engineering applications that include both sealing defects in wellbore cement [39, 42, 49] and modifying the permeability of rock formations for possible enhanced oil recovery applications [1, 169, 170]. Most research related to MICP has been conducted at the laboratory scale, though several studies of note have been performed at field scale. Fujita *et al*. (2008) stimulated native ureolytic microbes in a calcite-saturated aquifer to investigate the potential for co-precipitating radionuclides from contaminated groundwater [171]. Burbank *et al*. (2011) observed increased resistance to liquefaction in saturated soil following stimulation of indigenous ureolytic microbes and infiltration of calcium chloride solution [172]. Gomez *et al*. (2015) used surficial application of MICP to stabilize loose sands and reduce erosion at a mine site in Canada [35], and van Paassen *et al*. (2010) performed *in situ* seismic measurements during MICP bio-grouting in a 100 m^3 sand-filled test cell [173]. Cuthbert *et al*. (2013) applied MICP to reduce transmissivity in a rock fracture 24 m below ground surface (bgs)[43]. The first field demonstration in a wellbore environment successfully used MICP to seal a horizontal "pancake fracture" in tight sandstone at a depth of 340 m (1115 ft) bgs [40]. A subsequent demonstration in the same well resulted in MICP sealing of compromised wellbore cement 310 m (1017 ft) bgs [49]. To our knowledge, no field scale demonstrations of MICP have been performed in a working oil or gas well or in the presence of hydrocarbons prior to the current work.

The current study - overview

This field study was conducted in Indiana, USA, at a water injection well used for secondary oil recovery. Since the well had experienced a significant drop in waterflood efficiency, the goal of this field demonstration project was twofold: 1) to use available downhole characterization methods to develop a valid conceptual model of waterflood flow paths, and 2) provide proof-of-principle that MICP can significantly reduce system permeability in the presence of oil and using conventional oilfield fluid delivery methods. The well, located in Posey County, Indiana, had been used as a water injection well to sweep residual oil to production wells from 2010 – 2012 when injection pressure was lost, and the well was removed from service. We compared well logs performed at the time the well was drilled in 2006, including gamma ray, dual induction, and compensated density and neutron logs, with ultrasonic logs, sonic cement evaluation, and temperature logs conducted after the well failed. Analysis of these logs suggested that, rather than entering the formation targeted for waterflood, injectate was traveling through defects in the well cement to a higher permeability sandstone layer above the target formation (Figure 40). Formations like this sandstone layer are also referred to as 'thief zones.' We applied MICP to validate its potential to address oil and gas wellbore integrity challenges. Microbial cultures and urea-calcium media were delivered using a 3.75 gal (14.2 L) slickline dump bailer to promote mineralization and reduce flow through the undesired flow paths. Progress in the field was assessed by monitoring the relationship between injection flowrate and pressure. The pressure-flow relationship describes the capacity of the system to receive fluids without fracturing the formation, also known as the system's injectivity. At the end of the demonstration, samples of mineral precipitate were collected from the injection tubing for bio-chemical analyses.

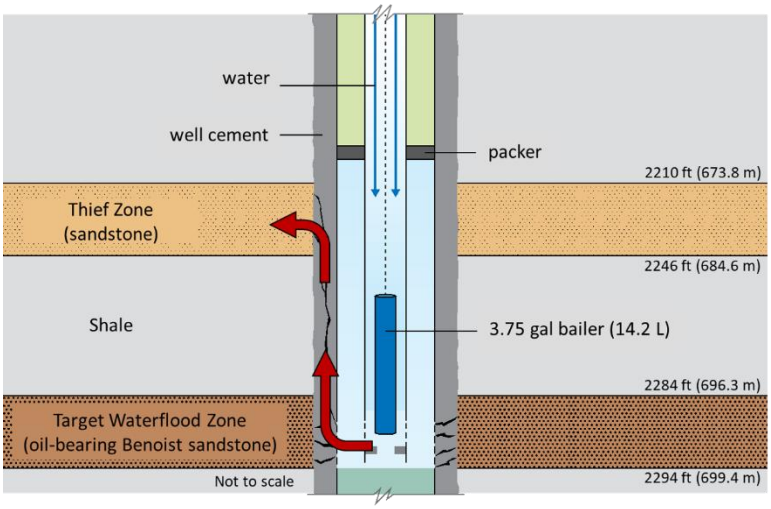

Figure 40. Conceptual model: a channel in the wellbore cement of the water injection well used for this field demonstration allowed injected fluids to travel to a more permeable sandstone layer 38-84 feet (10.4 – 25.6 m) above the target waterflood zone, which is a tight oil-bearing sandstone. Microbial cultures and urea-calcium media were delivered using a 3.75 gal (14.2 L) slickline dump bailer to promote mineralization and reduce flow through the undesired flow paths.

Materials and Methods (Experimental Methods)

Site characterization

The subject well consists of a 7-7/8 inch open hole drilled to 2540 ft (774.4 m) bgs. Gamma ray and dual induction logs (Figure 41), as well as compensated density and compensated neutron logs (not shown), were acquired prior to casing the well in 2006. These logs are typically used to identify the lithology and porosity of rock formations and differentiate between oil- and water-bearing strata. The logs showed tight oil-bearing Benoist sandstone between 2284 – 2294 ft (696.3 – 699.4 m) bgs, overlaid by shale up to approximately 2246 ft (684.6 m) bgs, and a higher permeability water-saturated sandstone between 2210 – 2246 ft (673.8 – 684.6 m) bgs. The well was fitted with a 5-1/2 inch 15.5 lb/ft steel casing to a depth of 2319 ft (707 m) (bgs). The annulus between the open hole and the steel casing was filled with well cement and the well casing was perforated between 2284 – 2294 ft (673.8 – 684.6 m) bgs to access the oil-bearing Benoist sandstone.

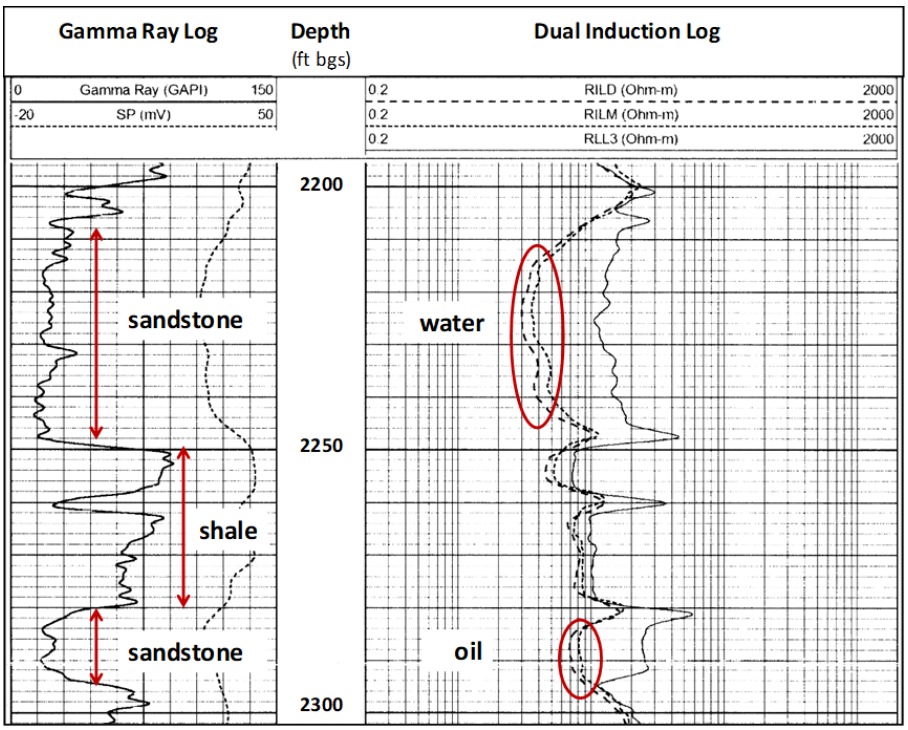

Figure 41. Gamma ray and dual induction logs completed in 2006 prior to casing the subject well identified an oil-bearing sandstone, overlaid by shale and a water-bearing sandstone.

Between 2010 - 2012, 966 barrels of water per month (BWPM) on average were injected at 1,400 – 1,500 psi (9.7 – 10.3 MPa), yielding 500 barrels of oil per month (BOPM) at a nearby producing well. In late 2012, injection pressure dropped to approximately 550 psi (3.8 MPa) and water injection increased to an average of 1,900 BWPM. Over the same period, oil production decreased to approximately 300 BOPM. The change in injectivity could have been caused by fracturing the Benoist sandstone with the high injection pressures or could indicate a failure of the wellbore cement.

To identify the cause of the change in injectivity, Loudon Technical Services (LTS) and Schlumberger Carbon Services (SLB) evaluated the well with sonic and ultrasonic wellbore logging tools. These borehole tools can be used to image the condition of the casing and cement annulus by transmitting acoustic waves into the formation and receiving the attenuated, reflected waves at the detector. Changes in waveform amplitude arise from differing densities of material through which the acoustic or ultrasonic waves pass. Based on the waveforms detected, these tools can identify the presence of solids, liquids, or gases behind the casing via flexural attenuation of the acoustic impedance (SLG map, Schlumberger), detect leaks in the well casing, or evaluate the cement-to-casing and cement-to-formation bond [174]. A conventional sonic cement bond log (CBL) with variable density logging (VDL) can indicate whether there is unbonded pipe or a good cement bond[175] but cannot identify small channels within the cement annulus.

The SLG map produced from an ultrasonic Isolation Scanner (IBC) log showed the presence of good cement bonding above the elevation where a packer was previously set at 2,218 ft (676.2 m) bgs (Figure 42). Below this depth and including the location of the perforations used for waterflooding, there were no valid waveforms detected with the tool, likely due to heavily corroded casing. The CBL-VDL log was collected with a different tool string and was less influenced by the condition of the casing. The CBL-VDL appears to suggest that good cement may extend to approximately 2245 ft (684.5 m) bgs as indicated by the wavy lines of the VDL (Figure 42). Parallel vertical lines indicate low signal attenuation due to poor cement bonding. No acoustic data, sonic or ultrasonic, were collected in the immediate vicinity of the perforations due to the presence of a bridge plug below the perforations.

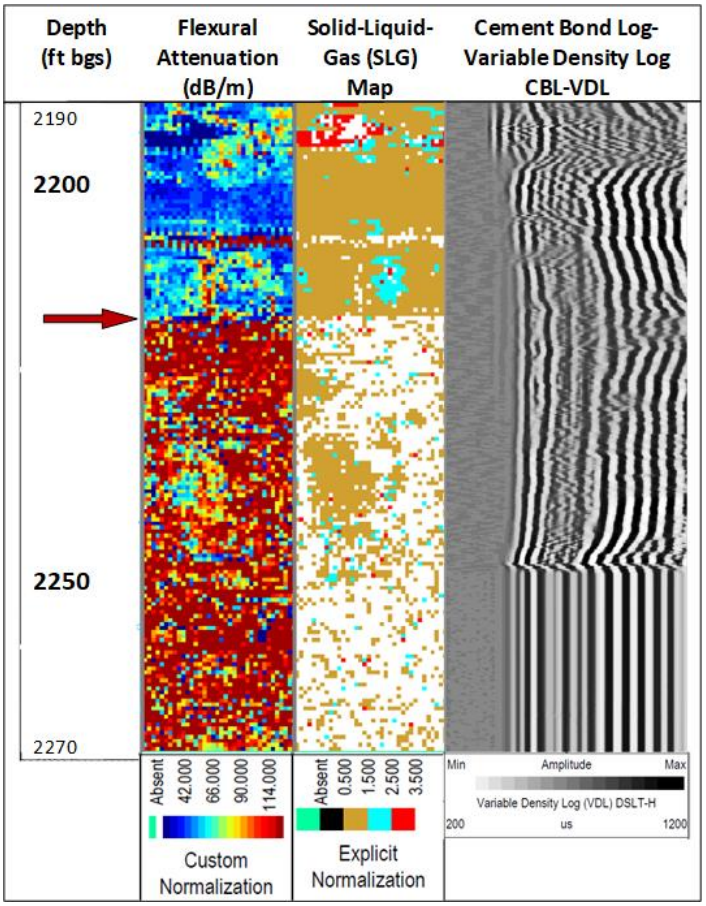

Figure 42. Sonic and ultrasonic well logging data collected to characterize well and identify cause of change in injectivity. The packer had been previously set at 2,218 ft (676.2 m) bgs (arrow) and well-bonded cement was observed above this elevation, shown as tan in the SLG map and in blue on the flexural attenuation log. Below 2,218 ft (676.2 m) bgs, corrosion of the casing prevented collection of useful data with the ultrasonic tool. The CBL-VDL appears to show good cement bonding to a depth of approximately 2245 ft (684.5 m) bgs, as indicated by the wavy lines of the VDL. Perforations for water flood injection are located 2284 – 2294 ft (696.3 – 699.4 m) bgs below the bottom of the well logs shown.

Since these well logs provided little information regarding the zone of interest, a wellbore temperature log was collected. Temperature logs can detect deviations from the reference temperature gradient in the well related to fluids of a different temperature entering or exiting the borehole [176]. Cool fluids are injected into the well and the temperature logging tool is passed through the wellbore zone of interest periodically, monitoring the change in temperature as the strata warm the well casing and fluids toward equilibrium. The measurement is sensitive to temperature anomalies in the region just outside the well casing and can be used to detect fluid flow through wellbore cement defects. Thus, the log was able to identify which failure scenario – fractured formation or failed cement - was more likely. The temperature log positively identified fluid travelling from the perforations along the outside of the casing in failed cement to an elevation of approximately 2230 ft (679.9 m) bgs. The temperature log appears later in the paper as Figure 44. Correlating the temperature log data to the original well logs collected in 2006 suggests that the well cement failed, possibly due to elevated injection pressures, up to an elevation where the formation transitioned from relatively impermeable shale to higher permeability sandstone thief zone above 2245 ft (684.5 m) bgs. As the injected water dispersed through the thief zone matrix, pressure on the wellbore cement and the volume of flow through it likely decreased. Certainly, above 2218 ft (676.2 m) bgs the cement provided a strong seal against upward fluid migration when the acoustic logs were collected.

In summary, based on knowledge of the lithology from the 2006 well logs, sparse information regarding cement condition from the acoustic logs, and evidence of flow through the cement annulus from the temperature log, the conceptual model shown in Figure 40 was developed and was used to design the injection strategies applied during the field demonstration. Pressure and flow data collected at the same time as the temperature log were used to estimate the aperture of the cement fracture. Assuming the flow passed through a single channel in the well cement and applying the cubic law [57] which describes a fluid's hydraulic behavior in a fracture, the aperture in the well cement was estimated to be approximately 400 μm at the narrowest point. MICP has been used to seal cement defects of similar dimensions in a laboratory study [177]. Moreover, the rock matrix of the sandstone thief zone provides an appropriate environment for MICP to occur [40, 178] thereby reducing permeability of the thief zone and system at large.

MICP field demonstration design

Collaborators on this project include the Center for Biofilm Engineering at Montana State University (CBE/MSU), Loudon Technical Services (LTS), and Montana Emergent Technologies (MET). Schlumberger (SLB) provided well services as a subcontractor to MET. Gallagher Drilling operates the subject well and provided access to it for the field demonstration. CBE/MSU designed the field demonstration protocol, oversaw implementation, and analyzed results. LTS provided field oversight, coordinated equipment and subcontractors for the field work, and helped with the analysis of the results. MET assisted with field implementation and design and construction of the mobile field laboratory.

Prior to the demonstration, Gallagher removed the plastic-lined injection tubing and injection packer. A 2-7/8 inch tubing "work string" with a tension-set packer was deployed in the well. The packer was set between 2187 – 2194 ft bgs (666.8 – 668.9 m) to isolate the region of interest

from the upper strata, and the tubing landed in the tubing head in preparation for the experiment. LTS and SLB flushed the well with approximately 700 gal (2650 L) of fresh water to establish an initial injection pressure and flow relationship. CBE/MSU and MET arrived on-site with the mobile laboratory where microbial cultivation was underway.

The 2-7/8 inch tubing accommodated a 3.75 gal (14.2 L) dump bailer used to deliver the biomineralization-promoting fluids. The bailer was lowered down the well tubing by a slickline rig until impact on a collar stop located at 2288 ft bgs (697.6 m). The force of impact was intended to shear a pin on the bailer, opening a valve and releasing the fluids contained within. Water injected down the 2-7/8 inch tubing flushed the biomineralization fluids out of the bailer through a perforated pup joint at 2285 – 2288 ft bgs (696.6 – 697.6 m) and out of perforations in the steel well casing. Once outside the well casing, the biomineralization fluids were assumed to follow the most hydraulically favorable path, i.e. through the fractured cement and into the thief zone sandstone where precipitation was desired. The duration of the bailer round trip was approximately 30 minutes.

Biomineralization-promoting media

Two types of fluids were injected into the well to promote MICP: 1) microbial cultures provided a source of the urease enzyme to catalyze ureolysis and a biofilm template for mineral nucleation and 2) urea-calcium media promoted supersaturated conditions favoring precipitation of calcium carbonate. Overnight cell cultures of *S. pasteurii* (ATCC11859) were started from frozen stocks in 18.5 g/L Brain Heart Infusion (BHI, Becton Dickinson, Franklin Lakes, NJ) media plus 2% urea in flasks placed in a 30°C incubating shaker. These overnight cultures varied in volume from 150 – 500 mL, with most being 300 mL. The overnight cultures were added directly to fresh yeast extract-based nutrient solution (YE-) consisting of 15.5 g/L yeast extract (Acros Organics, Geel, Belgium), 24 g/L urea (Dyno Nobel, Inc, Deer Island OR), and 1 g/L NH_4Cl (BASF USA, Florham Park, NJ) for a final volume of 15 L and mixed on a stir plate for approximately 24 hours prior to injection. During the second half of the experiment, some 15 L cultures were also inoculated with previous batches of inocula. Supplemental aeration was provided by aquarium air pumps (Aqua Culture MK-1504 and Topfin AIR-2000) fitted with 5-inch bubble diffusers (Aqua Culture, Walmart). The 15 L inoculum cultures were heated by seed heating mats wrapped around the carboy and by heating the mobile laboratory trailer to approximately 75 – 80 °F. Inocula injected on Day 6 were amended with 50 – 200 g Jack Bean meal (Sigma-Aldrich, St. Louis, MO), a plant-based source of the urease enzyme, and 100-250 g urea per 15 L batch immediately prior to filling the bailer to augment urea hydrolysis in the treatment zone. Before filling the bailer for an injection, the pH and electrical conductivity (EC) of the cultures were measured. Samples were collected for urea analysis with the Jung Assay [136], population analysis using the drop plate method [146], and optical density (OD 600).

Calcium media (YE+) (125 g/L $CaCl_2*2H_2O$ (Peladow, Occidental Chemical Corp., Dallas, TX), 72 g/L urea, 3 g/L NH_4Cl and 9 g/L yeast extract) was mixed several hours prior to injection in 15 L batches. Each batch was mixed with a drill-powered mixer and sampled for pH, urea, and Ca^{2+} prior to filling the bailer.

Recent laboratory studies have suggested that more frequent inoculation, or stimulation of bacterial growth with nutrient solution, improves the efficiency of ureolysis-driven calcite precipitation [177]. Therefore, a cycle of one inoculum injection followed by two calcium media injections was applied. The field demonstration design included 3 – 4 such cycles during a work-day at the field site.

Experiment termination and post-experiment analysis

The demonstration was concluded on Day 6 due to approaching inclement weather which would have created hazardous conditions at the wellhead. The crane, slickline truck, and mobile laboratory were removed from the site. There was no activity in the well for approximately 2 weeks until LTS returned to the site to conduct a post-MICP treatment injection test, acquire a temperature log, and remove the tubing string from the well.

Accumulated mineral material not present during the placement of the 2-7/8 inch tubing string was scraped from the perforated pup joint following removal of the tubing string from the well. Approximately 50 g of the mineral material was sampled for analysis at MSU. Some of the material was pulverized for analysis with XRD; some was digested with acid to quantify calcium content, while other samples of the material were imaged using FE-SEM and confocal microscopy. DNA was also extracted for sequencing from both the solid mineral and from a liquid enrichment inoculated with the mineral.

Sub-samples of the pup joint mineral material were crushed, dried, and weighed before being subjected to digestion in 10% trace metal grade nitric acid to dissolve the mineral components. The digestate was analyzed with a colorimetric assay to quantify the calcium content [179]. Sub-samples of the pup joint mineral material were also dried, pulverized with a mortar and pestle, and lightly sprinkled onto a glass slide coated with a thin layer of petroleum jelly for analysis with a Scintag X1 Powder X-ray diffractometer (XRD) and a Cu k-alpha X-ray source.

Sub-samples from both the outer surface and the inner region of the pup joint mineral material were dried and crushed prior to FE-SEM imaging. Sub-samples mounted for micro-imaging were sputter-coated with Ir for 1 minute at 20 mA. High resolution micrographs were collected on a Zeiss Supra 55VP field emission scanning electron microscope at 1.0 kV and a working distance of 3 – 5 mm.

An outer surface sub-sample of the mineral material was prepared for confocal microscopy by staining with 1 µL SYBR Green I nucleic acid stain in 1 mL Milli-Q deionized water for 1 hour in the dark. After staining, the sub-sample was rinsed with Milli-Q water and imaged using a 488 nm laser using an upright Leica SP5 confocal scanning laser microscope (CSLM). Images were processed for qualitative analysis using Imaris software (Bitplane, Zurich, Switzerland).

A small piece of the mineral material, approximately 2 g, was placed in a 500 mL media bottle containing 150 mL sterile CMM- media (3 g/L Difco Nutrient Broth, 20 g/L urea, 10 g/L NH_4Cl) to culture potential ureolytic microbes entrained in the mineral. The bottle was placed on a shaker table at 150 rpm at room temperature for 2 weeks. DNA was extracted from the liquid enrichment and also from an untreated 500mg sample of the mineral material using the MP

Biomedicals FastDNA™ Spin kit for soil along with the MP Biomedicals FastPrep®-24 bead beater. Extracted DNA concentrations were determined with an invitrogen™ Qubit® fluorometer. q-PCR and 16S rRNA gene sequencing was performed on both samples as described in the Supporting Information of [40]. Samples from the liquid enrichment were plated on BHI agar plates amended with 2% urea to isolate predominant microbes. Four of the isolates were identified with 16S rRNA gene sequencing and cultured for batch studies to assess their ureolytic activity.

Results and Discussion (Results and Discussion)

Reduced Injectivity

The flow – pressure ratio [gpm/psi] is an indication of the ease with which fluids can move through fractures, cement defects, or the pore space of a rock formation; a lower value implies lower permeability and limited injectivity. To improve readability, we will refer to this flow-to-pressure ratio hereafter as injectivity. After 25 inoculum injections (approximately 95 gal. (360 L)) and 49 calcium media injections (185 gal (700 L)), the injectivity of the system had decreased from 10.4×10^{-3} gpm/psi to 3×10^{-3} gpm/psi, a reduction of approximately 70% (Figure 43). During the first two days, the total volume of water injected after each bailer and actual pumping flow rates were recorded only periodically. On Day 4, several failed bailer dumps, shown as open markers in Figure 43, were followed by an increase in injectivity. In these instances, water pumped down the 2-7/8" tubing to push the bailer contents into the formation only further diluted the reactants in the cement defect and rock matrix since the bailer failed to release its contents. The cause of the pressure loss is unknown, though possible explanations include breakthrough of a thin MICP mineral seal, a new fracture in the wellbore cement, or expansion of flow to higher portions of the sandstone thief zone. The injectivity again decreased on Days 5 and 6 after the Day 4 increase. Pumping tests conducted approximately two weeks after the end of the field experiment yielded an injectivity consistent with those recorded at the end of Day 6, depicted as the last 3 data points in Figure 43.

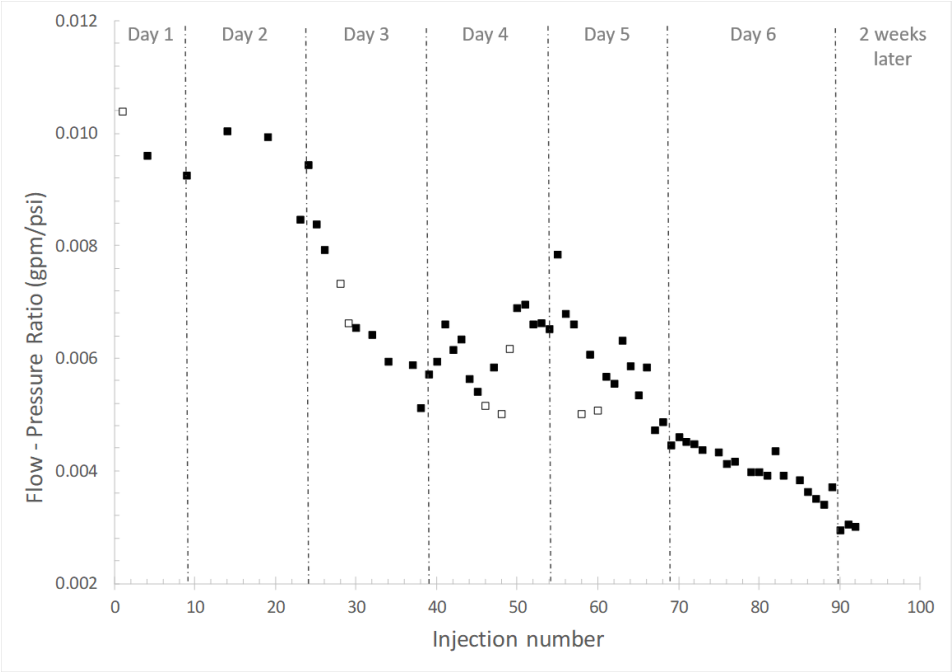

Figure 43. The flow-pressure ratio, or injectivity, declined by 70% over six days of injection of biomineralization-promoting fluids. Open markers indicate injections when the bailer delivering the fluids downhole failed to open and release the mineralization-promoting fluids. Vertical lines mark the days of the experiment. The last three data points were measured two weeks after the end of the field demonstration.

Post-experimental well characterization

Temperature logs were acquired over the zone of interest before and after the MICP treatment. Spacing of the lines indicates the rate at which the temperature recovers following injection of a colder fluid. More closely spaced lines indicate slower temperature recovery caused by higher volumes of cold water reaching the area. More widely spaced lines suggest that less water was injected into the region and temperature variation is dominated by the thermal gradient of the well. Relative to the temperature log conducted before the MICP treatment (Figure 44, left), the post-MICP temperature log shows more widely spaced temperature values between the passes of the instrument (Figure 44, right). Comparison of these two temperature logs provides evidence that significantly less water traveled into the channel above 2280 ft (695 m) bgs. There is little evidence of influence from the cooler fluids above 2245 ft (684.5 m) bgs. The post-demonstration temperature log suggests MICP treatment sealed or partially sealed the leakage pathway to the thief zone and provides validation of the conceptual model explaining the change in injectivity and mode of well failure.

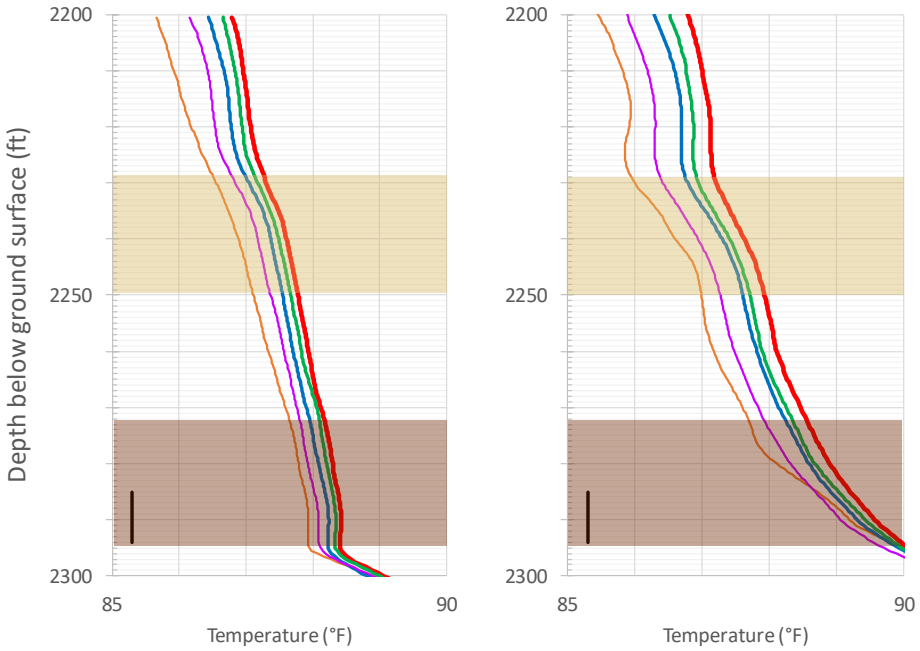

Figure 44. Temperature logs collected pre-MICP (left) show closer spacing of the temperature log lines indicating fluid flow through a channel between the perforated zone (black bar) in the target waterflood zone (brown shading) and the thief zone (tan shading). Post-MICP (right) shows reduced fluid flow through the region of the channel after treatment, indicated by the wider spacing of the measurement passes.

Mineral precipitate analysis

The outer surface of the mineral precipitate that formed on the perforated pup joint where the bailer dumped the biomineralization-promoting fluids was coated in a black substance while the inner layers were lighter colored and grainy in appearance (Figure 45). This material was not present when the tubing string was deployed in the well prior to the field demonstration. It is likely that the mineral material accumulated over the course of the field demonstration due to the injection of MICP-promoting fluids.

Figure 45. Mineral precipitation was observed on the downhole tubing following completion of the field demonstration, visible as the bumpy coating on the perforated pup joint (left). The outer surface was darker in color than the inner regions of the precipitate (right), perhaps due to exposure to wellbore fluids following the field demonstration.

Calcium assays of two samples of the mineral showed that calcium ion composed on average 39.6% of the sample mass, consistent with gravimetric measurements that indicate calcium accounted for 37.7% of the sample mass. By stoichiometry, calcium could be a maximum of 40% of digested $CaCO_3$ mass. XRD results for two sub-samples of the pup joint mineral indicate that the mineral consists entirely of calcite ($CaCO_3$), data not shown.

FE-SEM images of the pup joint mineral sample show crystal structures consistent with calcite minerals as well as round vaterite-like forms (Figure 46) and amorphous deposits. No cells were readily apparent in the FE-SEM micrographs, even after lightly washing the samples in a 1% HCl solution to dissolve the top layer of mineral. Chemical and microscopy analyses of the mineral material removed from the pup joint confirm the material to be calcium carbonate, as would be expected following the injection of MICP-promoting fluids.

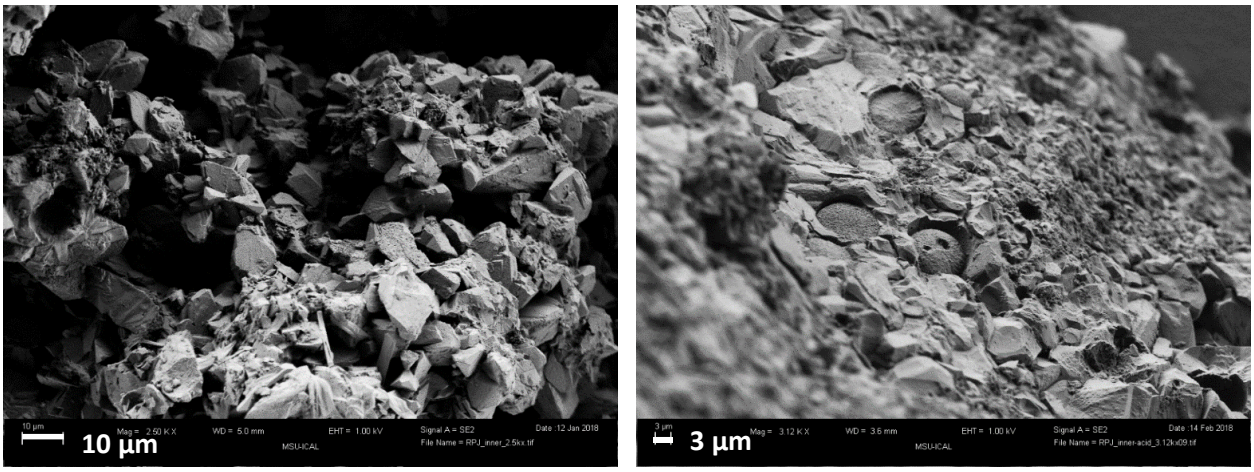

Figure 46. FE-SEM image of the mineral scale which accumulated on the surface of the pup joint downhole in the subject well after rinsing with 1% HCl solution. Material collected from the inner region of the scale shows angular crystals consistent with calcite and amorphous mineral forms (left) while the outer region of the mineral scale also includes examples of a round crystal morphology that is consistent with vaterite (right).

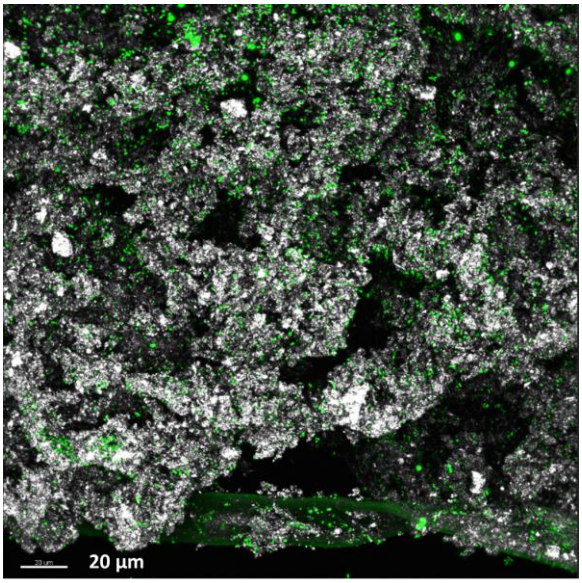

Figure 47. A 2D projection of a combined reflection and fluorescent image from a confocal microscope shows cells (SYBR Green I) in association with mineral precipitation. Scale bar is 20 µm. Image by Sobia Anjum, image analysis by Betsey Pitts.

Although no cells were observed during FE-SEM imaging, the confocal images revealed a dense microbial population associated with the precipitate, as would be expected with MICP. The 2D projection of combined reflection and fluorescent confocal images of the mineral is shown in Figure 47. The green flecks, labeled with SYBR-Green I nucleic acid stain, are likely bacteria though DNA-containing cell fragments could fluoresce as well. Since no attempt was made to use aseptic sampling methods, the microbes present may have been introduced at any time,

including after the tubing string was removed from the well though samples were taken as quickly as possible. Further microbiological analysis methods were applied to identify organisms that could have participated in the MICP process.

DNA was extracted both from the solid mineral and from a liquid enrichment. More microbial diversity was observed from the solid sample where the genus of bacterium injected, *Sporosarcina*, made up only 0.3% of the microbial community. In the enrichment, *Sporosarcina spp.* accounted for 41% of the community (Figure 48). This result is not unusual since the nutrient solution used in the enrichment is designed to culture ureolytic microbes. Isolations of microbes from the enrichment culture identified three organisms - *Sporosarcina pasteurii*, a *Shewanella* sp., and a *Sphingobacterium sp.* – that were capable of hydrolyzing urea in subsequent batch activity studies. This suggests that native ureolytic species of microbes may have been stimulated by the injections of nutrient solution and may have participated in the MICP process during the field demonstration.

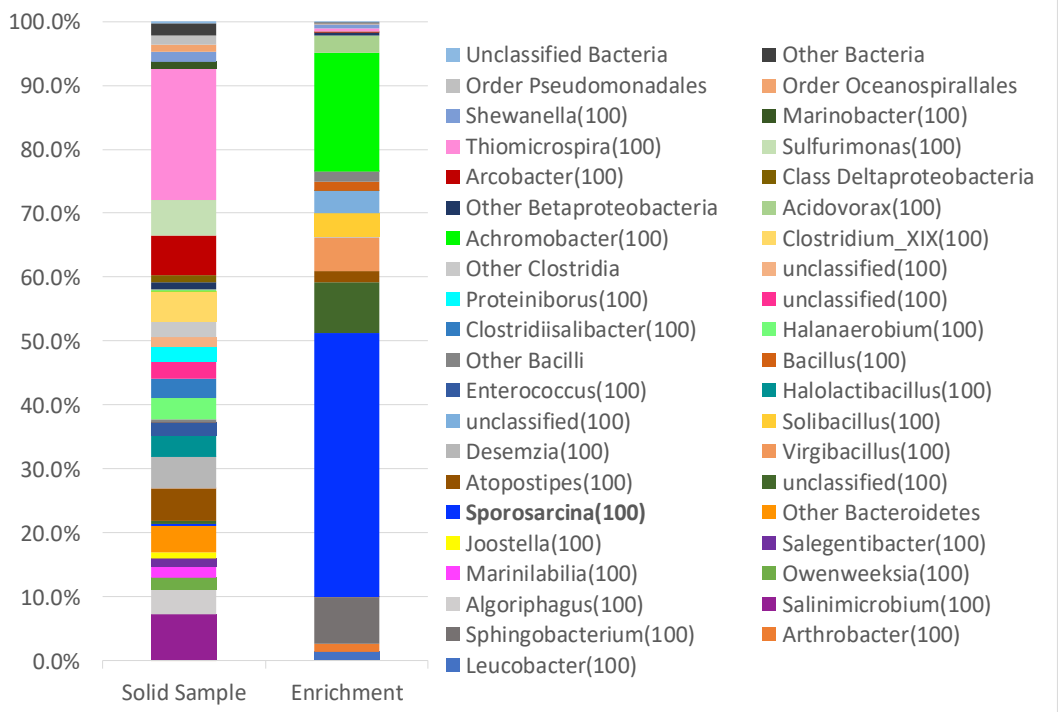

Figure 48. The microbial community extracted from the carbonate mineral itself resulted in a rich diversity with only a small percentage (0.3%) of the population identified as Sporosarcina spp., the injected microorganism. In contrast, in the liquid sample that was enriched in the laboratory Sporosarcina spp. were dominant making up 41% of the population.

Conclusions (Conclusions)

This field demonstration used injections of MICP-promoting fluids in a water injection well with the intent to 1) validate a conceptual model of wellbore cement failure derived from analysis of well logs and pressure – flow data and 2) provide proof of principle that MICP can reduce system permeability in the presence of oil and using conventional oilfield fluid delivery methods.

Pressure and flow rate were monitored during the MICP injections, revealing a 70% decrease in injectivity over the course of the demonstration. A post-treatment overnight injection test with a final rate of 2.25 gpm at 740.5 psia indicated the injectivity was stable two weeks after the end of the experiment. The post-treatment temperature log showed the majority of the injectate staying contained in an area within a few feet of the perforations, indicating that flow through the cement defect to the thief zone was significantly curtailed. When the MICP injection tubing was removed from the well there was considerable calcite precipitation apparent on the perforated pipe sections. Mineralogical and microbiological analyses of the mineral removed from the injection tubing confirm that MICP can occur downhole in the presence of oil.

The volume of calcium carbonate that formed in undesirable flow paths in the wellbore cement channel and sandstone thief zone was sufficient to reduce the leakage pathway but did not restore the historic injection flow–to–pressure relationship of approximately 1 gpm at 1400 psi (3.8 L/min at 9.7 MPa). In the authors' opinion, the most likely explanation is related to the volume of the void space to be filled by $CaCO_3$ precipitation relative to the ability of the bailer to deliver adequate volumes of microbes and calcium media in the timeframe allotted for the demonstration. A subsequent (or second) field demonstration was therefore planned in the same well where larger volumes of reactants were injected in an attempt to restore the historic injection flow–to–pressure relationship.

The work presented here shows that common well logs, including sonic, ultrasonic, and temperature logs, can be used to identify scenarios where MICP can be employed using conventional methods to reduce system permeability, remediate leakage pathways, and improve waterflood efficiency. Furthermore, this study verifies that the MICP biochemical reaction can occur in the presence of hydrocarbons.

Section 3.3 Restoring waterflood capacity with MICP using a continuous injection strategy

Abstract (Abstract)

This manuscript describes the second of two field demonstrations of microbially-induced calcium carbonate precipitation (MICP) performed in a failed waterflood injection well in Indiana, USA. In 2012 fracture-related flow pathways developed in the wellbore cement causing injection water to by-pass the oil-bearing formation and enter a high permeability sandstone thief zone, thereby substantially reducing injection pressure. In the first field demonstration (submitted for publication), our study team characterized the well's mode of failure and successfully applied MICP to reduce flow through the defective cement. However, because the MICP treatment was conducted using a bailer system, the degree of permeability reduction achievable was not adequate to fully restore the historic injection pressure of 1,400 psi at 1 gpm. For the second field demonstration injection scenario (reported herein) a continuous injection system was developed which substantially increased the injection volume of MICP-promoting fluids. Two strategies were implemented to produce more ureolytic microbes: 1) re-suspending concentrated frozen cells immediately prior to injection and 2) injecting fairly large amounts of live cells directly after growing them on site in large bioreactors. Multiple 'pulses' of microbes and urea-calcium media were delivered in sequence into a string of 1-inch diameter tubing separated by brine 'spacers' and injected continuously at a flowrate of 3.4 - 1.4 gpm (12.8-5.3 L/min). During the third day of injection, an injection pressure of 1384 psi (94.2 atm) at a flowrate of 1.4 gpm (5.3 L/min) was achieved and the experiment was terminated. This study demonstrates that MICP can be employed successfully in large-volume applications where the timeframe for the delivery of reactants is limited. This finding has significant relevance for commercialization of the MICP biotechnology in the oil and gas industry.

Introduction

Field Studies

As described in previous sections, there are a number of proposed engineering applications of MICP. Only a few field demonstrations have been described in the literature, our group has now performed five field tests using MICP in various subsurface applications. Two field demonstrations of microbially-induced calcium carbonate precipitation (MICP) have recently been performed in a waterflood injection well in Posey County, Indiana, USA. The second of the two field demonstrations is the subject of this section. The first field demonstration focused on characterizing the failure scenario of the waterflood injection well and demonstrating the proof-of-concept that MICP could be effective to reduce undesirable permeability in the presence of hydrocarbons[180]. For approximately two years, the subject well was used to improve secondary oil recovery by injecting waterflood fluids into a tight oil-bearing sandstone, thereby displacing residual oil and maintaining high formation pressure. Injection pressure was subsequently lost after the wellbore cement was compromised (channeled) and the well was removed from service. Analysis of gamma ray, dual induction, acoustic, and temperature well logs suggested that injectate was traveling through a leakage pathway in the wellbore cement to a higher permeability sandstone, or thief zone, located approximately 30-70 feet (9.1m-21.3m) above the oil-bearing formation targeted for waterflood.

In the first field demonstration, our study team used a 3.75-gal (14.2 L) slickline dump bailer to deliver MICP-promoting fluids, including microbial suspensions of *Sporosarcina pasteurii* (ATCC 11859) and urea–calcium (U+C) media, to reduce flow in the leakage pathway. Over 6 days, the bailer delivered 25 microbial culture and 49 U+C media injections amounting to approximately 95 gal (360L) of microbes and 185 gal (700L) of media. Injection testing at the end of the first field demonstration yielded an injection pressure of approximately 750 psi (51 atm) at a flowrate of 2.25 gpm (8.3 L/min). This result represents a 70% reduction in injectivity, defined here as the flowrate divided by the pressure [gpm/psi], marking a significant improvement in well performance and verifying that the biochemical reaction underlying MICP can occur in the presence of hydrocarbons in the subsurface. For a complete description of the field site and first field demonstration more information is found in Section 3.2.

Continuous injection strategy

Based on these favorable results, a second field demonstration was conducted in September 2018 to complete the sealing of the cement defect and thief zone so that the well could be returned to service as a waterflood injection well. The historic injection pressure of approximately 1,400 psi (95.3 atm) at a flowrate of 1 gpm (3.8 L/min) defines the capacity of the oil-bearing formation to receive waterflood fluids. The relatively high injectivity remaining after the first field demonstration was an indication that a significant additional volume of interconnected channels and pores remained open to flow within the defective cement and thief zone rock matrix. While appropriate for proof-of-concept experiments and small void volumes, our team determined that the bailer delivery method would not be suitable for the second field demonstration due to the limited delivery volume and time requirements of the method itself. To deliver the significantly larger volumes of both microbes and U+C media required to fill a large void volume, a new direct injection strategy was needed.

Controlling the placement of $CaCO_3$ precipitation is of paramount importance in field-scale MICP applications. Therefore, injection of biochemically reactive solutions thousands of feet deep in the subsurface poses several significant challenges. First, the proper sequence of solutions must be delivered without premature mixing for MICP to be successful. Ureolytic microbes act as the source of the urease enzyme catalyst and should precede delivery of the U+C media needed to complete the biomineralization. Premature mixing of microbial culture with U+C media results in spontaneous precipitation of floccular $CaCO_3$ due to residual HCO_3^- and CO_3^{2-} ions in the culture. Floccular $CaCO_3$ can be physically trapped in pores but may not provide the same sealing efficiency as bio-mineral attached to surfaces. Second, repeated applications of both microbial culture and U+C media are needed to produce enough bio-mineral to seal undesired flow paths. For the second field demonstration, the design location for mixing of fluids and precipitation of bio-mineral was in the thief zone rock matrix where fluid velocities decrease and the porous media structure promotes fluid mixing. As permeability decreased over time in the thief zone, bio-mineral was also expected to form in the cement defect and seal the undesirable flow path.

To address challenges related to premature fluid mixing, coiled tubing was considered to separate each fluid type during injection but was not economically viable for this field

demonstration. Instead, our team considered the feasibility of spotting the two MICP-promoting fluids into a string of 1-inch (2.54 cm) tubing, separated by a 'pulse' of non-reactive brine solution. Modeling suggested that flow faster than 1 gpm (3.8 L/min) would result in turbulent flow in the tubing string and reduce mixing between fluid types by minimizing the velocity gradient across the pipe and flattening/damping/blunting the parabolic flow profile typical of laminar flow regimes.

Since 1 gpm (3.8L/min) was approximately the desired endpoint flowrate, our study team hypothesized that 1) separating MICP-promoting fluids with a non-reactive brine in a single tubing string could minimize mixing in the tubing string provided that flow was continuous, and 2) the pore spaces of the thief zone would provide an appropriate environment for MICP to occur even without a static batch reaction period inherent in the bailer delivery process. The goal of this field demonstration was to determine the extent to which direct and continuous injection of MICP-promoting fluids via the tubing string could provide an additional tool to seal leakage pathways in wellbore cement and/or mitigate conformance problems for waterflooding or other enhanced oil recovery operations.

Field Demonstration Design (Experimental Methods)

Two strategies were employed to produce larger volumes of ureolytic microbes. Microbes were grown in the lab at Montana State University (MSU), centrifuged, and frozen. Immediately prior to injection in the field, the frozen cells were thawed and re-suspended in brine. In addition, the custom-built mobile laboratory was modified with an array of four 15-gal (57 L) bioreactors equipped with temperature control, mixing, aeration, and ventilation to cultivate large volumes of fresh microbes each day. Both methods are described in detail below. At the same time, the bailer delivery system was replaced with a continuous injection strategy to convey the MICP-promoting fluids downhole. Multiple 'pulses' of microbes and U+C media were spotted into a string of 1-inch (2.5 cm) diameter tubing separated by brine 'spacers' and injected continuously at a flowrate of 3.4 - 1.4 gpm (12.9 - 5.3 L/min) (Figure 49). A detailed description of the continuous injection method follows in a later section.

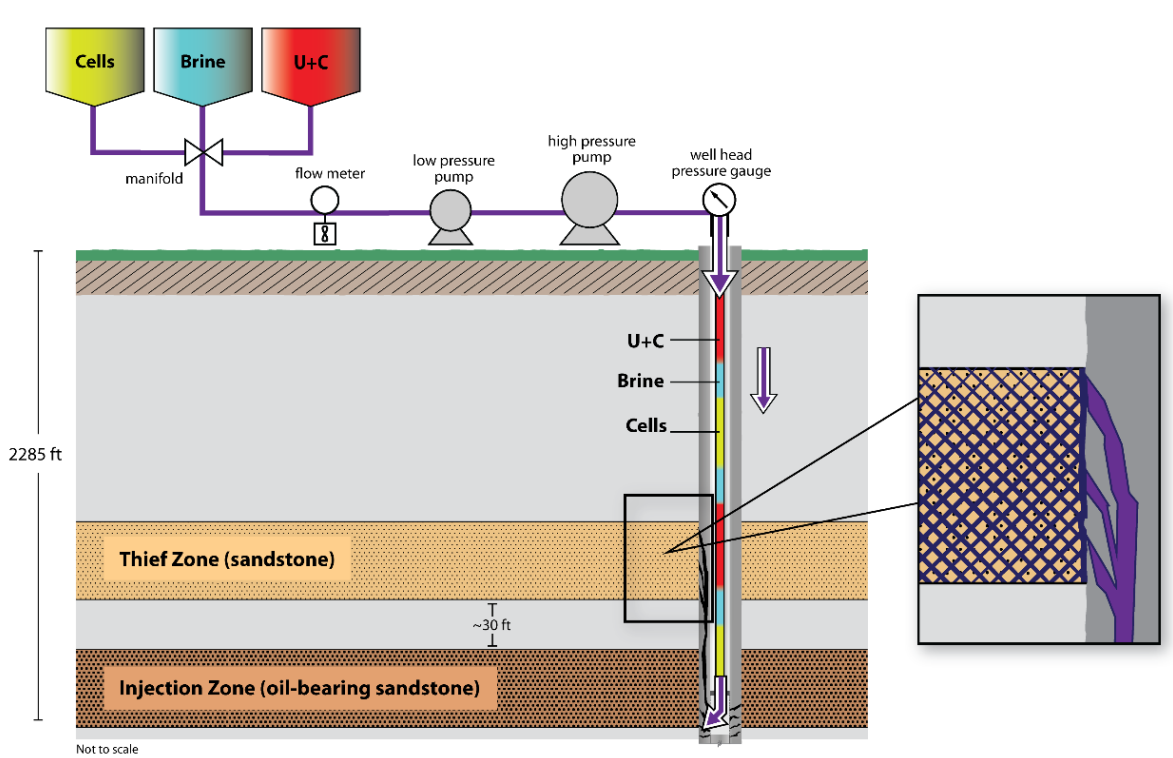

Figure 49. Continuous injection schematic. MICP-promoting solutions were injected down a 1-inch (2.54 cm) tubing string in the following order: microbes (represented in yellow), brine spacer (blue), U+C (red), followed by a brine spacer. The cycle was repeated until the desired injection pressure-flow relationship was achieved.

MICP-promoting fluids

Two methods of cell preparation were employed during the field demonstration. First, *Sporosarcina pasteurii* (ATCC 11859) cells were grown in the lab at MSU. Inoculum cultures were started from 1 mL frozen stock in Brain Heart Infusion (BHI, Becton Dickinson, Franklin Lakes, NJ) plus 20 g/L urea (Fisher Scientific) (BHI + 2% urea media) at a 1:100 ratio. The 100 mL cultures grew for 16 hrs in a 250 mL flask inside a 30°C incubating shaker. The cultures were used to inoculate 1900 mL lab grade yeast extract media (15.5 g/L yeast extract (Acros Organics, Geel, Belgium), 20 g/L urea (Fisher Scientific), 1 g/L NH_4Cl (Fisher Scientific)) (YE media) for a final volume of 2 L. After several 2L batches in YE media yielded lower than expected cell numbers, the cultures were grown in BHI + 2% urea media. The 2 L cultures grew for 24 hours in 4 or 6 L flasks on a stir plate with aluminum foil loosely wrapped around the stir plate and flask to passively insulate the culture. After 8 batches of cells were cultured in 2 L volumes, the culture volume in each flask was reduced to 1 L to improve cell counts. Several 1-2 L cultures were grown daily over a period of several weeks for a total of 68 L of cells. Each day, the 1-2 L cultures were combined into one batch and centrifuged in 750 mL centrifuge bottles at 4700 rpm for 15-25 minutes at 4°C in a Sorvall Legend XTR centrifuge. Supernatant was poured off to waste. Cells were removed from the centrifuge bottles and combined with 80% brine (10 g/L NH_4Cl) + 20% glycerol for a total volume of approximately 300 mL. Aliquots (30 mL) of each batch were frozen at -20°C in 50 mL conical tubes. A total of 103 vials of frozen cells were

shipped to the field site on dry ice for the field experiment. Prior to injection downhole, the cells were re-suspended in a 55-gallon (208L) tank of brine solution with 10 g/L NH_4Cl (BASF, non-food grade) and 24 g/L NaCl (Champion's Choice Mix N Fine, Cargill Inc., Wayzata, MN) using a design ratio of 30 mL frozen centrifuged cells per 4 gallons (15L) of solution.

Figure 50. The mobile lab was equipped with 4 15-gallon (57 L) conical bottom tanks (left) with integrated aeration, ventilation, mixing and temperature control to cultivate up to 96 gallons (363 L) of fresh microbial cultures per day. Two 55-gallon (208 L) storage reactors (right) were similarly outfitted and provided additional culturing or storage capacity.

The second method of cell preparation used the bioreactor system in the mobile laboratory, shown in Figure 50. Inoculum cultures in 1 L BHI + 2% urea media were started from 5 mL frozen *S. pasteurii* (ATCC 11859) stock and cultured in a 30°C incubator for 7-15 hours. These 1 L cultures were used to inoculate 12 gallons (45 L) of field grade yeast extract medium (15.5 g/L yeast extract (Acros Organics, Geel, Belgium), 24 g/L urea (Dyno Nobel, Inc, Deer Island OR), and 1 g/L NH_4Cl (BASF USA, Florham Park, NJ) in 15-gallon (57L) bioreactors that were equipped with aeration, ventilation, recirculation and temperature control at 30°C. Growth in the 15-gallon bioreactors occurred over 7-15 hours before the microbes were transferred to 55-gallon (208 L) storage reactors prior to downhole injection. The 55-gallon storage reactors were also equipped with aeration, ventilation, recirculation, and temperature control, providing additional time for microbial growth before injection. This system was able to produce 96 gallons (363 L) of actively growing *S. pasteurii* cells per day, with 48 gal (181 L) ready for injection in the morning and 48 gal ready for transfer to the 55-gallon (208L) storage reactors in the afternoon. Cultures in excess of the daily injection capacity were transferred to 100-gallon (378 L) static storage tanks to be held in reserve while freeing up volume in the 15- and 55-gallon (57L and 208L) reactors. Microbial cultures were sampled at various growth stages for pH and optical density (OD 600). Periodic samples were also collected and plated on BHI + 2% urea agar plates using the drop plate method for population analysis.[146]

Urea-calcium media (U+C) was prepared in 200-gallon (757 L) batches (104.3 g/L $CaCl_2$ (Peladow, Occidental Chemical Corp., Dallas, TX), 48 g/L urea (Dyno Nobel, Inc, Deer Island

OR) with mixing provided by a pressure washer and drill-powered mixer. Brine 'spacer' solution was mixed in 180-gallon (680 L) batches using the same ratio as for the frozen cell re-suspension. The purpose of the brine spacer was to separate microbes and U+C media to minimize spontaneous precipitation in the tubing during injection.

Continuous injection

The tanks containing the microbes, U+C media, and brine were connected with garden hose to a valved manifold (Figure 49). Fluids were pumped through the manifold by a low-pressure ½ hp transfer pump (Drummond) and flow was monitored by a digital turbine flow meter and totalizer (Assured Automation) to regulate the volume of each fluid type in sequence. Following an initial flushing of the well with 12 gallons (45 L) of fresh water, 12 gallons of microbes were pumped into the hose, followed by 10 gallons (37.8 L) of brine, 24 gallons (90.7 L) of U+C media, and 10 gallons of brine. Then the cycle of microbes-brine-U+C-brine repeated throughout the day of injection. The transfer pump fed the injection pump, a pressure-washer (PC4-3500, Landa), which delivered fluids via high-pressure hose to the tubing string at the wellhead. The initial injection flow rate was approximately 3.4 gpm, decreasing to 1.4 gpm at the end of the experiment. A 1-inch steel tubing string (1.049-inch ID) (2.5 cm) was laid down inside the 2-7/8-inch (7.3 cm) steel tubing string used in the first field demonstration to reduce the volumes of fluids required to fill the tubing and reach the perforations. A packer (AS1-X, Black Sands, Floresville, TX) was set at 2185.5 ft bgs (666 m) between the 2-7/8-inch tubing (7.3 cm) and 5-1/2-inch (14 cm) well casing. A second packer was set between the 2-7/8- and 1-inch tubing strings at 2166 ft bgs (660 m) to isolate the region of interest from the upper strata and provide support to the end of the 1-inch tubing.

The 2-7/8-inch (7.3 cm) tubing string extended to 2291 ft bgs (698 m) where perforations in the well casing allowed fluids to enter the rock formation and defects in the wellbore cement. There were approximately 127 gallons (480 L) of volume available in the tubing string between the surface and the perforations, which equates to approximately two cycles of microbes-brine-U+C-brine. Wellhead pressure was logged with an Omega pressure recorder (OM-CP-PR2000) to assess the injectivity of the formation and cement defect in real time. At the beginning of the field demonstration, the travel time of fluids in the tubing string was approximately 45 minutes between the surface and the perforations. Travel time increased to more than 90 minutes by the end of the demonstration as MICP reduced the system permeability.

Results and Discussion (Results and Discussion)

The continuous injection of MICP-promoting fluids was successful in restoring the well's historic pressure – flow relationship. During the third day of injection, a final pressure – flow relationship of 1384 psi (94.2 atm) at 1.4 gpm (5.3 L/min) was achieved. A total of 280 gallons (1062 L) of re-suspended frozen cells, 156 gallons (589L) of fresh cell cultures, 955 gallons (3608 L) of U+C, 647 gallons (2445 L) of brine, and 156 gallons (588L) of fresh water were injected during the field demonstration.

Microbial Cultures

S. pasteurii cultures grown in the lab, centrifuged, and subsequently frozen produced cell counts on average of 7.7×10^8 cfu/mL in the 30 mL aliquots with a large standard deviation of 5.9×10^8

cfu/mL. When re-suspended in brine in the field prior to injection, these cells were diluted 1:500. The re-suspended cell solution therefore had an estimated cell concentration of 1×10^6 cfu/mL. Plating of one batch of these cells in the field produced plate counts of 1.1×10^6 cfu/mL.

Cells grown in the bioreactor system in the mobile laboratory yielded higher cell numbers. Since two batches of cells were cultured each day, the data reported here combine cell counts of cultures grown in each system during the workday and those grown overnight. Inoculum cultures (1 L) produced plate counts of 3.0×10^7 cfu/mL and OD 600 values of 0.646 on average. The 12-gal (45.4 L) cultures grown in the bio-reactors produced plate counts of 4.7×10^7 cfu/mL and OD 600 values of 0.507 on average. Cultures sampled from the 55-gal (208 L) reactors prior to transfer to the injection storage tank showed cell counts of 1.5×10^8 cfu/mL and OD 600 values of 0.461 on average. Cell counts on the order of 10^8 cfu/mL are typical for laboratory cultures but are higher than have typically been achieved in non-ideal conditions during field demonstrations. Furthermore, plate counts are sensitive only to viable cells, but unculturable organisms have been shown to contain active urease enzyme.

Reduced Injectivity

Figure 51 shows the flow-to-pressure ratio [gpm/psi] recorded during injection in both field demonstrations as a function of the volume of fluids injected. A lower value means that it was more difficult to inject fluids into the formation and suggests that flow paths were restricted. For readability, this flow-to-pressure ratio will be called injectivity hereafter. Data from the first field demonstration used bailer delivery and was collected over a 6-day experimental period. The second field demonstration involved substantially larger fluid volumes but required half the time. The final data point shown in Figure 51 was collected during a subsequent injection test after the end of the second field demonstration from a flowrate of 0.8 gpm (3.0 L/min) at 1700 psi (115.7 atm), suggesting that the MICP biochemical reaction continued to completion in the formation for some time after the experiment ended.

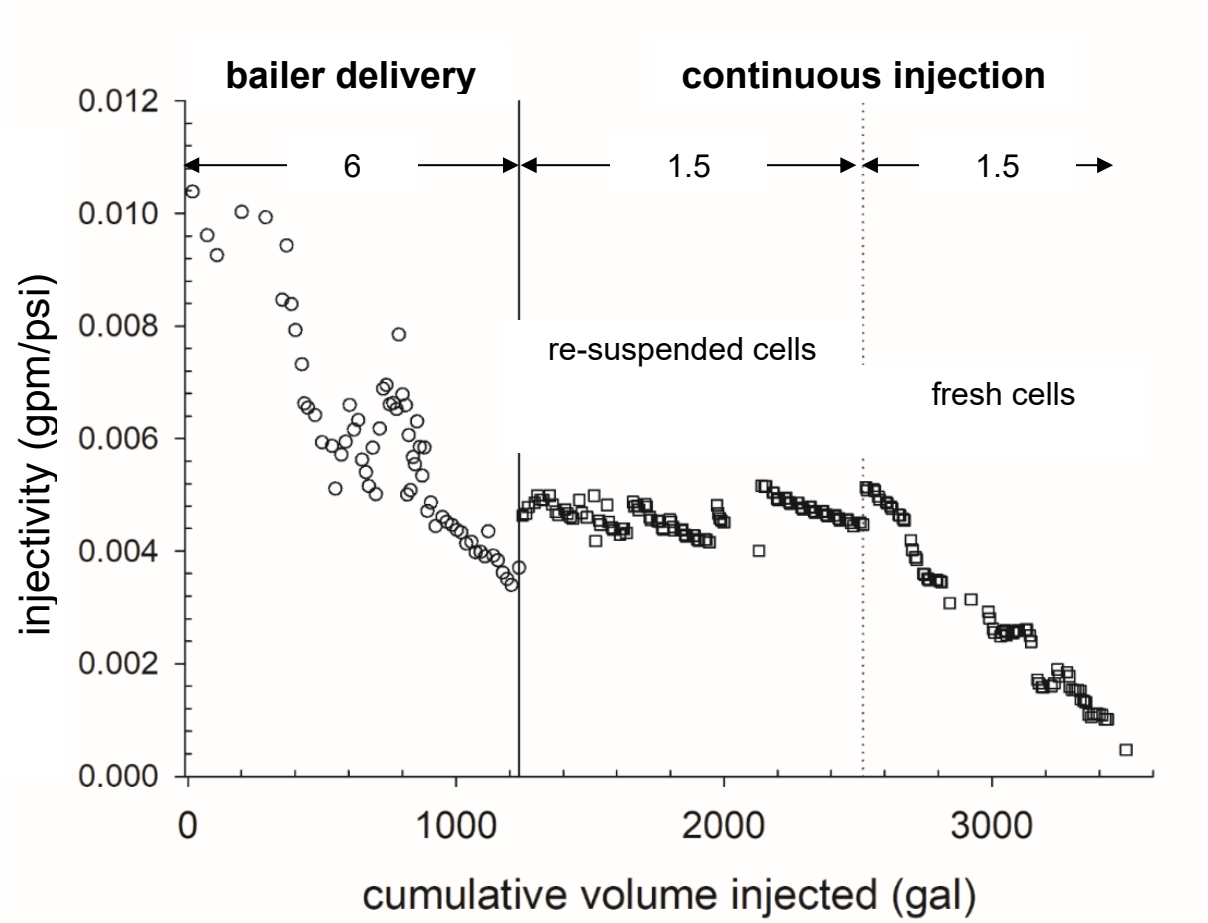

Figure 51. The continuous injection field demonstration began with injections of re-suspended frozen cells and U+C media. On Day 2 and after injecting approximately 280 gallons (1060 L) of the re-suspended cells, only a moderate pressure increase and little change in injectivity was observed. Injectivity decreased significantly during the injection of approximately 156 gallons (590.5L) of freshly cultured cells. A total of approximately 955 gallons (3605.1L) of U+C media was injected over the 3 days.

The period when re-suspended frozen cells were injected shows moderate reduction in injectivity that was not sustained. On the second day of the field demonstration, freshly grown cells were used, producing a rapid and sustained decrease in injectivity. This is noteworthy for several reasons. First, the slope of injectivity with respect to cumulative volume during continuous injection of fresh cell cultures is very similar to the slope observed when the bailer delivery method was used in the first field demonstration. This suggests that the volume of reactants delivered is more important than the timescale of delivery. Due to the round-trip travel time of the bailer, there were approximately 30 minutes of no-flow for ureolysis and precipitation reactions to occur between fluid injections in the first field demonstration. Laboratory experiments on MICP typically include a no-flow batch reaction period to promote precipitation. Such batch reaction periods in the formation do not appear to be necessary to achieve efficient permeability reduction.

Second, the continuous injection data shows a relatively smooth decrease in injectivity when using fresh cells, while the data collected using bailer delivery shows significantly more scatter. The 'noise' in the bailer delivery data is likely due to the bailer failing to release its contents on occasion. Continuous delivery may provide a more predictable avenue to a desired injectivity if/once the slope of the injectivity curve is determined for a given system. An important operational consideration during this field demonstration was estimating the endpoint and deciding when in the process to switch to non-reactive brine. Given the travel time and reaction capacity of fluids in the tubing string, our team began filling the tubing with brine when pressure reached 1320 psi (89.8 atm) at a flowrate of 2.35 gpm (8.9 L/min) to avoid excessive precipitation in the oil-bearing formation. The flowrate was reduced incrementally to maintain the injection pressure until reaching the pump's minimum flowrate of 1.4 gpm (5.3 L/min). Then the pressure increased as the final MICP-promoting fluids were injected at a constant flowrate. When the tubing was fully flushed and contained only brine, the final pressure – flow relationship was recorded and the experiment was terminated. Determining the appropriate time to stop injecting reactants, given fluid travel times and the potential costs and benefits of over- or under-biomineralizing the system, will require careful attention as MICP gains traction on the path to commercialization. Plotting injectivity data in real time during injection could be useful in this regard.

Conclusions (Conclusions)

The first field demonstration using bailer delivery occurred over a period of 6 days, while the fresh cell phase of the continuous injection demonstration required only 1.5 days. Again, this is likely related to the significantly larger volumes of reactants that can be delivered when using direct and continuous injection. These are positive findings for the future implementation of the MICP biotechnology in the oil and gas industry where non-productive time is costly.

Finally, in this study, re-suspended cells were not successful at reducing permeability in the system significantly or for long. It is possible that there were simply not enough cells present. The process of centrifuging, freezing, thawing, and re-suspending them in brine may also have negatively affected the cells' ureolytic activity and/or surface properties.

This study demonstrates that MICP can be employed successfully in large-volume applications where the timeframe for the delivery of reactants is limited. This finding has significant relevance for commercialization of the MICP biotechnology in the oil and gas industry.

Section 3.4 Design of a novel mobile laboratory for implementing engineered mineralization projects in field settings

Abstract (Abstract)

To advance the technology readiness level of the sealing technology, an additional task was added to the project scope, which was to design and construct a mobile laboratory to aid in implementation of field projects. An iterative design process was undertaken where a majority of the mobile lab was designed and constructed, followed by additional design and construction of custom bioreactors that were added to a portion of the lab trailer. The custom bioreactor system allowed for the continuous injection strategy to be implemented as described in Section 3.3 since large volumes of microbes could be grown in the field in short amounts of time.

Materials and Methods (Experimental Methods)

Characteristics of the mobile operations center

The mobile laboratory, a custom designed, 28 ft long, 8.5 ft wide, 8 ft tall cargo trailer was designed in a collaboration between MSU and Montana Emergent Technologies, a subcontractor on the project. In initial discussions, we evaluated the desired characteristics of the trailer which were determined to be:

1. Rapidly deployable;
2. Self-contained;
3. Field-ready;
4. Flexible;
5. Suitable for four-season use;
6. Equipped with built-in redundancy; and
7. Safe, i.e. Meet codes and standards.

In order to accommodate these desired characteristics, the major functions of the mobile operations center were determined which included: (1) operations control and communications; (2) laboratory activities; (3) storage, and (4) heating and tank systems for microbial growth (Figure 52). In consideration of operations control and communications is the ability for researchers inside to communicate with personnel outside of the trailer, via a window and/or radio. Thus, windows were installed in multiple sections of the trailer which will also contribute to reduce electricity needs for lighting. The trailer was equipped with storage such that chemicals can be procured prior to deployment, weighed out and standing ready for mixing in the field. Bringing the quality-checked chemicals along helped to minimize time spent on site in preparation for field activities. Tanks were used for microbial growth and mixing urea and calcium solutions and those fluids were pumped directly to storage tanks outside the trailer. The advantage of housing the tanks in the trailer is that the microbial growth can be accomplished in all four seasons since heating in the trailer alleviated the risk of freezing.

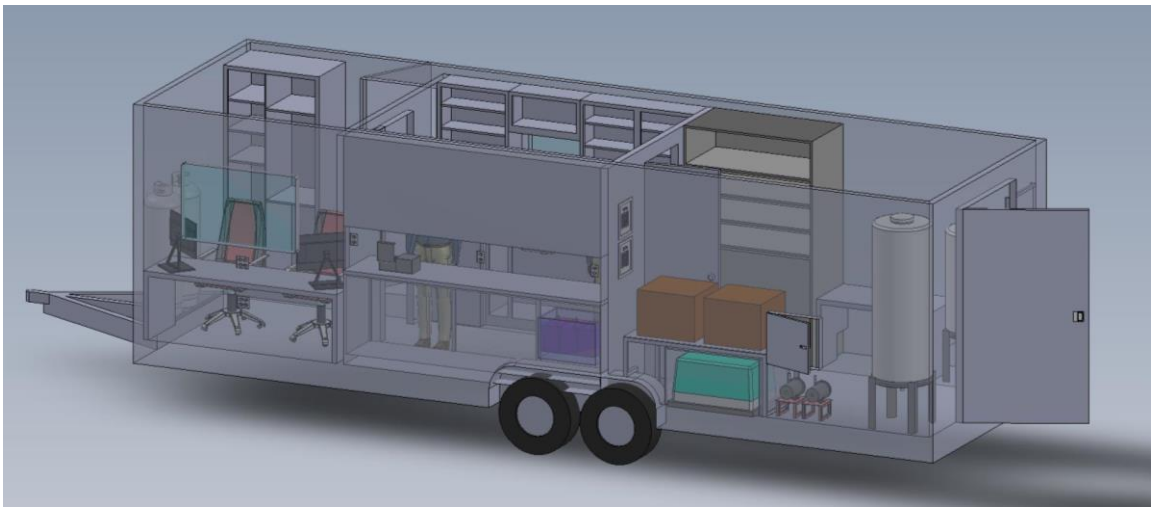

Figure 52. Conceptual design of the mobile laboratory.

Results and Discussion (Results and Discussion)

The purchase order from MSU to Becker Custom Trailer was executed on February 16, 2017. The mobile laboratory was delivered in August 2017 to Montana Emergent Technologies who were the subcontractors tasked with completing the construction and addition of shelves, desk space and water system.

Laboratory Section of the Trailer

The laboratory was equipped with bench space for sample analysis and instruments which can be stored in cabinets and drawers during transport. The laboratory section also housed a small refrigerator and freezer so microbial inoculum can be transported to the site without special shipping requirements or purchasing dry ice. Other major laboratory activities included inoculum/enzyme preparation and media and solution preparation and analysis of samples gathered and use of the required instruments to monitor quality of fluids to be injected. For example, a pH meter was used to check fluids before they were pumped downhole to make sure the fluids are not inhibitory to ureolysis. Finally, the laboratory section of the trailer was equipped with a carbon adsorption/ion exchange water treatment system that allows for purification of water that was used for microbial growth or sample analysis purposes. A sink was installed for cleaning laboratory glassware and hand washing (Figure 53).

Figure 53. Images of the build-out of the mobile operations center. left: sink and drying rack for laboratory glassware, middle: ion exchange water treatment system, right, the central lab space in the mobile laboratory provided adequate work and storage space for the necessary sampling and analysis of media solutions and microbial cultures.

Office Section/ Control Room

The control room was equipped with desk space for computers that were used to collect and store data and monitor experimental conditions. A dry erase board was used to track number of pulsed injections, keep lists of needed supplies and make quick calculations related to fluid volumes. The office area was also equipped with a storage cabinet that housed tools, emergency supplies, manuals for instruments and equipment, hard hats and other PPE (Figure 54).

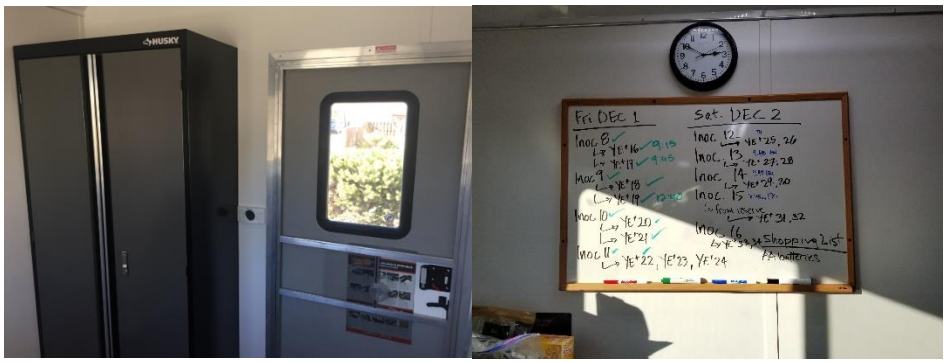

Figure 54. Images of the build-out of the mobile operations center. left: storage cabinet attached to wall, right dry erase board for calculations and list of needed supplies.

Fluid Handling and Microbial Growth Section of the Mobile Laboratory

In the back end of the trailer, the fluid handling equipment included recirculating pumps and tanks equipped with a heating coils attached to a hot water system, air pumps to bubble air into the media to promote oxygen transfer and ventilation to remove ammonia for large volume microbial growth in custom designed bioreactors (Figure 55). Portable benches were used in the back of the trailer where chemical storage, weighing, and mixing were performed.

Figure 55. Left, the conceptual design of growth tanks with heating coils and valved mixing systems. Right, installed bioreactors back of the trailer to cultivate large inoculum batches and mix calcium medium for injection.

Conclusions (Conclusions)

The trailer assisted in the efficiency of injections by making cultivation more efficient with the ability to heat the cultures to optimal temperature for microbial growth. Based on previous field experiences at the Gorgas well in Alabama, it was estimated that 9 injections could be completed each day. In the first Rexing #4 experiment, however, 12-15 injections were completed on days two-six. This enhanced productivity was attributable in part to the mobile lab, as well as to the efficiency of the team members operating the pumps at the wellhead and the slickline crew. In the second Rexing field experiment, with the custom bioreactors installed in the back of the trailer, over 2000 gallons (7571 L) of microbe suspensions, urea/calcium solutions and brine were injected and approximately 50 gallons (189 L) of microbes could be cultivated every 8-12 hours because of the heating coils, aeration system and recirculating pumps in the bioreactors.

FINAL REPORT SUMMARY AND CONCLUSION

The focus of the laboratory efforts (Section One) addressed the issue of fracture sealing in the near wellbore environment in cement and steel or cement and formation interfaces. These experiments were used to guide the efforts toward field application at the Gorgas well in Alabama during the first field demonstration; in that well channel sealing test, a bailer delivery system was used. Designing and developing the pulsed injection strategies in these laboratory scale experiments was necessary to understand and improve field delivery methods and their potential to be successful in reducing permeability of fractures in wellbore cement. The experiments conducted in the laboratory gave confidence to the field work that biomineralization could be used to significantly reduce permeability in engineered gaps between cement gap interfaces and that the resulting material was strong and could resist a differential pressure that might be seen with a leaking fluid from a subsurface formation.

In the scale-up experimental efforts (Section Two), reactor systems were designed to study the influence of biomineralization in wellbore configurations modeling not only fractures but also porous media systems (i.e. sand). The Rexing #4 well was the subject of the second and third field tests, therefore, it was necessary for us to determine how to increase volumes of fluids to impact increased pore space.

Section Three of this final report discussed the three field studies and summarized the mobile laboratory development. These studies allowed the team to enhance and improve the TRL level of the biomineralization sealing strategy by increasing the ability to grow large volumes of microbes and developing continuous injection strategies that decrease the overall time needed on-site which is a key cost factor in the implementation of this technology. The overall goal of this project was to develop a sealing method that was robust and implementable in a range of wellbore defects that would help assure the long-term integrity of boreholes and mitigate oil and gas leakage pathways to alleviate environmental impacts to water resources or the atmosphere. By utilizing a strategy of studying fundamentals on the laboratory scale to upscaling those developed methods to the field, we have developed a technology that can be added to the toolbox of oil field service providers to mitigate wellbore integrity problems in the field.

During this project, significant advancement of the MICP sealing technology was achieved. As described in the Executive Summary, the starting Technology Readiness Level (TRL) was TRL 3-4. The work described in Section One and Two of this report used laboratory-based wellbore analog reactors to move this technology to TRL5. Through the development and refinement of a mobile laboratory and optimization of injection strategies to support the field work conducted in this project, the technology advanced towards TRL 6 -7. Currently, Montana Emergent Technologies (MET), a partner to MSU and subcontractor on this project, has advanced the commercial application of the use of MICP specifically for the purpose of sealing channels in the annular space of wellbores to the TRL 8. They have commercialized the technology under the name BioSqueeze™ and have successfully sealed 13 wells in two states in commercial environments. In summary, throughout this project, methods to address wellbore integrity and sealing leakage pathways were successfully developed. The developed MICP wellbore sealing technology can now be used reliably to reduce the potential for leakage from oil and gas wells, reducing the environmental impact of conventional or unconventional oil and gas wells.

GRAPHICAL MATERIALS LIST

Figures

Tables

REFERENCES

1. Phillips, A. J.; Gerlach, R.; Lauchnor, E.; Mitchell, A. C.; Cunningham, A. B.; Spangler, L., Engineered applications of ureolytic biomineralization: a review. *Biofouling* **2013,** *29* (6), 715-733.
2. De Muynck, W.; De Belie, N.; Verstraete, W., Microbial carbonate precipitation in construction materials: A review. *Ecological Engineering* **2010,** *36* (2), 118-136.
3. De Belie, N.; Verstraete, W., Diatomaceous earth as a protective vehicle for bacteria applied for self-healing concrete. *Journal of Industrial Microbiology & Biotechnology* **2012,** *39* (4), 567-577.
4. Dhami, N. K.; Reddy, M. S.; Mukherjee, A., Improvement in strength properties of ash bricks by bacterial calcite. *Ecological Engineering* **2012,** *39* (0), 31-35.
5. Whiffin, V.; van Paassen, L.; Harkes, M., Microbial carbonate precipitation as a soil improvement technique. *Geomicrobiology Journal* **2007,** *24*, 417-423.
6. van Paassen, L.; Ghose, R.; van der Linden, T.; van der Star, W.; van Loosdrecht, M., Quantifying biomediated ground improvement by ureolysis: large-scale biogrout experiment. *Journal of Geotechnical and Geoenvironmental Engineering* **2010,** *136* (12), 1721-1728.
7. Al Qabany, A.; Soga, K.; Santamarina, C., Factors Affecting Efficiency of Microbially Induced Calcite Precipitation. *Journal of Geotechnical and Geoenvironmental Engineering* **2011,** *138* (8), 992-1001.
8. DeJong, J. T.; Mortensen, B. M.; Martinez, B. C.; Nelson, D. C., Bio-mediated soil improvement. *Ecological Engineering* **2010,** *36* (2), 197-210.
9. Tobler, D.; Maclachlan, E.; Phoenix, V., Microbially mediated plugging of porous media and the impact of differing injection strategies. *Ecological Engineering* **2012,** *42*, 270-278.
10. Fujita, Y.; Redden, G. D.; Ingram, J. C.; Cortez, M. M.; Ferris, F. G.; Smith, R. W., Strontium incorporation into calcite generated by bacterial ureolysis. *Geochimica et cosmochimica acta* **2004,** *68* (15), 3261.
11. Mitchell, A.; Dideriksen, K.; Spangler, L.; Cunningham, A.; Gerlach, R., Microbially enhanced carbon capture and storage by mineral-trapping and solubility-trapping. *Environmental Science & Technology* **2010**, 5270-5276.
12. Dupraz, S.; Parmentier, M.; Menez, B.; Guyot, F., Experimental and numerical modeling of bacterially induced pH increase and calcite precipitation in saline aquifers. *Chemical Geology* **2009,** *265*, 44-53.
13. Hammes, F.; Seka, A.; Van Hege, K.; Van de Wiele, T.; Vanderdeelen, J.; Siciliano, S.; Verstraete, W., Calcium removal from industrial wastewater by bio-catalytic $CaCO_3$ precipitation. *Journal of Chemical Technology and Biotechnology* **2003,** *78* (6), 670-677.
14. Okwadha, G. D. O.; Li, J., Biocontainment of polychlorinated biphenyls (PCBs) on flat concrete surfaces by microbial carbonate precipitation. *Journal of Environmental Management* **2011,** *92* (10), 2860-2864.

15. Lizak, K.; Zeltmann, T.; Crook, R. In *Permian Basin Operators Seal Casing Leaks with Small-Particle Cement*, Permian Basin Oil and Gas Recovery Conference, Midland, Texas, USA, Engineers, S. o. P., Ed. Society of Petroleum Engineers: Midland, Texas, USA, 1992; pp 429-434.
16. Harris, K.; Johnson, B. In *Successful remedial operations using ultrafine cement*, Mid-Continent Gas Symposium, Amarillo, Texas, Engineers, S. o. P., Ed. Society of Petroleum Engineers: Amarillo, Texas, 1992; pp 21-30.
17. Carey, J. W.; Svec, R.; Grigg, R.; Zhang, J. S.; Crow, W., Experimental investigation of wellbore integrity and CO2-brine flow along the casing-cement microannulus. *International Journal of Greenhouse Gas Control* **2010,** *4* (2), 272-282.
18. Carroll, S. A.; Keating, E.; Mansoor, K.; Dai, Z. X.; Sun, Y. W.; Trainor-Guitton, W.; Brown, C.; Bacon, D., Key factors for determining groundwater impacts due to leakage from geologic carbon sequestration reservoirs. *International Journal of Greenhouse Gas Control* **2014,** *29*, 153-168.
19. Dusseault, M., Why Oilwells Leak: Cement Behavior and Long-Term Consequences. *Society of Petroleum Engineers* **2000**.
20. Bai, M. X.; Zhang, Z. C.; Fu, X. F., A review on well integrity issues for CO2 geological storage and enhanced gas recovery. *Renew. Sust. Energ. Rev.* **2016,** *59*, 920-926.
21. Opedal, N. V.; Torsaeter, M.; Vralstad, T.; Cerasi, P., Potential Leakage Paths along Cement-Formation Interfaces in Wellbores; Implications for CO2 Storage. *7th Trondheim Conference on Co2 Capture, Transport and Storage (2013)* **2014,** *51*, 56-64.
22. Watson, T. L.; Bachu, S., Evaluation of the Potential for Gas and CO2 Leakage Along Wellbores. *Spe Drilling & Completion* **2009,** *24* (1), 115-126.
23. Carey, J. W.; Wigand, M.; Chipera, S. J.; WoldeGabriel, G.; Pawar, R.; Lichtner, P. C.; Wehner, S. C.; Raines, M. A.; Guthrie, G. D., Analysis and performance of oil well cement with 30 years Of CO(2) exposure from the SACROC Unit, West Texas, USA. *International Journal of Greenhouse Gas Control* **2007,** *1* (1), 75-85.
24. Huerta, N. J.; Hesse, M. A.; Bryant, S. L.; Strazisar, B. R.; Lopano, C., Reactive transport of CO2-saturated water in a cement fracture: Application to wellbore leakage during geologic CO2 storage. *International Journal of Greenhouse Gas Control* **2016,** *44*, 276-289.
25. Huerta, N. J.; Hesse, M. A.; Bryant, S. L.; Strazisar, B. R.; Lopano, C. L., Experimental Evidence for Self-Limiting Reactive Flow through a Fractured Cement Core: Implications for Time-Dependent Wellbore Leakage. *Environmental Science & Technology* **2013,** *47* (1), 269-275.
26. Kutchko, B. G.; Strazisar, B. R.; Huerta, N.; Lowry, G. V.; Dzombak, D. A.; Thaulow, N., CO2 Reaction with Hydrated Class H Well Cement under Geologic Sequestration Conditions: Effects of Flyash Admixtures. *Environmental Science & Technology* **2009,** *43* (10), 3947-3952.

27. Kutchko, B. G.; Strazisar, B. R.; Lowry, G. V.; Dzombak, D. A.; Thaulow, N., Rate of CO(2) attack on hydrated Class H well cement under geologic sequestration conditions. *Environmental Science & Technology* **2008,** *42* (16), 6237-6242.
28. Um, W.; Jung, H.; Kabilan, S.; Fernandez, C. A.; Brown, C. F., Geochemical and geomechanical effects on wellbore cement fractures. *12th International Conference on Greenhouse Gas Control Technologies, Ghgt-12* **2014,** *63*, 5808-5812.
29. Li, Z. Y.; Zhang, K.; Guo, X. Y.; Liu, J.; Cheng, X. W.; Du, J. B., Study of the failure mechanisms of a cement sheath based on an equivalent physical experiment. *Journal of Natural Gas Science and Engineering* **2016,** *31*, 331-339.
30. Loizzo, M.; Akemu, O. A. P.; Jammes, L.; Desroches, J.; Lombardi, S.; Annunziatellis, A., Quantifying the Risk of CO2 Leakage Through Wellbores. *Spe Drilling & Completion* **2011,** *26* (3), 324-331.
31. Todorovic, J.; Raphaug, M.; Lindeberg, E.; Vralstad, T.; Buddensiek, M. L., Remediation of Leakage through Annular Cement Using a Polymer Resin: a Laboratory Study. *8th Trondheim Conference on Co2 Capture, Transport and Storage* **2016,** *86*, 442-449.
32. Rike, J. L.; Rike, E., Squeeze Cementing: State of the Art. *Journal of Petroleum Technology* **1982,** *34* (1), 37-45.
33. Phillips, A. J.; Gerlach, R.; Lauchnor, E.; Mitchell, A. C.; Cunningham, A. B.; Spangler, L., Engineered applications of ureolytic biomineralization: a review. *Biofouling* **2013,** *29* (6), 715-33.
34. Fujita, Y.; Redden, G. D.; Ingram, J. C.; Cortez, M. M.; Ferris, F. G.; Smith, R. W., Strontium incorporation into calcite generated by bacterial ureolysis. *Geochimica Et Cosmochimica Acta* **2004,** *68* (15), 3261-3270.
35. Gomez, M. G.; Martinez, B. C.; DeJong, J. T.; Hunt, C. E.; deVlaming, L. A.; Major, D. W.; Dworatzek, S. M., Field-scale bio-cementation tests to improve sands. *Proceedings of the Institution of Civil Engineers-Ground Improvement* **2015,** *168* (3), 206-216.
36. Lauchnor, E. G.; Schultz, L. N.; Bugni, S.; Mitchell, A. C.; Cunningham, A. B.; Gerlach, R., Bacterially Induced Calcium Carbonate Precipitation and Strontium Coprecipitation in a Porous Media Flow System. *Environ. Sci. Technol.* **2013,** *47* (3), 1557-1564.
37. van Paassen, L. A.; Ghose, R.; van der Linden, T. J. M.; van der Star, W. R. L.; van Loosdrecht, M. C. M., Quantifying Biomediated Ground Improvement by Ureolysis: Large-Scale Biogrout Experiment. *Journal of Geotechnical and Geoenvironmental Engineering* **2010,** *136* (12), 1721-1728.
38. Cunningham, A. B.; Gerlach, R.; Spangler, L.; Mitchell, A. C.; Parks, S.; Phillips, A., Reducing the risk of well bore leakage of CO2 using engineered biomineralization barriers. In *10th International Conference on Greenhouse Gas Control Technologies*, Gale, J.; Hendriks, C.; Turkenberg, W., Eds. 2011; Vol. 4, pp 5178-5185.
39. Cunningham, A. B.; Phillips, A. J.; Troyer, E.; Lauchnor, E.; Hiebert, R.; Gerlach, R.; Spangler, L., Wellbore leakage mitigation using engineered biomineralization. In *12th*

International Conference on Greenhouse Gas Control Technologies, Ghgt-12, Dixon, T.; Herzog, H.; Twinning, S., Eds. 2014; Vol. 63, pp 4612-4619.
40. Phillips, A. J.; Cunningham, A. B.; Gerlach, R.; Hiebert, R.; Hwang, C.; Lomans, B. P.; Westrich, J.; Mantilla, C.; Kirksey, J.; Esposito, R.; Spangler, L., Fracture Sealing with Microbially-Induced Calcium Carbonate Precipitation: A Field Study. *Environmental Science & Technology* **2016,** *50* (7), 4111-4117.
41. Phillips, A. J.; Eldring, J.; Hiebert, R.; Lauchnor, E.; Mitchell, A. C.; Cunningham, A.; Spangler, L.; Gerlach, R., Design of a meso-scale high pressure vessel for the laboratory examination of biogeochemical subsurface processes. *Journal of Petroleum Science and Engineering* **2015,** *126*, 55-62.
42. Phillips, A. J.; Lauchnor, E.; Eldring, J.; Esposito, R.; Mitchell, A. C.; Gerlach, R.; Cunningham, A. B.; Spangler, L. H., Potential CO2 Leakage Reduction through Biofilm-Induced Calcium Carbonate Precipitation. *Environ. Sci. Technol.* **2013,** *47* (1), 142-149.
43. Cuthbert, M. O.; McMillan, L. A.; Handley-Sidhu, S.; Riley, M. S.; Tobler, D. J.; Phoenix, V. R., A Field and Modeling Study of Fractured Rock Permeability Reduction Using Microbially Induced Calcite Precipitation. *Environmental Science & Technology* **2013,** *47* (23), 13637-13643.
44. Mitchell, A. C.; Dideriksen, K.; Spangler, L. H.; Cunningham, A. B.; Gerlach, R., Microbially Enhanced Carbon Capture and Storage by Mineral-Trapping and Solubility-Trapping. *Environmental Science and Technology* **2010,** *44* (13), 5270-5276.
45. Tobler, D. J.; Maclachlan, E.; Phoenix, V. R., Microbially mediated plugging of porous media and the impact of differing injection strategies. *Ecological Engineering* **2012,** *42*, 270-278.
46. Hammes, F.; Verstraete, W., Key roles of pH and calcium metabolism in microbial carbonate precipitation. *Re/Views in Environmental Science and Bio/Technology* **2002,** *1* (1), 3-7.
47. De Muynck, W.; Debrouwer, D.; De Belie, N.; Verstraete, W., Bacterial carbonate precipitation improves the durability of cementitious materials. *Cement and Concrete Research* **2008,** *38* (7), 1005-1014.
48. Stocks-Fischer, S.; Galinat, J. K.; Bang, S. S., Microbiological precipitation of CaCO3. *Soil Biology & Biochemistry* **1999,** *31* (11), 1563-1571.
49. Phillips, A. J.; Troyer, E.; Hiebert, R.; Kirkland, C. M.; Gerlach, R.; Cunningham, A.; Spangler, L.; Kirksey, J.; Rowe, W.; Esposito, R., Enhancing wellbore cement integrity with microbially induced calcite precipitation (MICP): a field scale demonstration. *Journal of Petroleum Science and Engineering* **2018,** *171*, 1141-1148.
50. Mortensen, B. M.; Haber, M. J.; DeJong, J. T.; Caslake, L. F.; Nelson, D. C., Effects of environmental factors on microbial induced calcium carbonate precipitation. *Journal of Applied Microbiology* **2011,** *111* (2), 338-349.
51. Whiffin, V. S.; van Paassen, L. A.; Harkes, M. P., Microbial carbonate precipitation as a soil improvement technique. *Geomicrobiology Journal* **2007,** *24* (5), 417-423.

52. Ebigbo, A.; Phillips, A.; Gerlach, R.; Helmig, R.; Cunningham, A. B.; Class, H.; Spangler, L. H., Darcy-scale modeling of microbially induced carbonate mineral precipitation in sand columns. *Water Resources Research* **2012,** *48*.
53. Hommel, J.; Lauchnor, E.; Phillips, A.; Gerlach, R.; Cunningham, A. B.; Helmig, R.; Ebigbo, A.; Class, H., A revised model for microbially induced calcite precipitation: Improvements and new insights based on recent experiments. *Water Resour. Res.* **2015,** *51* (5), 3695-3715.
54. Martin, D.; Dodds, K.; Ngwenya, B. T.; Butler, I. B.; Elphick, S. C., Inhibition of Sporosarcina pasteurii under Anoxic Conditions: Implications for Subsurface Carbonate Precipitation and Remediation via Ureolysis. *Environmental Science & Technology* **2012,** *46* (15), 8351-8355.
55. Phillips, A. Biofilm-Induced Calcium Carbonate Precipitation: Application in the Subsurface. Montana State University, 2013.
56. Jung, D.; Biggs, H.; Erikson, J.; Ledyard, P., New colorimetric reaction for end-point, continuous-flow, and kinetic measurement of urea. *Clinical Chemistry* **1975,** *21* (8), 1136-1140.
57. Zimmerman, R. W.; Bodvarsson, G. S., Hydraulic conductivity of rock fractures. *Transp. Porous Media* **1996,** *23* (1), 1-30.
58. Feldkamp, L. A.; Davis, L. C.; Kress, J. W., Practical cone-beam algorithm. *J. Opt. Soc. Am. A-Opt. Image Sci. Vis.* **1984,** *1* (6), 612-619.
59. Fan, S.; Li, M., X-ray computed microtomography of threedimensional microcracks and self-healing in engineered cementitious composites. *Smart Mater. Struct.* **2015,** *24* (1), 14.
60. El Mountassir, G.; Lunn, R. J.; Moir, H.; MacLachlan, E., Hydrodynamic coupling in microbially mediated fracture mineralization: Formation of self-organized groundwater flow channels. *Water Resources Research* **2014,** *50* (1), 1-16.
61. Minto, J. M.; MacLachlan, E.; El Mountassir, G.; Lunn, R. J., Rock fracture grouting with microbially induced carbonate precipitation. *Water Resources Research* **2016,** *52* (11), 8810-8827.
62. Tobler, D. J.; Minto, J. M.; El Mountassir, G.; Lunn, R. J.; Phoenix, V. R., Microscale Analysis of Fractured Rock Sealed With Microbially Induced CaCO3 Precipitation: Influence on Hydraulic and Mechanical Performance. *Water Resources Research* **2018,** *54* (10), 8295-8308.
63. Stocks-Fischer, S.; Galinat, J. K.; Bang, S. S., Microbiological precipitation of CaCO3. *Soil Biology and Biochemistry* **1999,** *31* (11), 1563-1571.
64. Watson, T. L.; Bachu, S., Evaluation of the potential for gas and CO_2 leakage along wellbores. *SPE-106817-PA* **2009,** *24* (01), 1115-126.
65. Dusseault, M. B.; Gray, M. N.; Nawrocki, P. A., Why Oilwells Leak: Cement Behavior and Long-Term Consequences. In *International Oil and Gas Conference and Exhibition in China*, Society of Petroleum Engineers: Beijing, China, 2000; p 8.

66. Jackson, R. E.; Dusseault, M. B., Gas release mechanisms from energy wellbores. In *48th Rock Mechanics/Geomechanics Symposium*, American Rock Mechanics Association: Minneapolis, Minnesota, USA, 2014; p 5.
67. Carroll, S.; McNab, W.; Torres, S.; Singleton, M.; Zhao, P., Wellbore integrity in carbon sequestration environments: 1. Experimental study of Cement-Sandstone/Shale-Brine-CO2. *Energy Procedia* **2011,** *4*, 5186-5194.
68. Carroll, S.; Carey, J. W.; Dzombak, D.; Huerta, N. J.; Li, L.; Richard, T.; Um, W.; Walsh, S. D. C.; Zhang, L., Review: Role of chemistry, mechanics, and transport on well integrity in CO2 storage environments. *International Journal of Greenhouse Gas Control* **2016,** *49*, 149-160.
69. Loizzo, M.; Akemu, O. A.; Jammes, L.; Desroches, J.; Lombardi, S.; Annunziatellis, A., Quantifying the Risk of CO2 Leakage Through Wellbores. *SPE Drilling & Completion* **2011,** *26* (03), 324-331.
70. Carey, W. J.; Svec, R.; Grigg, R.; Zhang, J.; Crow, W., Experimental investigation of wellbore integrity and CO_2–brine flow along the casing–cement microannulus. *International Journal of Greenhouse Gas Control* **2010,** *4* (2), 272-282.
71. Crow, W.; Williams, B.; Carey, J. W.; Celia, M.; Gasda, S., Wellbore integrity of a natural CO2 producer. *Energy Procedia* **2009,** *1*, 3561-3569.
72. Huerta, N. J.; Bryant, S. L.; Strazisar, B. R.; Kutchko, B. G.; Conrad, L. C., The influence of confining stress and chemical alteration on conductive pathways within wellbore cement. *Energy Procedia* **2009,** *1* (1), 3571-3578.
73. Newell, D. L.; Carey, J. W., Experimental evaluation of wellbore integrity along the cement-rock boundary. *Environmental Science & Technology* **2012,** *47* (1), 276-282.
74. Opedal, N.; Torsæter, M.; Vrålstad, T.; Cerasi, P., Potential Leakage Paths along Cement-formation Interfaces in Wellbores; Implications for CO2 Storage. *Energy Procedia* **2014,** *51* (0), 56-64.
75. Todorovic, J.; Raphaug, M.; Lindeberg, E.; Vrålstad, T.; Buddensiek, M.-L., Remediation of Leakage through Annular Cement Using a Polymer Resin: A Laboratory Study. *Energy Procedia* **2016,** *86* (Supplement C), 442-449.
76. Genedy, M.; Stormont, J.; Matteo, E.; Taha, M. R., Examining Epoxy-based Nanocomposites in Wellbore Seal Repair for Effective CO2 Sequestration. *Energy Procedia* **2014,** *63* (Supplement C), 5798-5807.
77. Reinhardt, H. W., Ultra-fine cements for special applications. *Advanced Cement Based Materials* **1993,** *1* (2), 106-107.
78. Tamura, M.; Goto, T.; Ogino, T.; Shimizu, K., Injection with ultra-fine cement into fine sand layer. In *International Offshore and Polar Engineering Conference*, International Society of Offshore and Polar Engineers: Osaka, Japan, 1994; pp 567-571.
79. Cunningham, A. B.; Phillips, A. J.; Troyer, E.; Lauchnor, E.; Hiebert, R.; Gerlach, R.; Spangler, L., Wellbore leakage mitigation using engineered biomineralization. *Energy Procedia* **2014,** *63* (0), 4612-4619.

80. Phillips, A.; Gerlach, R.; Lauchnor, E.; Mitchell, A.; Cunningham, A.; Spangler, L., Engineered applications of ureolytic biomineralization: a review. *Biofouling* **2013,** *29* (6), 715-733.
81. Phillips, A. J.; Gerlach, R.; Cunningham, A. B.; Spangler, L.; Hiebert, R.; Kirksey, J.; Esposito, R., Biological influences in the subsurface: A method to seal fractures and reduce permeability with microbially-induced calcite precipitation. In *49th US Rock Mechanics / Geomechanics Symposium*, Association, A. R. M., Ed. San Francisco, CA, USA, 28 June- 1 July 2015, 2015; p 6.
82. Phillips, A. J.; Troyer, E.; Hiebert, R.; Kirkland, C.; Gerlach, R.; Cunningham, A. B.; Spangler, L.; Kirksey, J.; Rowe, W.; Esposito, R., Enhancing wellbore cement integrity with microbially induced calcite precipitation (MICP): A field scale demonstration. *Journal of Petroleum Science and Engineering* **2018,** *171*, 1141-1148.
83. Ebigbo, A.; Phillips, A.; Gerlach, R.; Helmig, R.; Cunningham, A. B.; Class, H.; Spangler, L. H., Darcy-scale modeling of microbially induced carbonate mineral precipitation in sand columns. *Water Resour. Res.* **2012,** *48* (7), W07519.
84. Phillips, A. J.; Eldring, J.; Hiebert, R.; Lauchnor, E.; Mitchell, A. C.; Cunningham, A.; Spangler, L.; Gerlach, R., Design of a meso-scale high pressure vessel for the laboratory examination of biogeochemical subsurface processes. *Journal of Petroleum Science and Engineering* **2015,** *126* (0), 55-62.
85. In *Bioprocess Engineering Principles (Second Edition)*, Doran, P. M., Ed. Academic Press: London, 2013; pp 899-919.
86. Fidaleo, M.; Lavecchia, R., Kinetic study of enzymatic urea hydrolysis in the pH range 4-9. *Chemical and Biochemical Engineering Quarterly* **2003,** *17* (4), 311-318.
87. Lauchnor, E. G.; Topp, D. M.; Parker, A. E.; Gerlach, R., Whole cell kinetics of ureolysis by Sporosarcina pasteurii. *J Appl Microbiol* **2015,** *118* (6), 1321-32.
88. Stocks-Fischer, S.; Galinat, J.; Bang, S., Microbiological precipitation of $CaCO_3$. *Soil Biology & Biochemistry* **1999,** *31* (11), 1563-1571.
89. Hommel, J.; Cunningham, A. B.; Helmig, R.; Ebigbo, A.; Class, H., Numerical Investigation of Microbially Induced Calcite Precipitation as a Leakage Mitigation Technology. *Energy Procedia* **2013,** *40* (0), 392-397.
90. Hommel, J.; Lauchnor, E.; Gerlach, R.; Cunningham, A. B.; Ebigbo, A.; Helmig, R.; Class, H., Investigating the influence of the initial biomass distribution and injection strategies on biofilm-mediated calcite precipitation in porous media. . *Transport in Porous Media* **2015**, 1-23.
91. Cunningham, A.; Class, H.; Ebigbo, A.; Gerlach, R.; Phillips, A.; Hommel, J., Field-scale modeling of microbially induced calcite precipitation. *In revision, Computational Geosciences* **2018,** *Manuscript #COMG-D-18-00040R1*.
92. Hendricks, C. A. W., E.; Dejagar, D.; Block, K.; Riemer, P., Emission Reduction of Greenhouse Gases from the Cement Industry. *IEA Greenhouse Gas R&D Programme* **2004**.
93. USGS - Mineral Commodity Summaries 2018. **2018**, 43-44.

94. Van Tittelboom, K.; De Belie, N.; De Muynck, W.; Verstraete, W., Use of bacteria to repair cracks in concrete. *Cement and Concrete Research* **2010,** *40* (1), 157-166.
95. Hamed Khodadadi, T.; Kavazanjian, E.; van Paassen, L.; Dejong, J., *Bio-Grout Materials: A Review*. 2017; p 1-12.
96. Halder, B. K.; Roy, D.; Tandon, V.; Ramana, C. V.; Tarquin, A. J., Use of mutated micro-organism to produce sustainable mortar. *ACI Materials Journal* **2014,** *111* (5).
97. Bundur, Z. B.; Kirisits, M. J.; Ferron, R. In *Bacterial calcification in cement paste and mortars containing mineral admixtures*, 1st International Congress on Bio-Based Building Materials, 2015.
98. Jonkers, H. M.; Thijssen, A.; Muyzer, G.; Copuroglu, O.; Schlangen, E., Application of bacteria as self-healing agent for the development of sustainable concrete. *Ecological Engineering* **2010,** *36* (2), 230-235.
99. American Petroleum Institute, Specification for Cements and Materials for Well Cementing Petroleum and natural gas industries—Cements and materials for well cementing—Part 1. 2005.
100. ASTM Standard C39 *Standard Test Method for Compressive Strength of Cylindrical Concrete Specimens*; ASTM International, West Conshohocken, PA: 2012.
101. ASTM Standard C109 *Standard Test Method for Compressive Strength of Hydraulic Cement Mortars*; ASTM International, West Conshohocken, PA: 2013.
102. C469, A. S., Standard Test Method for Static Modulus of Elasticity and Poisson's Ratio of Concrete in Compression. ASTM International, West Conshohocken, PA: 2014.
103. ASTM Standard C305 *Standard Practice for Mechanical Mixing of Hydraulic Cement Pastes and Mortars of Plastic Consistency*; ASTM International, West Conshohocken, PA: 2014.
104. Lauchnor, E. G.; Schultz, L. N.; Bugni, S.; Mitchell, A. C.; Cunningham, A. B.; Gerlach, R., Bacterially induced calcium carbonate precipitation and strontium coprecipitation in a porous media flow system. *Environ Sci Technol* **2013,** *47* (3), 1557-64.
105. Micro-Measurements *Strain Gage (Strain Gauge) Installations on Concrete Structures* 2015.
106. Shapiro, S. S.; Wilk, M. B., An analysis of variance test for normality (complete samples). *Biometrika* **1965,** *52* (3/4), 591-611.
107. Dunn, O. J., Multiple comparisons among means. *Journal of the American Statistical Association* **1961,** *56* (293), 52-64.
108. Li, M.; Li, L.; Ogbonnaya, U.; Wen, K.; Tian, A.; Amini, F., Influence of Fiber Addition on Mechanical Properties of MICP-Treated Sand. *Journal of Materials in Civil Engineering* **2016,** *28* (4), 04015166.
109. Yasuhara, H.; Neupane, D.; Hayashi, K.; Okamura, M., Experiments and predictions of physical properties of sand cemented by enzymatically-induced carbonate precipitation. *Soils and Foundations* **2012,** *52* (3), 539-549.
110. Park, S.-S.; Choi, S.-G.; Nam, I.-H., Effect of Plant-Induced Calcite Precipitation on the Strength of Sand. 2014; Vol. 26, p 06014017.

111. Cheng, L.; Cord-Ruwisch, R.; Shahin, M. A., Cementation of sand soil by microbially induced calcite precipitation at various degrees of saturation. *Canadian Geotechnical Journal* **2013,** *50* (1), 81-90.
112. Edward Kavazanjian, N. H., Enzyme Induced Carbonate Precipitation (EICP) Columns for Ground Improvement. In *2015 Geo-Congress*, 2015.
113. Stoodley, P.; Sauer, K.; Davies, D. G.; Costerton, J. W., Biofilms as complex differentiated communities. *Annual Review of Microbiology* **2002,** *56*, 187-209.
114. Beech, I. B.; Sunner, J., Biocorrosion: towards understanding interactions between biofilms and metals. *Curr. Opin. Biotechnol.* **2004,** *15* (3), 181-6.
115. Costerton, J. W.; Stewart, P. S.; Greenberg, E. P., Bacterial biofilms: A common cause of persistent infections. *Science* **1999,** *284* (5418), 1318-1322.
116. de Kreuk, M.; Heijnen, J. J.; van Loosdrecht, M. C. M., Simultaneous COD, nitrogen, and phosphate removal by aerobic granular sludge. *Biotechnology and Bioengineering* **2005,** *90* (6), 761-769.
117. Cunningham, A. B.; Sharp, R. R.; Hiebert, R.; James, G., Subsurface biofilm barriers for the containment and remediation of contaminated groundwater. *Biorem. J.* **2003,** *7* (3-4), 151-164.
118. Decho, A. W., Overview of biopolymer-induced mineralization: What goes on in biofilms? *Ecol. Eng.* **2010,** *36* (2), 137-144.
119. Ferris, F. G.; Phoenix, V.; Fujita, Y.; Smith, R. W., Kinetics of calcite precipitation induced by ureolytic bacteria at 10 to 20 degrees C in artificial groundwater. *Geochim. Cosmochim. Acta* **2003,** *67* (8), 1701-1722.
120. Fridjonsson, E. O.; Seymour, J. D.; Schultz, L. N.; Gerlach, R.; Cunningham, A. B.; Codd, S. L., NMR measurement of hydrodynamic dispersion in porous media subject to biofilm mediated precipitation reactions. *J. Contam. Hydrol.* **2011,** *120-21*, 79-88.
121. Mitchell, A. C.; Dideriksen, K.; Spangler, L. H.; Cunningham, A. B.; Gerlach, R., Microbially Enhanced Carbon Capture and Storage by Mineral-Trapping and Solubility-Trapping. *Environ. Sci. Technol.* **2010,** *44* (13), 5270-5276.
122. Behroozmand, A. A.; Keating, K.; Auken, E., A Review of the Principles and Applications of the NMR Technique for Near-Surface Characterization. *Surv Geophys* **2015,** *36* (1), 27-85.
123. Walsh, D.; Turner, P.; Grunewald, E.; Zhang, H.; Butler, J. J.; Reboulet, E.; Knobbe, S.; Christy, T.; Lane, J. W.; Johnson, C. D.; Munday, T.; Fitzpatrick, A., A small-diameter NMR logging tool for groundwater investigations. *Groundwater* **2013,** *51* (6), 914-926.
124. Sham, E.; Mantle, M. D.; Mitchell, J.; Tobler, D. J.; Phoenix, V. R.; Johns, M. L., Monitoring bacterially induced calcite precipitation in porous media using magnetic resonance imaging and flow measurements. *Journal of Contaminant Hydrology* **2013,** *152*, 35-43.
125. Kirkland, C. M.; Hiebert, R.; Phillips, A.; Grunewald, E.; Walsh, D. O.; Seymour, J. D.; Codd, S. L., Biofilm Detection in a Model Well-Bore Environment Using Low-Field NMR. *Groundwater Monitoring & Remediation* **2015**, DOI:10.1111/gwmr.12117.

126. Kirkland, C. M.; Herrling, M. P.; Hiebert, R.; Bender, A. T.; Grunewald, E.; Walsh, D. O.; Codd, S. L., In Situ Detection of Subsurface Biofilm Using Low-Field NMR: A Field Study. *Environmental Science & Technology* **2015,** *49* (18), 11045-11052.
127. Grunewald, E.; Knight, R., A laboratory study of NMR relaxation times in unconsolidated heterogeneous sediments. *Geophysics* **2011,** *76* (4), G73-G83.
128. Kleinberg, R. L.; Horsfield, M. A., Transverse relaxation processes in porous sedimentary rock. *Journal of Magnetic Resonance* **1990,** *88* (1), 9-19.
129. Kleinberg, R. L., Kenyon, W.E., Mitra, P.P., Mechanism of NMR relaxation of fluids in rock. *Journal of Magnetic Resonance Series A* **1994,** *108*, 206-214.
130. Bryar, T. R.; Daughney, C. J.; Knight, R. J., Paramagnetic effects of iron(III) species on nuclear magnetic relaxation of fluid protons in porous media. *Journal of Magnetic Resonance* **2000,** *142* (1), 74-85.
131. Foley, I.; Farooqui, S. A.; Kleinberg, R. L., Effect of paramagnetic ions on NMR relaxation of fluids at solid surfaces. *Journal of Magnetic Resonance Series A* **1996,** *123* (1), 95-104.
132. Kenyon, W. E.; Kolleeny, J. A., NMR surface relaxivity of calcite with adsorbed Mn2+. *Journal of Colloid and Interface Science* **1995,** *170* (2), 502-514.
133. Coates, G. R.; Marschall, D.; Mardon, D.; Galford, J., A new characterization of bulk-volume irreducible using magnetic resonance. *Log Analyst* **1998,** *39* (1), 51-63.
134. Zhang, Q.; Lo, S. W.; Huang, C. C.; Hirasaki, G. J.; Kobayashi, R.; House, W. V. In *Some exceptions to default NMR rock and fluid properties*, Transactions of the SPWLA Annual Logging Symposium (Society of Professional Well Log Analysts), 1998; pp FF1-FF14.
135. Wheeler, L. A. Establishment of ureolytic biofilms and their influence on the permeability of pulse-flow porous media column systems. Master's Thesis, Montana State University, Bozeman, MT, 2009.
136. Jung, D.; Biggs, H.; Erikson, J.; Ledyard, P. U., New colorimetric reaction for endpoint, continuous-flow and kinetic measurement of urea *Clin. Chem.* **1975,** *21* (8), 1136-1140.
137. Brufatto, C.; Cochran, J.; Conn, L.; Power, D.; El-Zeghaty, S.; Fraboulet, B.; Griffin, T.; James, S.; Munk, T.; Justus, F.; Levine, J.; Montgomery, C.; Murphy, D.; Pfeiffer, J.; Pornpoch, T.; Rishmani, L., From mud to cement- building gas wells. *Oilfield Review* **2003,** *15* (3), 62-76.
138. Choi, Y.-S.; Young, D.; Nešić, S.; Gray, L. G. S., Wellbore integrity and corrosion of carbon steel in CO_2 geologic storage environments: A literature review. *International Journal of Greenhouse Gas Control* **2013,** *Accepted proof*.
139. Crow, W.; Brian Williams, D.; William Carey, J.; Celia, M.; Gasda, S., Wellbore integrity analysis of a natural CO_2 producer. *Energy Procedia* **2009,** *1* (1), 3561-3569.
140. Gasda, S. E.; Bachu, S.; Celia, M. A., Spatial characterization of the location of potentially leaky wells penetrating a deep saline aquifer in a mature sedimentary basin. *Environmental Geology* **2004,** *46* (6/7), 707-720.

141. Bagal, J.; Onadeko, G.; Hazel, P.; Dagestad, V., Annular Barrier as an Alternative to Squeezes in Challenging Wells: Technology Review and Case Histories. In *SPE/AAPG Africa Energy and Technology Conference*, Society of Petroleum Engineers: Nairobi City, Kenya, 2016.
142. Genedy, M.; Kandil, U. F.; Matteo, E. N.; Stormont, J.; Reda Taha, M. M., A new polymer nanocomposite repair material for restoring wellbore seal integrity. *International Journal of Greenhouse Gas Control* **2017,** *58*, 290-298.
143. Jones, P. J.; Karcher, J.; Ruch, A.; Beamer, A.; Smit, P.; Hines, S.; Olson, M. R.; Day, D., Rigless Operation to Restore Wellbore Integrity using Synthetic-based Resin Sealants. Society of Petroleum Engineers.
144. Phillips, A. J. Biofilm-Induced Calcium Carbonate Precipitation: Application in the Subsurface. Montana State University, Bozeman, MT, 2013.
145. Gomez, M. G.; Martinez, B. C.; DeJong, J. T.; Hunt, C. E.; deVlaming, L. A.; Major, D. W.; Dworatzek, S. M., Field-scale bio-cementation tests to improve sands. *Proceedings of the Institution of Civil Engineers - Ground Improvement* **2015,** *168* (3), 206-216.
146. Herigstad, B.; Hamilton, M.; Heersink, J., How to optimize the drop plate method for enumerating bacteria. *Journal of Microbiological Methods* **2001,** *44* (2), 121-129.
147. Koplos, J.; Kobelski, B.; Karimjee, A.; Sham, C. UIC Program Mechanical Integrtiy Testing: Lessons for Carbon Capture and Storage? Fifth Annual Conference on Carbon Capture and Sequestration - DOE/NETL, Virginia, USA, Department of Energy: Virginia, USA, 2006; p 21.

148. US EPA. Determination of the mechanical integrity of injection wells. www.epa.gov/region5/water/uic/r5guid/r5_05_2008.htm.
149. Oil and Gas Conservation Act. Colorado Oil and Gas Commission Ed. http://cogcc.state.co.us/reg.html#/rules, Updated 2016; Vol. Rule 326: Mechanical Integrity Testing.
150. Montana Board of Oil & Gas Conservation Underground Injection Control Rules.
151. State Oil and Gas Board of Alabama David E. Bolin, E., Oil and Gas Report 1(The Gold Book) http://www2.ogb.state.al.us/documents/misc_ogb/goldbook.pdf, 2014.

152. Texas Railroad Commission, Injection/Disposal Well Permitting, Testing, and Monitoring Manual-Summary of Testing Requirements.
153. Energy Information Administration, The Distribution of U.S. Oil and Natural Gas Wells by Production Rate. US Department of Energy: Washington, DC 2018.
154. Yuan, B.; Wood, D. A., A comprehensive review of formation damage during enhanced oil recovery. *Journal of Petroleum Science and Engineering* **2018,** *167*, 287-299.
155. Udy, J.; Hansen, B.; Maddux, S.; Petersen, D.; Heilner, S.; Stevens, K.; Lignell, D.; Hedengren, J. D., Review of Field Development Optimization of Waterflooding, EOR, and Well Placement Focusing on History Matching and Optimization Algorithms. *Processes* **2017,** *5* (3).

156. Ahmed, A. A.; Mohamed, A. P. I., In-depth permeability modifier for improvement of sweep efficiency in a heterogeneous oil reservoir: a review. *Research Journal of Applied Sciences, Engineering and Technology* **2015,** *9* (1), 18-28.
157. Kargozarfard, Z.; Riazi, M.; Ayatollahi, S., Viscous fingering and its effect on areal sweep efficiency during waterflooding: an experimental study. *Petroleum Science* **2019,** *16* (1), 105-116.
158. Feng, Q.; Wang, S.; Zhang, W.; Song, Y.; Song, S., Characterization of high-permeability streak in mature waterflooding reservoirs using pressure transient analysis. *Journal of Petroleum Science and Engineering* **2013,** *110*, 55-65.
159. Davies, R. J.; Almond, S.; Ward, R. S.; Jackson, R. B.; Adams, C.; Worrall, F.; Herringshaw, L. G.; Gluyas, J. G.; Whitehead, M. A., Oil and gas wells and their integrity: Implications for shale and unconventional resource exploitation. *Marine and Petroleum Geology* **2014,** *56*, 239-254.
160. Ingraffea, A. R.; Wells, M. T.; Santoro, R. L.; Shonkoff, S. B. C., Assessment and risk analysis of casing and cement impairment in oil and gas wells in Pennsylvania, 2000–2012. *Proceedings of the National Academy of Sciences* **2014,** *111* (30), 10955-10960.
161. Wang, W.; Taleghani, A. D., Three-dimensional analysis of cement sheath integrity around wellbores. *Journal of Petroleum Science and Engineering* **2014,** *121*, 38-51.
162. Carroll, S. A.; Iyer, J.; Walsh, S. D. C., Influence of Chemical, Mechanical, and Transport Processes on Wellbore Leakage from Geologic CO2 Storage Reservoirs. *Accounts of Chemical Research* **2017,** *50* (8), 1829-1837.
163. De Andrade, J.; Sangesland, S., Cement Sheath Failure Mechanisms: Numerical Estimates to Design for Long-Term Well Integrity. *Journal of Petroleum Science and Engineering* **2016,** *147*, 682-698.
164. Haagsma, A.; Weber, S.; Moody, M.; Sminchak, J.; Gerst, J.; Gupta, N., Comparative wellbore integrity evaluation across a complex of oil and gas fields within the Michigan Basin and implications for CO_2 storage. *Greenhouse Gases-Science and Technology* **2017,** *7* (5), 828-842.
165. Newell, D. L.; Carey, J. W., Experimental Evaluation of Wellbore Integrity Along the Cement-rock Boundary. *Environmental Science & Technology* **2013,** *47* (1), 276-282.
166. Clarke, W. J.; McNally, A. C., Ultrafine Cement for Oilwell Cementing. In *Low Permeability Reservoirs Symposium*, Society of Petroleum Engineers: Denver, Colorado, 1993; p 8.
167. Bagal, J.; Onadeko, G.; Hazel, P.; Dagestad, V., Annular barrier as an alternative to squeezes in challenging wells: technology review and case histories. In *Africa Energy and Technology Conference*, American Association of Petroleum Geologists (AAPG) and Society of Petroleum Engineers (SPE): Nairobi, Kenja, 2016.
168. Oppenheimer-Shaanan, Y.; Sibony-Nevo, O.; Bloom-Ackermann, Z.; Suissa, R.; Steinberg, N.; Kartvelishvily, E.; Brumfeld, V.; Kolodkin-Gal, I., Spatio-temporal assembly of functional mineral scaffolds within microbial biofilms. *Npj Biofilms and Microbiomes* **2016,** *2*.

169. Wu, J.; Wang, X.-B.; Wang, H.-F.; Zeng, R. J., Microbially induced calcium carbonate precipitation driven by ureolysis to enhance oil recovery. *RSC Advances* **2017,** *7* (59), 37382-37391.
170. Ferris, F. G.; Stehmeier, L. G.; Kantzas, A.; Mourits, F. M., Bacteriogenic mineral plugging. *Journal of Canadian Petroleum Technology* **1996,** *35* (8), 56-61.
171. Fujita, Y.; Taylor, J. L.; Gresham, T. L. T.; Delwiche, M. E.; Colwell, F. S.; McLing, T. L.; Petzke, L. M.; Smith, R. W., Stimulation of microbial urea hydrolysis in groundwater to enhance calcite precipitation. *Environmental Science & Technology* **2008,** *42* (8), 3025-3032.
172. Burbank, M. B.; Weaver, T. J.; Green, T. L.; Williams, B. C.; Crawford, R. L., Precipitation of Calcite by Indigenous Microorganisms to Strengthen Liquefiable Soils. *Geomicrobiology Journal* **2011,** *28* (4), 301-312.
173. van Paassen Leon, A.; Ghose, R.; van der Linden, T. J. M.; van der Star, W. R. L.; van Loosdrecht, M. C. M., Quantifying Biomediated Ground Improvement by Ureolysis: Large-Scale Biogrout Experiment. *Journal of Geotechnical and Geoenvironmental Engineering* **2010,** *136* (12), 1721-1728.
174. Johns, J. E.; Blount, C. G.; Dethlefs, J. C.; Loveland, M. J.; McConnell, M. L.; Schwartz, G. L.; Julian, J. Y., Applied Ultrasonic Technology in Wellbore-Leak Detection and Case Histories in Alaska North Slope Wells. *Spe Production & Operations* **2009,** *24* (2), 225-232.
175. Frisch, G. J.; Graham, L.; Wyatt, D., Economic evaluation of the use of well logs for diagnosing conformance problems. In *SPE Gas Technology Symposium*, Society of Petroleum Engineers: Calgary, Alberta, Canada, 1998.
176. Loeb, J.; Poupon, A., Temperature logs in production and injection wells. In *27th Meeting of the the European Association of Exploration Geophysicists*, SPE Schlumberger: Madrid, Spain, May, 1965.
177. Kirkland, C. M.; Norton, D.; Firth, O.; Eldring, J.; Cunningham, A. B.; Gerlach, R.; Phillips, A. J., Visualizing MICP with X-ray uCT to enhance cement defect sealing. *International Journal of Greenhouse Gas Control* **2019,** *86*, 93 - 100
178. Verba, C.; Thurber, A. R.; Alleau, Y.; Koley, D.; Colwell, F.; Torres, M. E., Mineral changes in cement-sandstone matrices induced by biocementation. *International Journal of Greenhouse Gas Control* **2016,** *49*, 312-322.
179. Phillips, A. J. Biofilm-Induced Calcium Carbonate Precipitation: Application in the Subsurface. Montana State University, 2013.

180. Kirkland, C. M.; Thane, A.; Cunningham, A. B.; Gerlach, R.; Hiebert, R.; Hyatt, R.; Kirksey, J.; Spangler, L.; Phillips, A. J., Improving waterflood efficiency using microbially-induced calcium carbonate precipitation (MICP): a field demonstration. *J Pet Sci Eng* **submitted**.

BIBLIOGRAPHY

None

LIST OF ACRONYMS AND ABBREVIATIONS

Nomenclature

A = cross-sectional area of the defect,
A= area of loaded surface mm^2 or $[in^2]$
b = aperture of the channel gap,
$[Ca^{2+}]$ and $[CO_3^{2-}]$ are the activities of the calcium and carbonate ions
E = chord modulus of elasticity MPa [psi]
ε_2 = longitudinal strain produced by stress S_2
g= gravitational constant,
Δh, P = injection pressure
JBM= jack bean meal
k= apparent fracture permeability,
K_{so} is the solubility constant of $CaCO_3$ ($5x10^{-9}$ at 25°C)
L = length of the channel
MICP= microbially-induced calcium carbonate precipitation
MSU=Montana State University
μ = dynamic viscosity of the fluid
NMR= nuclear magnetic resonance
P = total maximum load N or [kip]
Q = flow rate,
ρ = density of the fluid,
S_2 = stress corresponding to 40 % of ultimate load
S_1 = stress corresponding to a longitudinal strain
S is the saturation state of $CaCO_3$
σ = compressive strength in MPa or [psi]
w = width of the channel

PUBLICATIONS

Cunningham, A.B., Class, H., Ebigbo, A., Gerlach, R., Phillips, A.J. and Hommel, J., Field-scale modeling of microbially induced calcite precipitation. Computational Geosciences, 2019. 23(2): p. 399-414 DOI: 10.1007/s10596-018-9797-6.

Kirkland, C.M., Norton, D., Firth, O., Eldring, J., Cunningham, A.B., Gerlach, R. and Phillips, A.J., Visualizing MICP with X-ray µ-CT to enhance cement defect sealing. International Journal of Greenhouse Gas Control, 2019. 86(July 2019): p. 93-100 DOI: 10.1016/j.ijggc.2019.04.019.

Phillips, A.J., Troyer, E., Heibert, R., Kirkland, C.M., Gerlach, R., Cunningham, A.B., Spangler, L., Kirksey, J., Rowe, W. and Esposito, R., Enhancing wellbore cement integrity with microbially induced calcite precipitation (MICP): A field scale demonstration. Journal of

Petroleum Science and Engineering, 2018. 171(December 2018): p. 1141-1148 DOI: 10.1016/j.petrol.2018.08.012.

Besser, D. (2018). Ureolysis induced mineral precipitation material properties compared to oil and gas well cements. Civil Engineering. Bozeman, MT. Masters.

Norton, D. (2017). Visualizing and Quantifying Biomineralization in Wellbore Analog Reactors. Masters Defense. Civil & Environmental Engineering. Bozeman, MT. Masters.

Kirkland, C.M., Zanetti, S., Grunewald, E., Walsh, D.O., Codd, S.L. and Phillips, A., Detecting microbially induced calcite precipitation (MICP) in a model well-bore using downhole low-field NMR. Environmental Science and Technology, 2016. 51(3): p. 1537-1543 DOI: 10.1021/acs.est.6b04833.

Phillips, A., Cunningham, A., Gerlach, R., Hiebert, R., Hwang, C., Lomans, B., Westridge, J., Mantilla, C., Kirksey, J., Esposito, A. and Spangler, L., Fracture Sealing with Microbially-Induced Calcium Carbonate Precipitation: A Field Study. Environmental Science & Technology Journal, 2016. 50(7): p. 4111-4117 DOI: 10.1021/acs.est.5b05559.

PRESENTATIONS

Kirkland, C.M., Norton, D., Thane, A., Heibert, R., Hommel, J., Kirksey, J., Esposito, R., Cunningham, A.B., Gerlach, R., Spangler, L. and Phillips, A.J. Biomineralization and Wellbore Integrity: A Microscopic Solution to Subsurface Fluid Migration. in 14th Greenhouse Gas Control Technologies Conference. 2019. Melbourne, Australia.

Phillips, A.J., Methods to Enhance Wellbore Cement Integrity with Microbially-Induced Calcite Precipitation (MICP), in U.S. Department of Energy, National Energy Technology Laboratory Mastering the Subsurface Through Technology Innovation, Partnerships and Collaboration: Carbon Storage and Oil and Natural Gas Technologies Review Meeting. 2019: Pittsburgh, PA

Gerlach, R., Controlling Stone-Producing Microbes – The Good Ones and the Evil Ones in Montana State University 125th Anniversary, Faculty Symposium. 2018: Bozeman, MT

Phillips, A., Morasko, V., Daily, R., Kirkland, C.M., Gerlach, R., Cunningham, A. and Spangler, L., Urease: a journey from laboratory to field, in Montana State University Center for Biofilm Engineering Weekly Seminar Series. 2018: Bozeman, MT

Besser, D., C., W., Daily, R., Cunningham, A., Gerlach, R., Fick, D., Spangler, L. and Phillips, A., Assessment of ureolysis induced mineral precipitation material properties compared to oil and gas well cements, in American Rock Mechanics Association 51st Annual Meeting Proceedings. Paper # 588. 2017: San Francisco, CA

Besser, D., C., W., Daily, R., Cunningham, A., Gerlach, R., Fick, D., Spangler, L. and Phillips, A., Assessment of ureolysis induced mineral precipitation material properties compared to oil and gas well cements, in Montana Biofilms Meeting. 2017: Bozeman, MT

Besser, D., West, C., Cunningham, A., Fick, D., Phillips, A.J., Daily, R., Gerlach, R. and Spangler, L. Assessment of Ureolysis Induced Mineral Precipitation Material Properties Compared to Oil and Gas Well Cements. in 51st U.S. Rock Mechanics/Geomechanics Symposium. 2017. San Francisco, CA: American Rock Mechanics Association.

Besser, D., West, C., Daily, R., Cunningham, A., Gerlach, R., Fick, D., Spangler, L. and Phillips, A. Assessment of ureolysis induced mineral precipitation material properties compared to oil and gas well cements. in American Rock Mechanics Association 51st Annual Meeting. 2017. San Francisco, CA.

Phillips, A., Cunningham, A., Gerlach, R. and Spangler, L., Methods to Enhance Wellbore Cement Integrity with Microbially-induced Calcite Precipitation (MICP), in Mastering the Subsurface Through Technology Innovation, Partnerships and Collaboration: Carbon Storage and Oil and Natural Gas Technologies Review Meeting, U.S. Department of Energy Fossil Energy and National Energy Technology Laboratory. 2017: Pittsburgh, PA

Phillips, A., Gerlach, R., Cunningham, A., Hommel, J., Helmig, R., Hiebert, R., Kirksey, J., Rowe, W., Esposito, A. and Spangler, L., Biomineralization: a strategy to modify permeability in the subsurface, in 9th International Conference on Porous Media & Annual Meeting. 2017: Rotterdam, Netherlands

Phillips, A., Gerlach, R., Cunningham, A. and Spangler, L., (Bio)mineralization for Permeability Modification and Wellbore Sealing, in Society of Petroleum Engineers Annual Spring Symposium. 2017: Butte, MT

Troyer, E., West, C., Berninghaus, A., Joyce, J., Gerlach, R., Phillips, A. and Foreman, C. Biomineralized Art: Using Microbes and Minds to Make Mountains. in American Rock Mechanics Association 51st Annual Meeting. 2017. San Francisco, CA.

Gerlach, R., Cunningham, A., Spangler, L., Phillips, A., Hiebert, R., Kirksey, J., Rowe, W., Esposito, R., Lomans, B. and Busch, A., Biocementation for Wellbore Integrity Restoration and Enhanced Resource Recovery, in RMF2016: 22nd Reservoir Microbiology Forum. 2016: London, UK

Gerlach, R., Phillips, A., Cunningham, A. and Spangler, L. Biofilm-Mediated Mineral Precipitation Technology – From the Microscale to the Field-Scale. in Goldschmidt Conferenece. 2016. Yokohama, Japan.

Gerlach, R., Phillips, A., Cunningham, A. and Spangler, L., Controlling Fluid Flow in the Subsurface through Ureolysis-Controlled Mineral Precipitation, in American Geophysical Union Fall Meeting. 2016: San Francisco, CA

Norton, D., Gerlach, R., Eldring, J., Thane, J., Hiebert, R., Cunningham, A., Spangler, L. and Phillips, A.J., Visualizing and Quantifying Biomineralization in a Wellbore Analog Reactor, in Geologic Society of America Annual Meeting. Poster. 2016: Denver, CO

Norton, D., Gerlach, R., Eldring, J., Thane, J., Hiebert, R., Cunningham, A., Spangler, L. and Phillips, A.J., Visualizing and Quantifying Biomineralization in a Wellbore Analog Reactor, in Montana Biofilm Meeting. Poster. 2016: Bozeman, MT

Phillips, A., Cunningham, A., Gerlach, R. and Spangler, L., Biomineralization Sealing Technology- A Technology Developed in Montana, in Montana Energy Conference 2016. 2016: Billings, MT

Phillips, A., Gerlach, R., Cunningham, A. and Spangler, L., Methods to Enhance Wellbore Cement Integrity with Microbially-induced Calcite Precipitation (MICP), in Mastering the

Subsurface through Technology Innovation and Collaboration: Carbon Storage and Oil and Natural Gas Technologies Review Meeting U.S. Department of Energy Fossil Energy and National Energy Technology Laboratory. 2016: Pittsburgh, PA

Phillips, A., Gerlach, R., Cunningham, A., Troyer, E., Norton, D., Hiebert, R., Kirksey, J., Rowe, W., Esposito, A. and Spangler, L., Biomineralization: a strategy to modify permeability in the subsurface, in Geologic Society of America Annual Meeting. 2016: Denver, CO

Phillips, A.J., Gerlach, R., Cunningham, A., Troyer, E., West, D., Norton, D., Hiebert, R., Kirksey, J., Rowe, W., Esposito, A. and Spangler, L., Biomineralization: A Promising Method to Improve Wellbore Integrity, in Workshop on Natural Gas Storage in Depleted Reservoirs or Aquifers, US DOE National Laboratories. Poster. 2016: Broomfield, CO

Gerlach, R., Cunningham, A., Phillips, A., Hiebert, R., Lauchnor, E., Mitchell, A. and Spangler, L. Biofilm-Mediated Mineral Precipitation Technology – from the Microscale to the Field-Scale. in 7th American Society of Microbiology Biofilms Conference. 2015. Chicago, IL.

Gerlach, R., Cunningham, A. and Spangler, L., Field Test and Evaluation of Engineered Biomineralization Technology for Sealing Existing Wells, in U.S. Department of Energy, National Energy Technology Laboratory, Carbon Storage R&D Project Review Meeting. 2015: Pittsburgh, PA

Phillips, A., Gerlach, R., Cunningham, A., Spangler, L., Hiebert, R., Kirksey, J. and Esposito, A. Biological Influences In the Subsurface: A Method to Seal Fractures and Reduce Permeability with Microbially-Induced Calcite Precipitation. in ARMA (American Rock Mechanics/Geomechanics) Symposium. 2015. San Francisco, CA.

Spangler, L., Gerlach, R., Cunningham, A. and Phillips, A. Biofilm-Mediated Mineral Precipitation Technology – From the Microscale to the Field-Scale. in IEAGHG Risk Management Network and Environmental Research Network Meeting. 2015. Southampton, UK.

OTHER PRODUCTS PRODUCED

Inventions/Patent Applications:
MSU reported the below invention disclosure, and a patent has not been filed yet. The technology is currently on hold for further development. MSU filed and received an extension to elect title through 4/12/2021.

Title: A METHOD TO PREVENT FLOW OF PARTICULATES INTO WELLBORES

Inventors

First Name	**Middle Ini**	**Last Name**
Adrienne	J	Phillips
Robin		Gerlach
Vincent	John	Morasko
Dwight	R	Hiebert
Alfred	B	Cunningham
Burt		Todd
Lee	H	Spangler

Date Reported 6/20/2017
DOE “S” No. S-148,083

APPENDIX: Rights and Permissions from Publication Copyright Holders

Leonti, Michelle

From: Peter Smeallie <peterhsmeallie@gmail.com>
Sent: Wednesday, January 22, 2020 12:01 PM
To: Leonti, Michelle
Subject: RE: Permission for re-use of ARMA paper?

Dear Michelle,

ARMA is pleased to grant a copyright waiver to use the paper below as specified with proper attribution.

As a matter of courtesy, the professor may wish to inform the paper authors.

Sincerely,

Peter

Peter Smeallie
Executive Director
American Rock Mechanics Association
600 Woodland Terrace
Alexandria, VA 22302
703-683-1808 (office)
703-801-1088 (cell)
703-997-6112 (fax)
www.armarocks.org

From: Leonti, Michelle [mailto:michelle.leonti@montana.edu]
Sent: Wednesday, January 22, 2020 1:33 PM
To: peterhsmeallie@gmail.com
Subject: RE: Permission for re-use of ARMA paper?

Hello Again,

I came across the attached copy of the paper, which does indicate ARMA holds the copyright; however, the webpage does not mention copyright.

Thanks again,
Michelle

Michelle Leonti, CWCA
Administration Manager
Energy Research Institute
Montana State University
PO Box 172465
Bozeman, MT 59717-2465
Phone: (406) 994-1658
michelle.leonti@montana.edu

http://www.montana.edu/energy/

From: Leonti, Michelle
Sent: Wednesday, January 22, 2020 9:48 AM
To: peterhsmeallie@gmail.com
Subject: FW: Permission for re-use of ARMA paper?

Hello Peter,

Thank you for taking my call today. Below is the original request made by the Principal Investigator for the project. As stated in our conversation, we would like to use the conference proceeding "Assessment of Ureolysis Induced Mineral Precipitation Material Properties Compared to Oil and Gas Well Cements" (https://www.onepetro.org/conference-paper/ARMA-2017-0588) in a final report to the US Department of Energy which will be available to the public. The copyright holder is not clear to us.

Thank you,
Michelle

Michelle Leonti, CWCA
Administration Manager
Energy Research Institute
Montana State University
PO Box 172465
Bozeman, MT 59717-2465
Phone: (406) 994-1658
michelle.leonti@montana.edu
http://www.montana.edu/energy/

From: Adrienne Phillips <adrienne.phillips@montana.edu>
Sent: Thursday, January 2, 2020 11:14 AM
To: info@armarocks.org
Cc: Leonti, Michelle <michelle.leonti@montana.edu>
Subject: Permission for re-use of ARMA paper?

Good morning,
I would like to request to reuse a modified version of a paper that was published as part of an ARMA conference proceeding in a final report for the funding agency. However, there is no button on the paper's link (at the One Petro website) called "rights and permissions" as was instructed in the directions found here: https://www.onepetro.org/static-pages/Copyright

Can you please instruct us where to find information about how to request permission for the reuse of the paper? Here is a link to the paper: https://www.onepetro.org/conference-paper/ARMA-2017-0588

Thanks in advance for the information.

My best,
Adie

Adrienne (Adie) Phillips
Assistant Professor
Civil Engineering Department
Center for Biofilm Engineering

Energy Research Institute
Montana State University
406.994.2119

Permission To Copy or To Use Copyrighted Material

Guneycan Dicle Beser provides MSU permission to copy and use copyrighted materials listed below for the purposes of the Methods to Enhance Wellbore Cement Integrity with Microbially-Induced Calcite Precipitation (MICP) (DE-FE0024296) final scientific/technical report by MSU. This material will be used solely for nonprofit educational or research purposes in accordance with the mission of Montana State University. The copied material will not be sold.

This permission is non-exclusive, royalty-free (no cost to the Montana State University), world-wide, and perpetual.

By giving MSU permission to use the copyrighted material, permission is also granted to the Department of Energy and the U.S. Government to use the copyrighted material. The Government reserves for itself and others acting on its behalf a royalty-free, nonexclusive, irrevocable, worldwide license for Governmental purposes to publish, distribute, translate, duplicate, exhibit, and perform this copyrighted paper.

Please sign the release form below to signify agreement.

Permission for use only as stated above is granted.

Guneycan Dicle Beser Digitally signed by Guneycan Dicle Beser
DN: C=US, E=dbeser@mccarthy.com, CN=Guneycan Dicle Beser
Date: 2020.01.15 14:55:23-06'00'

Copyright Holder's Signature _____ Date _____

Permission extends to the following materials:

Beser, GD. Ureolysis induced mineral precipitation material properties compared to oil and gas well cements. MS Thesis, Civil Engineering, Montana State University, April 2018

Permission To Copy or To Use Copyrighted Material

Alfred Cunningham provides MSU permission to copy and use copyrighted materials listed below for the purposes of the Methods to Enhance Wellbore Cement Integrity with Microbially-Induced Calcite Precipitation (MICP) (DE-FE0024296) final scientific/technical report by MSU. This material will be used solely for nonprofit educational or research purposes in accordance with the mission of Montana State University. The copied material will not be sold.

This permission is non-exclusive, royalty-free (no cost to the Montana State University), world-wide, and perpetual.

By giving MSU permission to use the copyrighted material, permission is also granted to the Department of Energy and the U.S. Government to use the copyrighted material. The Government reserves for itself and others acting on its behalf a royalty-free, nonexclusive, irrevocable, worldwide license for Governmental purposes to publish, distribute, translate, duplicate, exhibit, and perform this copyrighted paper.

Please sign the release form below to signify agreement.

Permission for use only as stated above is granted.

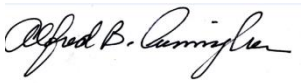

_____01/06/2020_____

Copyright Holder's Signature Date

Permission extends to the following materials:

Kirkland, C, Norton, D, Cunningham, A, Thane, A, Gerlach, R, Hiebert, R, Hommel, J, Kirksey, J, Esposito, R, Spangler, L, Phillips, AJ. (2018) Biomineralization and wellbore integrity: a microscopic solution to subsurface fluid migration 14th Greenhouse Gas Control Technologies Conference Melbourne, Australia October 21-25, 2018 (SSRN published online April 2019) https://papers.ssrn.com/sol3/papers.cfm?abstract_id=3366088

Permission To Copy or To Use Copyrighted Material

Richard Esposito provides MSU permission to copy and use copyrighted materials listed below for the purposes of the Methods to Enhance Wellbore Cement Integrity with Microbially-Induced Calcite Precipitation (MICP) (DE-FE0024296) final scientific/technical report by MSU. This material will be used solely for nonprofit educational or research purposes in accordance with the mission of Montana State University. The copied material will not be sold.

This permission is non-exclusive, royalty-free (no cost to the Montana State University), world-wide, and perpetual.

By giving MSU permission to use the copyrighted material, permission is also granted to the Department of Energy and the U.S. Government to use the copyrighted material. The Government reserves for itself and others acting on its behalf a royalty-free, nonexclusive, irrevocable, worldwide license for Governmental purposes to publish, distribute, translate, duplicate, exhibit, and perform this copyrighted paper.

Please sign the release form below to signify agreement.

Permission for use only as stated above is granted.

Copyright Holder's Signature

1/9/2020

Date

Permission extends to the following materials:

Kirkland, C, Norton, D, Cunningham, A, Thane, A, Gerlach, R, Hiebert, R, Hommel, J, Kirksey, J, Esposito, R, Spangler, L, Phillips, AJ. (2018) Biomineralization and wellbore integrity: a microscopic solution to subsurface fluid migration 14th Greenhouse Gas Control Technologies Conference Melbourne, Australia October 21-25, 2018 (SSRN published online April 2019) https://papers.ssrn.com/sol3/papers.cfm?abstract_id=3366088

Permission To Copy or To Use Copyrighted Material

Robin Gerlach provides MSU permission to copy and use copyrighted materials listed below for the purposes of the Methods to Enhance Wellbore Cement Integrity with Microbially-Induced Calcite Precipitation (MICP) (DE-FE0024296) final scientific/technical report by MSU. This material will be used solely for nonprofit educational or research purposes in accordance with the mission of Montana State University. The copied material will not be sold.

This permission is non-exclusive, royalty-free (no cost to the Montana State University), world-wide, and perpetual.

By giving MSU permission to use the copyrighted material, permission is also granted to the Department of Energy and the U.S. Government to use the copyrighted material. The Government reserves for itself and others acting on its behalf a royalty-free, nonexclusive, irrevocable, worldwide license for Governmental purposes to publish, distribute, translate, duplicate, exhibit, and perform this copyrighted paper.

Please sign the release form below to signify agreement.

Permission for use only as stated above is granted.

Copyright Holder's Signature

Jan 08, 2020
Date

Permission extends to the following materials:

Kirkland, C, Norton, D, Cunningham, A, Thane, A, Gerlach, R, Hiebert, R, Hommel, J, Kirksey, J, Esposito, R, Spangler, L, Phillips, AJ. (2018) Biomineralization and wellbore integrity: a microscopic solution to subsurface fluid migration 14th Greenhouse Gas Control Technologies Conference Melbourne, Australia October 21-25, 2018 (SSRN published online April 2019) https://papers.ssrn.com/sol3/papers.cfm?abstract_id=3366088

Permission To Copy or To Use Copyrighted Material

Randy Hiebert provides MSU permission to copy and use copyrighted materials listed below for the purposes of the Methods to Enhance Wellbore Cement Integrity with Microbially-Induced Calcite Precipitation (MICP) (DE-FE0024296) final scientific/technical report by MSU. This material will be used solely for nonprofit educational or research purposes in accordance with the mission of Montana State University. The copied material will not be sold.

This permission is non-exclusive, royalty-free (no cost to the Montana State University), world-wide, and perpetual.

By giving MSU permission to use the copyrighted material, permission is also granted to the Department of Energy and the U.S. Government to use the copyrighted material. The Government reserves for itself and others acting on its behalf a royalty-free, nonexclusive, irrevocable, worldwide license for Governmental purposes to publish, distribute, translate, duplicate, exhibit, and perform this copyrighted paper.

Please sign the release form below to signify agreement.

Permission for use only as stated above is granted.

Randy Hiebert — Jan. 8, 2020

Copyright Holder's Signature — Date

Permission extends to the following materials:

Kirkland, C, Norton, D, Cunningham, A, Thane, A, Gerlach, R, Hiebert, R, Hommel, J, Kirksey, J, Esposito, R, Spangler, L, Phillips, AJ. (2018) Biomineralization and wellbore integrity: a microscopic solution to subsurface fluid migration 14th Greenhouse Gas Control Technologies Conference Melbourne, Australia October 21-25, 2018 (SSRN published online April 2019) https://papers.ssrn.com/sol3/papers.cfm?abstract_id=3366088

Permission To Copy or To Use Copyrighted Material

Johannes Hommel provides MSU permission to copy and use copyrighted materials listed below for the purposes of the Methods to Enhance Wellbore Cement Integrity with Microbially-Induced Calcite Precipitation (MICP) (DE-FE0024296) final scientific/technical report by MSU. This material will be used solely for nonprofit educational or research purposes in accordance with the mission of Montana State University. The copied material will not be sold.

This permission is non-exclusive, royalty-free (no cost to the Montana State University), world-wide, and perpetual.

By giving MSU permission to use the copyrighted material, permission is also granted to the Department of Energy and the U.S. Government to use the copyrighted material. The Government reserves for itself and others acting on its behalf a royalty-free, nonexclusive, irrevocable, worldwide license for Governmental purposes to publish, distribute, translate, duplicate, exhibit, and perform this copyrighted paper.

Please sign the release form below to signify agreement.

Permission for use only as stated above is granted.

Copyright Holder's Signature Date

Permission extends to the following materials:

Kirkland, C, Norton, D, Cunningham, A, Thane, A, Gerlach, R, Hiebert, R, Hommel, J, Kirksey, J, Esposito, R, Spangler, L, Phillips, AJ. (2018) Biomineralization and wellbore integrity: a microscopic solution to subsurface fluid migration 14th Greenhouse Gas Control Technologies Conference Melbourne, Australia October 21-25, 2018 (SSRN published online April 2019) https://papers.ssrn.com/sol3/papers.cfm?abstract_id=3366088

Permission To Copy or To Use Copyrighted Material

Catherine M. Kirkland provides MSU permission to copy and use copyrighted materials listed below for the purposes of the Methods to Enhance Wellbore Cement Integrity with Microbially-Induced Calcite Precipitation (MICP) (DE-FE0024296) final scientific/technical report by MSU. This material will be used solely for nonprofit educational or research purposes in accordance with the mission of Montana State University. The copied material will not be sold.

This permission is non-exclusive, royalty-free (no cost to the Montana State University), world-wide, and perpetual.

By giving MSU permission to use the copyrighted material, permission is also granted to the Department of Energy and the U.S. Government to use the copyrighted material. The Government reserves for itself and others acting on its behalf a royalty-free, nonexclusive, irrevocable, worldwide license for Governmental purposes to publish, distribute, translate, duplicate, exhibit, and perform this copyrighted paper.

Please sign the release form below to signify agreement.

Permission for use only as stated above is granted.

Catherine M. Kirkland — 1/8/2020

Copyright Holder's Signature — Date

Permission extends to the following materials:

Kirkland, C, Norton, D, Cunningham, A, Thane, A, Gerlach, R, Hiebert, R, Hommel, J, Kirksey, J, Esposito, R, Spangler, L, Phillips, AJ. (2018) Biomineralization and wellbore integrity: a microscopic solution to subsurface fluid migration 14th Greenhouse Gas Control Technologies Conference Melbourne, Australia October 21-25, 2018 (SSRN published online April 2019) https://papers.ssrn.com/sol3/papers.cfm?abstract_id=3366088

Permission To Copy or To Use Copyrighted Material

Jim Kirksey provides MSU permission to copy and use copyrighted materials listed below for the purposes of the Methods to Enhance Wellbore Cement Integrity with Microbially-Induced Calcite Precipitation (MICP) (DE-FE0024296) final scientific/technical report by MSU. This material will be used solely for nonprofit educational or research purposes in accordance with the mission of Montana State University. The copied material will not be sold.

This permission is non-exclusive, royalty-free (no cost to the Montana State University), world-wide, and perpetual.

By giving MSU permission to use the copyrighted material, permission is also granted to the Department of Energy and the U.S. Government to use the copyrighted material. The Government reserves for itself and others acting on its behalf a royalty-free, nonexclusive, irrevocable, worldwide license for Governmental purposes to publish, distribute, translate, duplicate, exhibit, and perform this copyrighted paper.

Please sign the release form below to signify agreement.

Permission for use only as stated above is granted.

Recoverable Signature

X

Jim Kirksey
Principal
Signed by: bc1708ed-298a-4e3e-945e-034428bce4ef 1/08/2020

Copyright Holder's Signature Date

Permission extends to the following materials:

Kirkland, C, Norton, D, Cunningham, A, Thane, A, Gerlach, R, Hiebert, R, Hommel, J, Kirksey, J, Esposito, R, Spangler, L, Phillips, AJ. (2018) Biomineralization and wellbore integrity: a microscopic solution to subsurface fluid migration 14th Greenhouse Gas Control Technologies Conference Melbourne, Australia October 21-25, 2018 (SSRN published online April 2019) https://papers.ssrn.com/sol3/papers.cfm?abstract_id=3366088

Permission To Copy or To Use Copyrighted Material

Drew Owen Norton provides MSU permission to copy and use copyrighted materials listed below for the purposes of the Methods to Enhance Wellbore Cement Integrity with Microbially-Induced Calcite Precipitation (MICP) (DE-FE0024296) final scientific/technical report by MSU. This material will be used solely for nonprofit educational or research purposes in accordance with the mission of Montana State University. The copied material will not be sold.

This permission is non-exclusive, royalty-free (no cost to the Montana State University), world-wide, and perpetual.

By giving MSU permission to use the copyrighted material, permission is also granted to the Department of Energy and the U.S. Government to use the copyrighted material. The Government reserves for itself and others acting on its behalf a royalty-free, nonexclusive, irrevocable, worldwide license for Governmental purposes to publish, distribute, translate, duplicate, exhibit, and perform this copyrighted paper.

Please sign the release form below to signify agreement.

Permission for use only as stated above is granted.

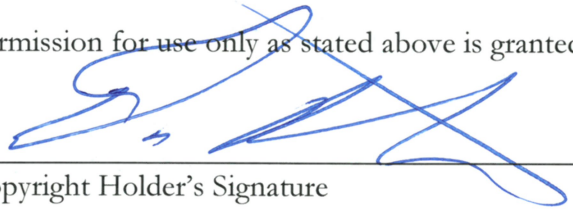

Copyright Holder's Signature

1/8/2020

Date

Permission extends to the following materials:

Kirkland, C, Norton, D, Cunningham, A, Thane, A, Gerlach, R, Hiebert, R, Hommel, J, Kirksey, J, Esposito, R, Spangler, L, Phillips, AJ. (2018) Biomineralization and wellbore integrity: a microscopic solution to subsurface fluid migration 14th Greenhouse Gas Control Technologies Conference Melbourne, Australia October 21-25, 2018 (SSRN published online April 2019) https://papers.ssrn.com/sol3/papers.cfm?abstract_id=3366088

Permission To Copy or To Use Copyrighted Material

Adrienne Phillips provides MSU permission to copy and use copyrighted materials listed below for the purposes of the Methods to Enhance Wellbore Cement Integrity with Microbially-Induced Calcite Precipitation (MICP) (DE-FE0024296) final scientific/technical report by MSU. This material will be used solely for nonprofit educational or research purposes in accordance with the mission of Montana State University. The copied material will not be sold.

This permission is non-exclusive, royalty-free (no cost to the Montana State University), world-wide, and perpetual.

By giving MSU permission to use the copyrighted material, permission is also granted to the Department of Energy and the U.S. Government to use the copyrighted material. The Government reserves for itself and others acting on its behalf a royalty-free, nonexclusive, irrevocable, worldwide license for Governmental purposes to publish, distribute, translate, duplicate, exhibit, and perform this copyrighted paper.

Please sign the release form below to signify agreement.

Permission for use only as stated above is granted.

Copyright Holder's Signature

1/9/2020
Date

Permission extends to the following materials:

Kirkland, C, Norton, D, Cunningham, A, Thane, A, Gerlach, R, Hiebert, R, Hommel, J, Kirksey, J, Esposito, R, Spangler, L, Phillips, AJ. (2018) Biomineralization and wellbore integrity: a microscopic solution to subsurface fluid migration 14th Greenhouse Gas Control Technologies Conference Melbourne, Australia October 21-25, 2018 (SSRN published online April 2019) https://papers.ssrn.com/sol3/papers.cfm?abstract_id=3366088

Permission To Copy or To Use Copyrighted Material

Lee H. Spangler provides MSU permission to copy and use copyrighted materials listed below for the purposes of the Methods to Enhance Wellbore Cement Integrity with Microbially-Induced Calcite Precipitation (MICP) (DE-FE0024296) final scientific/technical report by MSU. This material will be used solely for nonprofit educational or research purposes in accordance with the mission of Montana State University. The copied material will not be sold.

This permission is non-exclusive, royalty-free (no cost to the Montana State University), world-wide, and perpetual.

By giving MSU permission to use the copyrighted material, permission is also granted to the Department of Energy and the U.S. Government to use the copyrighted material. The Government reserves for itself and others acting on its behalf a royalty-free, nonexclusive, irrevocable, worldwide license for Governmental purposes to publish, distribute, translate, duplicate, exhibit, and perform this copyrighted paper.

Please sign the release form below to signify agreement.

Permission for use only as stated above is granted.

Copyright Holder's Signature

1/8/2020
Date

Permission extends to the following materials:

Kirkland, C, Norton, D, Cunningham, A, Thane, A, Gerlach, R, Hiebert, R, Hommel, J, Kirksey, J, Esposito, R, Spangler, L, Phillips, AJ. (2018) Biomineralization and wellbore integrity: a microscopic solution to subsurface fluid migration 14th Greenhouse Gas Control Technologies Conference Melbourne, Australia October 21-25, 2018 (SSRN published online April 2019) https://papers.ssrn.com/sol3/papers.cfm?abstract_id=3366088

Permission To Copy or To Use Copyrighted Material

Abby Thane provides MSU permission to copy and use copyrighted materials listed below for the purposes of the Methods to Enhance Wellbore Cement Integrity with Microbially-Induced Calcite Precipitation (MICP) (DE-FE0024296) final scientific/technical report by MSU. This material will be used solely for nonprofit educational or research purposes in accordance with the mission of Montana State University. The copied material will not be sold.

This permission is non-exclusive, royalty-free (no cost to the Montana State University), world-wide, and perpetual.

By giving MSU permission to use the copyrighted material, permission is also granted to the Department of Energy and the U.S. Government to use the copyrighted material. The Government reserves for itself and others acting on its behalf a royalty-free, nonexclusive, irrevocable, worldwide license for Governmental purposes to publish, distribute, translate, duplicate, exhibit, and perform this copyrighted paper.

Please sign the release form below to signify agreement.

Permission for use only as stated above is granted.

Copyright Holder's Signature

1/15/2020
Date

Permission extends to the following materials:

Kirkland, C, Norton, D, Cunningham, A, Thane, A, Gerlach, R, Hiebert, R, Hommel, J, Kirksey, J, Esposito, R, Spangler, L, Phillips, AJ. (2018) Biomineralization and wellbore integrity: a microscopic solution to subsurface fluid migration 14th Greenhouse Gas Control Technologies Conference Melbourne, Australia October 21-25, 2018 (SSRN published online April 2019) https://papers.ssrn.com/sol3/papers.cfm?abstract_id=3366088

Permission To Copy or To Use Copyrighted Material

Drew Owen Norton provides MSU permission to copy and use copyrighted materials listed below for the purposes of the Methods to Enhance Wellbore Cement Integrity with Microbially-Induced Calcite Precipitation (MICP) (DE-FE0024296) final scientific/technical report by MSU. This material will be used solely for nonprofit educational or research purposes in accordance with the mission of Montana State University. The copied material will not be sold.

This permission is non-exclusive, royalty-free (no cost to the Montana State University), world-wide, and perpetual.

By giving MSU permission to use the copyrighted material, permission is also granted to the Department of Energy and the U.S. Government to use the copyrighted material. The Government reserves for itself and others acting on its behalf a royalty-free, nonexclusive, irrevocable, worldwide license for Governmental purposes to publish, distribute, translate, duplicate, exhibit, and perform this copyrighted paper.

Please sign the release form below to signify agreement.

Permission for use only as stated above is granted.

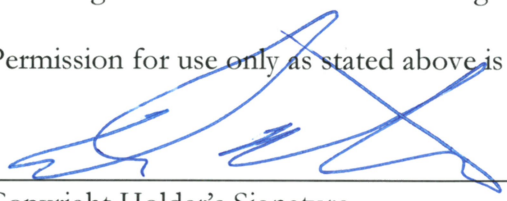

Copyright Holder's Signature

1/8/2020

Date

Permission extends to the following materials:

Norton, D. Visualizing and Quantifying Biomineralization in Wellbore Analog Reactors. MS Thesis, Environmental Engineering, Montana State University, June 2017

Detecting Microbially Induced Calcite Precipitation in a Model Well-Bore Using Downhole Low-Field NMR

Author: Catherine M. Kirkland, Sam Zanetti, Elliot Grunewald, et al

Publication: Environmental Science & Technology

Publisher: American Chemical Society

Date: Feb 1, 2017

PERMISSION/LICENSE IS GRANTED FOR YOUR ORDER AT NO CHARGE

This type of permission/license, instead of the standard Terms & Conditions, is sent to you because no fee is being charged for your order. Please note the following:

- Permission is granted for your request in both print and electronic formats, and translations.
- If figures and/or tables were requested, they may be adapted or used in part.
- Please print this page for your records and send a copy of it to your publisher/graduate school.
- Appropriate credit for the requested material should be given as follows: "Reprinted (adapted) with permission from (COMPLETE REFERENCE CITATION). Copyright (YEAR) American Chemical Society." Insert appropriate information in place of the capitalized words.
- One-time permission is granted only for the use specified in your request. No additional uses are granted (such as derivative works or other editions). For any other uses, please submit a new request.

BACK CLOSE WINDOW

ELSEVIER LICENSE
TERMS AND CONDITIONS

Feb 18, 2020

This Agreement between Montana State University -- Michelle Leonti ("You") and Elsevier ("Elsevier") consists of your license details and the terms and conditions provided by Elsevier and Copyright Clearance Center.

All payments must be made in full to CCC. For payment instructions, please see information listed at the bottom of this form.

License Number	4772191065903
License date	Feb 18, 2020
Licensed Content Publisher	Elsevier
Licensed Content Publication	International Journal of Greenhouse Gas Control
Licensed Content Title	Visualizing MICP with X-ray μ-CT to enhance cement defect sealing
Licensed Content Author	Catherine M. Kirkland,Drew Norton,Olivia Firth,Joachim Eldring,Alfred B. Cunningham,Robin Gerlach,Adrienne J. Phillips
Licensed Content Date	Jul 1, 2019
Licensed Content Volume	86
Licensed Content Issue	n/a

Licensed Content Pages	8
Start Page	93
End Page	100
Type of Use	reuse in a government report
Requestor type	academic/educational institute
Portion	full article
My number of copies...	1
Format	electronic
Are you the author of this Elsevier article?	No
Will you be translating?	No
Title	Final Scientific/Technical Report of Project Methods to Enhance Wellbore Cement Integrity with Microbially-Induced Calcite Precipitation (MICP)
Lead author	Adrienne Phillips
Produced by	Montana State University
Expected publication date	Jan 2020
Requestor Location	Montana State University PO Box 172465

BOZEMAN, MT 59717
United States
Attn: Michelle Leonti

Publisher Tax ID	98-0397604
Billing Type	Credit Card
Credit card info	Visa ending in 6804
Credit card expiration	06/2020
Total	192.00 USD

Terms and Conditions

INTRODUCTION

1. The publisher for this copyrighted material is Elsevier. By clicking "accept" in connection with completing this licensing transaction, you agree that the following terms and conditions apply to this transaction (along with the Billing and Payment terms and conditions established by Copyright Clearance Center, Inc. ("CCC"), at the time that you opened your Rightslink account and that are available at any time at http://myaccount.copyright.com).

GENERAL TERMS

2. Elsevier hereby grants you permission to reproduce the aforementioned material subject to the terms and conditions indicated.

3. Acknowledgement: If any part of the material to be used (for example, figures) has appeared in our publication with credit or acknowledgement to another source, permission must also be sought from that source. If such permission is not obtained then that material may not be included in your publication/copies. Suitable acknowledgement to the source must be made, either as a footnote or in a reference list at the end of your publication, as follows:

"Reprinted from Publication title, Vol /edition number, Author(s), Title of article / title of chapter, Pages No., Copyright (Year), with permission from Elsevier [OR APPLICABLE SOCIETY COPYRIGHT OWNER]." Also Lancet special credit - "Reprinted from The Lancet, Vol. number, Author(s), Title of article, Pages No., Copyright (Year), with permission from Elsevier."

4. Reproduction of this material is confined to the purpose and/or media for which permission is hereby given.

5. Altering/Modifying Material: Not Permitted. However figures and illustrations may be altered/adapted minimally to serve your work. Any other abbreviations, additions, deletions

and/or any other alterations shall be made only with prior written authorization of Elsevier Ltd. (Please contact Elsevier at permissions@elsevier.com). No modifications can be made to any Lancet figures/tables and they must be reproduced in full.

6. If the permission fee for the requested use of our material is waived in this instance, please be advised that your future requests for Elsevier materials may attract a fee.

7. Reservation of Rights: Publisher reserves all rights not specifically granted in the combination of (i) the license details provided by you and accepted in the course of this licensing transaction, (ii) these terms and conditions and (iii) CCC's Billing and Payment terms and conditions.

8. License Contingent Upon Payment: While you may exercise the rights licensed immediately upon issuance of the license at the end of the licensing process for the transaction, provided that you have disclosed complete and accurate details of your proposed use, no license is finally effective unless and until full payment is received from you (either by publisher or by CCC) as provided in CCC's Billing and Payment terms and conditions. If full payment is not received on a timely basis, then any license preliminarily granted shall be deemed automatically revoked and shall be void as if never granted. Further, in the event that you breach any of these terms and conditions or any of CCC's Billing and Payment terms and conditions, the license is automatically revoked and shall be void as if never granted. Use of materials as described in a revoked license, as well as any use of the materials beyond the scope of an unrevoked license, may constitute copyright infringement and publisher reserves the right to take any and all action to protect its copyright in the materials.

9. Warranties: Publisher makes no representations or warranties with respect to the licensed material.

10. Indemnity: You hereby indemnify and agree to hold harmless publisher and CCC, and their respective officers, directors, employees and agents, from and against any and all claims arising out of your use of the licensed material other than as specifically authorized pursuant to this license.

11. No Transfer of License: This license is personal to you and may not be sublicensed, assigned, or transferred by you to any other person without publisher's written permission.

12. No Amendment Except in Writing: This license may not be amended except in a writing signed by both parties (or, in the case of publisher, by CCC on publisher's behalf).

13. Objection to Contrary Terms: Publisher hereby objects to any terms contained in any purchase order, acknowledgment, check endorsement or other writing prepared by you, which terms are inconsistent with these terms and conditions or CCC's Billing and Payment terms and conditions. These terms and conditions, together with CCC's Billing and Payment terms and conditions (which are incorporated herein), comprise the entire agreement between you and publisher (and CCC) concerning this licensing transaction. In the event of any conflict between your obligations established by these terms and conditions and those established by CCC's Billing and Payment terms and conditions, these terms and conditions shall control.

14. Revocation: Elsevier or Copyright Clearance Center may deny the permissions described in this License at their sole discretion, for any reason or no reason, with a full refund payable to you. Notice of such denial will be made using the contact information provided by you. Failure to receive such notice will not alter or invalidate the denial. In no event will Elsevier or Copyright Clearance Center be responsible or liable for any costs, expenses or damage

incurred by you as a result of a denial of your permission request, other than a refund of the amount(s) paid by you to Elsevier and/or Copyright Clearance Center for denied permissions.

LIMITED LICENSE

The following terms and conditions apply only to specific license types:

15. **Translation**: This permission is granted for non-exclusive world **English** rights only unless your license was granted for translation rights. If you licensed translation rights you may only translate this content into the languages you requested. A professional translator must perform all translations and reproduce the content word for word preserving the integrity of the article.

16. **Posting licensed content on any Website**: The following terms and conditions apply as follows: Licensing material from an Elsevier journal: All content posted to the web site must maintain the copyright information line on the bottom of each image; A hyper-text must be included to the Homepage of the journal from which you are licensing at http://www.sciencedirect.com/science/journal/xxxxx or the Elsevier homepage for books at http://www.elsevier.com; Central Storage: This license does not include permission for a scanned version of the material to be stored in a central repository such as that provided by Heron/XanEdu.

Licensing material from an Elsevier book: A hyper-text link must be included to the Elsevier homepage at http://www.elsevier.com . All content posted to the web site must maintain the copyright information line on the bottom of each image.

Posting licensed content on Electronic reserve: In addition to the above the following clauses are applicable: The web site must be password-protected and made available only to bona fide students registered on a relevant course. This permission is granted for 1 year only. You may obtain a new license for future website posting.

17. **For journal authors:** the following clauses are applicable in addition to the above:

Preprints:

A preprint is an author's own write-up of research results and analysis, it has not been peer-reviewed, nor has it had any other value added to it by a publisher (such as formatting, copyright, technical enhancement etc.).

Authors can share their preprints anywhere at any time. Preprints should not be added to or enhanced in any way in order to appear more like, or to substitute for, the final versions of articles however authors can update their preprints on arXiv or RePEc with their Accepted Author Manuscript (see below).

If accepted for publication, we encourage authors to link from the preprint to their formal publication via its DOI. Millions of researchers have access to the formal publications on ScienceDirect, and so links will help users to find, access, cite and use the best available version. Please note that Cell Press, The Lancet and some society-owned have different preprint policies. Information on these policies is available on the journal homepage.

Accepted Author Manuscripts: An accepted author manuscript is the manuscript of an article that has been accepted for publication and which typically includes author-

incorporated changes suggested during submission, peer review and editor-author communications.

Authors can share their accepted author manuscript:

- immediately
  - via their non-commercial person homepage or blog
  - by updating a preprint in arXiv or RePEc with the accepted manuscript
  - via their research institute or institutional repository for internal institutional uses or as part of an invitation-only research collaboration work-group
  - directly by providing copies to their students or to research collaborators for their personal use
  - for private scholarly sharing as part of an invitation-only work group on commercial sites with which Elsevier has an agreement
- After the embargo period
  - via non-commercial hosting platforms such as their institutional repository
  - via commercial sites with which Elsevier has an agreement

In all cases accepted manuscripts should:

- link to the formal publication via its DOI
- bear a CC-BY-NC-ND license - this is easy to do
- if aggregated with other manuscripts, for example in a repository or other site, be shared in alignment with our hosting policy not be added to or enhanced in any way to appear more like, or to substitute for, the published journal article.

Published journal article (JPA): A published journal article (PJA) is the definitive final record of published research that appears or will appear in the journal and embodies all value-adding publishing activities including peer review co-ordination, copy-editing, formatting, (if relevant) pagination and online enrichment.

Policies for sharing publishing journal articles differ for subscription and gold open access articles:

Subscription Articles: If you are an author, please share a link to your article rather than the full-text. Millions of researchers have access to the formal publications on ScienceDirect, and so links will help your users to find, access, cite, and use the best available version.

Theses and dissertations which contain embedded PJAs as part of the formal submission can be posted publicly by the awarding institution with DOI links back to the formal publications on ScienceDirect.

If you are affiliated with a library that subscribes to ScienceDirect you have additional private sharing rights for others' research accessed under that agreement. This includes use for classroom teaching and internal training at the institution (including use in course packs and courseware programs), and inclusion of the article for grant funding purposes.

Gold Open Access Articles: May be shared according to the author-selected end-user license and should contain a CrossMark logo, the end user license, and a DOI link to the formal publication on ScienceDirect.

Please refer to Elsevier's posting policy for further information.

18. **For book authors** the following clauses are applicable in addition to the above: Authors are permitted to place a brief summary of their work online only. You are not

allowed to download and post the published electronic version of your chapter, nor may you scan the printed edition to create an electronic version. **Posting to a repository:** Authors are permitted to post a summary of their chapter only in their institution's repository.

19. **Thesis/Dissertation**: If your license is for use in a thesis/dissertation your thesis may be submitted to your institution in either print or electronic form. Should your thesis be published commercially, please reapply for permission. These requirements include permission for the Library and Archives of Canada to supply single copies, on demand, of the complete thesis and include permission for Proquest/UMI to supply single copies, on demand, of the complete thesis. Should your thesis be published commercially, please reapply for permission. Theses and dissertations which contain embedded PJAs as part of the formal submission can be posted publicly by the awarding institution with DOI links back to the formal publications on ScienceDirect.

Elsevier Open Access Terms and Conditions

You can publish open access with Elsevier in hundreds of open access journals or in nearly 2000 established subscription journals that support open access publishing. Permitted third party re-use of these open access articles is defined by the author's choice of Creative Commons user license. See our open access license policy for more information.

Terms & Conditions applicable to all Open Access articles published with Elsevier:

Any reuse of the article must not represent the author as endorsing the adaptation of the article nor should the article be modified in such a way as to damage the author's honour or reputation. If any changes have been made, such changes must be clearly indicated.

The author(s) must be appropriately credited and we ask that you include the end user license and a DOI link to the formal publication on ScienceDirect.

If any part of the material to be used (for example, figures) has appeared in our publication with credit or acknowledgement to another source it is the responsibility of the user to ensure their reuse complies with the terms and conditions determined by the rights holder.

Additional Terms & Conditions applicable to each Creative Commons user license:

CC BY: The CC-BY license allows users to copy, to create extracts, abstracts and new works from the Article, to alter and revise the Article and to make commercial use of the Article (including reuse and/or resale of the Article by commercial entities), provided the user gives appropriate credit (with a link to the formal publication through the relevant DOI), provides a link to the license, indicates if changes were made and the licensor is not represented as endorsing the use made of the work. The full details of the license are available at http://creativecommons.org/licenses/by/4.0.

CC BY NC SA: The CC BY-NC-SA license allows users to copy, to create extracts, abstracts and new works from the Article, to alter and revise the Article, provided this is not done for commercial purposes, and that the user gives appropriate credit (with a link to the formal publication through the relevant DOI), provides a link to the license, indicates if changes were made and the licensor is not represented as endorsing the use made of the work. Further, any new works must be made available on the same conditions. The full details of the license are available at http://creativecommons.org/licenses/by-nc-sa/4.0.

CC BY NC ND: The CC BY-NC-ND license allows users to copy and distribute the Article, provided this is not done for commercial purposes and further does not permit distribution of the Article if it is changed or edited in any way, and provided the user gives appropriate credit (with a link to the formal publication through the relevant DOI), provides a link to the license, and that the licensor is not represented as endorsing the use made of the work. The full details of the license are available at http://creativecommons.org/licenses/by-nc-nd/4.0. Any commercial reuse of Open Access articles published with a CC BY NC SA or CC BY NC ND license requires permission from Elsevier and will be subject to a fee.

Commercial reuse includes:

- Associating advertising with the full text of the Article
- Charging fees for document delivery or access
- Article aggregation
- Systematic distribution via e-mail lists or share buttons

Posting or linking by commercial companies for use by customers of those companies.

20. **Other Conditions**:

v1.9

Questions? customercare@copyright.com or +1-855-239-3415 (toll free in the US) or +1-978-646-2777.

ELSEVIER LICENSE
TERMS AND CONDITIONS

Feb 18, 2020

This Agreement between Montana State University -- Michelle Leonti ("You") and Elsevier ("Elsevier") consists of your license details and the terms and conditions provided by Elsevier and Copyright Clearance Center.

All payments must be made in full to CCC. For payment instructions, please see information listed at the bottom of this form.

License Number	4772191414200
License date	Feb 18, 2020
Licensed Content Publisher	Elsevier
Licensed Content Publication	Journal of Petroleum Science and Engineering
Licensed Content Title	Enhancing wellbore cement integrity with microbially induced calcite precipitation (MICP): A field scale demonstration
Licensed Content Author	A.J. Phillips,E. Troyer,R. Hiebert,C. Kirkland,R. Gerlach,A.B. Cunningham,L. Spangler,J. Kirksey,W. Rowe,R. Esposito
Licensed Content Date	Dec 1, 2018
Licensed Content Volume	171
Licensed Content Issue	n/a

Licensed Content Pages	8
Start Page	1141
End Page	1148
Type of Use	reuse in a government report
Requestor type	academic/educational institute
Portion	full article
My number of copies...	1
Format	electronic
Are you the author of this Elsevier article?	No
Will you be translating?	No
Title	Final Scientific/Technical Report of Project Methods to Enhance Wellbore Cement Integrity with Microbially-Induced Calcite Precipitation (MICP)
Lead author	Adrienne Phillips
Produced by	Montana State University
Expected publication date	Jan 2020
Expected number of pages	1

Requestor Location	Montana State University PO Box 172465 BOZEMAN, MT 59717 United States Attn: Michelle Leonti
Publisher Tax ID	98-0397604
Billing Type	Credit Card
Credit card info	Visa ending in 6804
Credit card expiration	06/2020
Total	192.00 USD

Terms and Conditions

INTRODUCTION

1. The publisher for this copyrighted material is Elsevier. By clicking "accept" in connection with completing this licensing transaction, you agree that the following terms and conditions apply to this transaction (along with the Billing and Payment terms and conditions established by Copyright Clearance Center, Inc. ("CCC"), at the time that you opened your Rightslink account and that are available at any time at http://myaccount.copyright.com).

GENERAL TERMS

2. Elsevier hereby grants you permission to reproduce the aforementioned material subject to the terms and conditions indicated.

3. Acknowledgement: If any part of the material to be used (for example, figures) has appeared in our publication with credit or acknowledgement to another source, permission must also be sought from that source. If such permission is not obtained then that material may not be included in your publication/copies. Suitable acknowledgement to the source must be made, either as a footnote or in a reference list at the end of your publication, as follows:

"Reprinted from Publication title, Vol /edition number, Author(s), Title of article / title of chapter, Pages No., Copyright (Year), with permission from Elsevier [OR APPLICABLE SOCIETY COPYRIGHT OWNER]." Also Lancet special credit - "Reprinted from The Lancet, Vol. number, Author(s), Title of article, Pages No., Copyright (Year), with permission from Elsevier."

4. Reproduction of this material is confined to the purpose and/or media for which permission is hereby given.

5. Altering/Modifying Material: Not Permitted. However figures and illustrations may be altered/adapted minimally to serve your work. Any other abbreviations, additions, deletions and/or any other alterations shall be made only with prior written authorization of Elsevier Ltd. (Please contact Elsevier at permissions@elsevier.com). No modifications can be made to any Lancet figures/tables and they must be reproduced in full.

6. If the permission fee for the requested use of our material is waived in this instance, please be advised that your future requests for Elsevier materials may attract a fee.

7. Reservation of Rights: Publisher reserves all rights not specifically granted in the combination of (i) the license details provided by you and accepted in the course of this licensing transaction, (ii) these terms and conditions and (iii) CCC's Billing and Payment terms and conditions.

8. License Contingent Upon Payment: While you may exercise the rights licensed immediately upon issuance of the license at the end of the licensing process for the transaction, provided that you have disclosed complete and accurate details of your proposed use, no license is finally effective unless and until full payment is received from you (either by publisher or by CCC) as provided in CCC's Billing and Payment terms and conditions. If full payment is not received on a timely basis, then any license preliminarily granted shall be deemed automatically revoked and shall be void as if never granted. Further, in the event that you breach any of these terms and conditions or any of CCC's Billing and Payment terms and conditions, the license is automatically revoked and shall be void as if never granted. Use of materials as described in a revoked license, as well as any use of the materials beyond the scope of an unrevoked license, may constitute copyright infringement and publisher reserves the right to take any and all action to protect its copyright in the materials.

9. Warranties: Publisher makes no representations or warranties with respect to the licensed material.

10. Indemnity: You hereby indemnify and agree to hold harmless publisher and CCC, and their respective officers, directors, employees and agents, from and against any and all claims arising out of your use of the licensed material other than as specifically authorized pursuant to this license.

11. No Transfer of License: This license is personal to you and may not be sublicensed, assigned, or transferred by you to any other person without publisher's written permission.

12. No Amendment Except in Writing: This license may not be amended except in a writing signed by both parties (or, in the case of publisher, by CCC on publisher's behalf).

13. Objection to Contrary Terms: Publisher hereby objects to any terms contained in any purchase order, acknowledgment, check endorsement or other writing prepared by you, which terms are inconsistent with these terms and conditions or CCC's Billing and Payment terms and conditions. These terms and conditions, together with CCC's Billing and Payment terms and conditions (which are incorporated herein), comprise the entire agreement between you and publisher (and CCC) concerning this licensing transaction. In the event of any conflict between your obligations established by these terms and conditions and those established by CCC's Billing and Payment terms and conditions, these terms and conditions shall control.

14. Revocation: Elsevier or Copyright Clearance Center may deny the permissions described in this License at their sole discretion, for any reason or no reason, with a full refund payable to you. Notice of such denial will be made using the contact information provided by you. Failure to receive such notice will not alter or invalidate the denial. In no event will Elsevier or Copyright Clearance Center be responsible or liable for any costs, expenses or damage incurred by you as a result of a denial of your permission request, other than a refund of the amount(s) paid by you to Elsevier and/or Copyright Clearance Center for denied permissions.

LIMITED LICENSE

The following terms and conditions apply only to specific license types:

15. **Translation**: This permission is granted for non-exclusive world **English** rights only unless your license was granted for translation rights. If you licensed translation rights you may only translate this content into the languages you requested. A professional translator must perform all translations and reproduce the content word for word preserving the integrity of the article.

16. **Posting licensed content on any Website**: The following terms and conditions apply as follows: Licensing material from an Elsevier journal: All content posted to the web site must maintain the copyright information line on the bottom of each image; A hyper-text must be included to the Homepage of the journal from which you are licensing at http://www.sciencedirect.com/science/journal/xxxxx or the Elsevier homepage for books at http://www.elsevier.com; Central Storage: This license does not include permission for a scanned version of the material to be stored in a central repository such as that provided by Heron/XanEdu.

Licensing material from an Elsevier book: A hyper-text link must be included to the Elsevier homepage at http://www.elsevier.com . All content posted to the web site must maintain the copyright information line on the bottom of each image.

Posting licensed content on Electronic reserve: In addition to the above the following clauses are applicable: The web site must be password-protected and made available only to bona fide students registered on a relevant course. This permission is granted for 1 year only. You may obtain a new license for future website posting.

17. **For journal authors:** the following clauses are applicable in addition to the above:

Preprints:

A preprint is an author's own write-up of research results and analysis, it has not been peer-reviewed, nor has it had any other value added to it by a publisher (such as formatting, copyright, technical enhancement etc.).

Authors can share their preprints anywhere at any time. Preprints should not be added to or enhanced in any way in order to appear more like, or to substitute for, the final versions of articles however authors can update their preprints on arXiv or RePEc with their Accepted Author Manuscript (see below).

If accepted for publication, we encourage authors to link from the preprint to their formal publication via its DOI. Millions of researchers have access to the formal publications on ScienceDirect, and so links will help users to find, access, cite and use the best available

version. Please note that Cell Press, The Lancet and some society-owned have different preprint policies. Information on these policies is available on the journal homepage.

Accepted Author Manuscripts: An accepted author manuscript is the manuscript of an article that has been accepted for publication and which typically includes author-incorporated changes suggested during submission, peer review and editor-author communications.

Authors can share their accepted author manuscript:

- immediately
  - via their non-commercial person homepage or blog
  - by updating a preprint in arXiv or RePEc with the accepted manuscript
  - via their research institute or institutional repository for internal institutional uses or as part of an invitation-only research collaboration work-group
  - directly by providing copies to their students or to research collaborators for their personal use
  - for private scholarly sharing as part of an invitation-only work group on commercial sites with which Elsevier has an agreement
- After the embargo period
  - via non-commercial hosting platforms such as their institutional repository
  - via commercial sites with which Elsevier has an agreement

In all cases accepted manuscripts should:

- link to the formal publication via its DOI
- bear a CC-BY-NC-ND license - this is easy to do
- if aggregated with other manuscripts, for example in a repository or other site, be shared in alignment with our hosting policy not be added to or enhanced in any way to appear more like, or to substitute for, the published journal article.

Published journal article (JPA): A published journal article (PJA) is the definitive final record of published research that appears or will appear in the journal and embodies all value-adding publishing activities including peer review co-ordination, copy-editing, formatting, (if relevant) pagination and online enrichment.

Policies for sharing publishing journal articles differ for subscription and gold open access articles:

Subscription Articles: If you are an author, please share a link to your article rather than the full-text. Millions of researchers have access to the formal publications on ScienceDirect, and so links will help your users to find, access, cite, and use the best available version.

Theses and dissertations which contain embedded PJAs as part of the formal submission can be posted publicly by the awarding institution with DOI links back to the formal publications on ScienceDirect.

If you are affiliated with a library that subscribes to ScienceDirect you have additional private sharing rights for others' research accessed under that agreement. This includes use for classroom teaching and internal training at the institution (including use in course packs and courseware programs), and inclusion of the article for grant funding purposes.

Gold Open Access Articles: May be shared according to the author-selected end-user license and should contain a CrossMark logo, the end user license, and a DOI link to the formal publication on ScienceDirect.

Please refer to Elsevier's posting policy for further information.

18. **For book authors** the following clauses are applicable in addition to the above: Authors are permitted to place a brief summary of their work online only. You are not allowed to download and post the published electronic version of your chapter, nor may you scan the printed edition to create an electronic version. **Posting to a repository:** Authors are permitted to post a summary of their chapter only in their institution's repository.

19. **Thesis/Dissertation**: If your license is for use in a thesis/dissertation your thesis may be submitted to your institution in either print or electronic form. Should your thesis be published commercially, please reapply for permission. These requirements include permission for the Library and Archives of Canada to supply single copies, on demand, of the complete thesis and include permission for Proquest/UMI to supply single copies, on demand, of the complete thesis. Should your thesis be published commercially, please reapply for permission. Theses and dissertations which contain embedded PJAs as part of the formal submission can be posted publicly by the awarding institution with DOI links back to the formal publications on ScienceDirect.

Elsevier Open Access Terms and Conditions

You can publish open access with Elsevier in hundreds of open access journals or in nearly 2000 established subscription journals that support open access publishing. Permitted third party re-use of these open access articles is defined by the author's choice of Creative Commons user license. See our open access license policy for more information.

Terms & Conditions applicable to all Open Access articles published with Elsevier:

Any reuse of the article must not represent the author as endorsing the adaptation of the article nor should the article be modified in such a way as to damage the author's honour or reputation. If any changes have been made, such changes must be clearly indicated.

The author(s) must be appropriately credited and we ask that you include the end user license and a DOI link to the formal publication on ScienceDirect.

If any part of the material to be used (for example, figures) has appeared in our publication with credit or acknowledgement to another source it is the responsibility of the user to ensure their reuse complies with the terms and conditions determined by the rights holder.

Additional Terms & Conditions applicable to each Creative Commons user license:

CC BY: The CC-BY license allows users to copy, to create extracts, abstracts and new works from the Article, to alter and revise the Article and to make commercial use of the Article (including reuse and/or resale of the Article by commercial entities), provided the user gives appropriate credit (with a link to the formal publication through the relevant DOI), provides a link to the license, indicates if changes were made and the licensor is not represented as endorsing the use made of the work. The full details of the license are available at http://creativecommons.org/licenses/by/4.0.

CC BY NC SA: The CC BY-NC-SA license allows users to copy, to create extracts, abstracts and new works from the Article, to alter and revise the Article, provided this is not done for commercial purposes, and that the user gives appropriate credit (with a link to the formal publication through the relevant DOI), provides a link to the license, indicates if changes were made and the licensor is not represented as endorsing the use made of the

work. Further, any new works must be made available on the same conditions. The full details of the license are available at http://creativecommons.org/licenses/by-nc-sa/4.0.

CC BY NC ND: The CC BY-NC-ND license allows users to copy and distribute the Article, provided this is not done for commercial purposes and further does not permit distribution of the Article if it is changed or edited in any way, and provided the user gives appropriate credit (with a link to the formal publication through the relevant DOI), provides a link to the license, and that the licensor is not represented as endorsing the use made of the work. The full details of the license are available at http://creativecommons.org/licenses/by-nc-nd/4.0. Any commercial reuse of Open Access articles published with a CC BY NC SA or CC BY NC ND license requires permission from Elsevier and will be subject to a fee.

Commercial reuse includes:

- Associating advertising with the full text of the Article
- Charging fees for document delivery or access
- Article aggregation
- Systematic distribution via e-mail lists or share buttons

Posting or linking by commercial companies for use by customers of those companies.

20. **Other Conditions**:

v1.9

Questions? customercare@copyright.com or +1-855-239-3415 (toll free in the US) or +1-978-646-2777.